Doctoral theses at NTNU, 2017:317

Joakim Johnsen

Thermomechanical behaviour of semi-crystalline polymers: experiments, modelling and simulation

NTNU
Norwegian University of
Science and Technology

Doctoral thesis

Joakim Johnsen

ISBN 978-82-326-2702-8 (printed ver.)
ISBN 978-82-326-2703-5 (electronic ver.)
ISSN 1503-8181

NTNU
Norwegian University of Science and Technology
Thesis for the Degree of
Philosophiae Doctor
Faculty of Engineering
Department of Structural Engineering

Doctoral theses at NTNU, 2017:317

NTNU

Joakim Johnsen

Thermomechanical behaviour of semi-crystalline polymers: experiments, modelling and simulation

Thesis for the Degree of Philosophiae Doctor

Trondheim, November 2017

Norwegian University of Science and Technology
Faculty of Engineering
Department of Structural Engineering

NTNU
Norwegian University of
Science and Technology

NTNU
Norwegian University of Science and Technology

Thesis for the Degree of Philosophiae Doctor

Faculty of Engineering
Department of Structural Engineering

ISBN 978-82-326-2702-8 (printed ver.)
ISBN 978-82-326-2703-5 (electronic ver.)
ISSN 1503-8181

Doctoral theses at NTNU, 2017:317

Printed by NTNU Grafisk senter

Preface

This thesis is submitted in partial fulfilment of the requirements for the degree of Philosophiae Doctor in Structural Engineering at the Norwegian University of Science and Technology (NTNU). The work has been conducted at the Structural Impact Laboratory (SIMLab) at the Department of Structural Engineering, NTNU. Funding was provided by the Arctic Materials II programme, hosted by SINTEF Materials and Chemistry. The work was supervised by Professor Arild Holm Clausen, Dr. Frode Grytten and Professor Odd Sture Hopperstad.

The thesis consists of three main parts which are referred to as Parts 1-3. Each part contains a journal article, Parts 1 and 2 are already published, while Part 3 is in preparation for submission to an international peer-reviewed journal. As such, each part can be read separately. Part 1 presents the experimental set-up, Part 2 contains the experimental results, and Part 3 presents the proposed material model. A synopsis binds the individual parts together.

The first author has been responsible for the experimental work, material modelling, numerical work and the preparation of all the manuscripts.

Joakim Johnsen
Trondheim, Norway
October 18, 2017

Abstract

This work presents experimental investigations on two semi-crystalline materials: a rubber-modified polypropylene (PP) and a cross-linked low density polyethylene (XLPE). Uniaxial tension and compression tests were performed at different temperatures and strain rates using a novel experimental set-up that involves optical measurements of the deformation. A thermomechanical constitutive model was developed, implemented and used to describe the mechanical behaviour of the XLPE material. The thesis is organized as follows: A synopsis presents the background, motivation, objectives and scope along with a summary of the work, while the three journal articles in Parts 1 to 3 describe the scientific contributions in detail.

Part 1 presents the experimental set-up established to conduct tests at low temperatures. The experimental set-up consists of a transparent polycarbonate (PC) temperature chamber which, in contrast to conventional temperature chambers, allows the use of several digital cameras to monitor the test specimen during experiments. Consequently, local strain measurements could be performed by using for example digital image correlation (DIC). To facilitate instrumentation with an infrared thermal camera, a slit was added in the front window of the PC temperature chamber to obtain a free line-of-sight between the test specimen and the infrared camera. Utilizing this experimental set-up, a semi-crystalline XLPE under quasi-static tensile loading was successfully analysed using DIC at four different temperatures, $T = 25$ °C, $T = 0$ °C, $T = -15$ °C and $T = -30$ °C. At the lower temperatures, the conventional spray-paint speckle became brittle and cracked during deformation. An alternative method was developed using white grease with a black powder added for contrast. It was shown that neither the PC chamber nor replacing the conventional spray-paint speckle pattern with grease and black powder influenced the stress-strain curves as determined by DIC.

Part 2 presents uniaxial tension and compression experiments performed on both materials: the semi-crystalline rubber-modified polypropylene (PP) and the semi-crystalline cross-linked low density polyethylene (XLPE). The experimental set-up presented in Part 1 was used to perform uniaxial tension and compression tests at four different temperatures ($T = 25$ °C, $T = 0$ °C, $T = -15$ °C and $T = -30$ °C) and three initial nominal strain rates ($\dot{e} = 0.01$ s^{-1}, $\dot{e} = 0.1$ s^{-1} and $\dot{e} = 1.0$ s^{-1}). DIC was used to obtain local stress-strain data from the tension experiments, while a combination of point tracking and edge tracing was used in the compression experiments. A scanning electron microscopy (SEM) study was performed to give a qualitative understanding of the substantial volumetric strain observed in the PP material and the small volumetric strains

in the XLPE material. The mechanical behaviour of both materials was shown to be dependent on temperature and strain rate. More specifically, Young's modulus increased for decreasing temperatures in both materials and for increasing strain rate in the XLPE material. The Ree-Eyring flow theory was used to successfully capture the temperature and strain rate dependent yield stress in both materials. In terms of volume change, the XLPE material was found to be nearly incompressible at room temperature, while it became slightly compressible at the lower temperatures. For the PP material the observed volumetric strains were substantial, ranging from approximately 0.5 to 0.9.

Part 3 presents the proposed thermoelastic-thermoviscoplastic constitutive model consisting of two parts: an intermolecular part described by an elastic Hencky spring coupled with two Ree-Eyring dashpots augmented with kinematic hardening from an inelastic Hencky spring, and an orientational part capturing entropic strain hardening due to alignment of the polymer chains using an eight chain spring. The objective of the study is to describe the effect of temperature and strain rate on the mechanical behaviour of the XLPE material investigated in Parts 1 and 2. The constitutive model was implemented in the commercial finite element (FE) program Abaqus/Standard as a UMAT subroutine. A numerical method was used to establish the consistent tangent operator together with a sub-stepping scheme to ensure convergence. The FE model yields accurate predictions of the stress-strain behaviour of the material, along with the volumetric strains, self-heating, strain rate and force vs. global displacement.

Acknowledgements

First of all I would like to thank my supervisors: Professor Arild Holm Clausen, Dr. Frode Grytten and Professor Odd Sture Hopperstad. Your knowledge of the field, attention to detail and mathematical rigour have been truly inspiring. I could not have asked for better guidance.

The financial support for this project comes from Arctic Materials II, a programme consisting of a consortium of companies and with substantial funding from the Research Council of Norway. I am forever grateful for being given the opportunity to do academic research.

This thesis could never have been finished without the outstanding working environment at SIMLab. A big thank you to all who made, and continue to make, this a truly wonderful place to work – both at the office and outside. A special thanks goes to Dr. Jens Kristian Holmen for providing inside information from SIMLab while I lived in Oslo – thus easing my worries regarding the Ph.D. life, for all the time you have spent giving advice regarding my work and for putting up with me for 10 years. Mr. Lars Edvard Dæhli deserves honorable mention for enduring 2.5 years sharing an office with me, thank you for always taking the time to answer my questions, for talking to yourself as much as I do, and for all the interesting (and not so interesting) discussions at the office. I also wish to acknowledge Mr. Christian Oen Paulsen for his help procuring the SEM micrographs of my materials. I will always be indebted to Dr. Marius Andersen for all the help related to my work. Your DIC program and your tensile specimen design were game changers.

Mr. Tore Wisth and Mr. Trond Auestad were invaluable in the development of the experimental set-up, in the machining of the test specimens and in the execution of the experimental programme – thank you for all your help. I would also like to thank Dr. Norbert Jansen and Mr. Thomas Stark at Borealis, without whom the polypropylene testing campaign would have been devastating.

The help from Associate Professor David Didier Morin and Dr. Torodd Berstad regarding the implementation of the constitutive model is greatly appreciated. Thank you for taking time for all the discussions and for the sporadic debugging (even though you added an Easter egg in my code, David).

I would also like to thank my family for always being there for me and for all the encouragement and support. I am also thankful for my friends for being persistent in the claim that there is more to life than work.

Contents

Chapter 1

Synopsis

1.1 Introduction

The use of polymeric materials in industrial applications is widespread. In the automotive industry for instance, polymers are used in a variety of applications – ranging from components in the interior to pedestrian safety devices designed to dissipate energy during impacts. A potential problem in this regard is that material characterization and impact tests are frequently performed close to room temperature, thus failing to account for the change in material behaviour as the temperature is decreased. It is likely that cars in arctic environments will encounter low air temperatures, and since polymeric materials tend to become stiffer and more brittle when cooled, the ramifications of a collision with a pedestrian may be devastating. Another industry where the use of polymeric materials is manifold is the oil and gas industry. Here polymeric materials can be used as gaskets, shock-absorbers in load bearing structures and coatings on pipelines and umbilicals. Estimates from The United States Geological Survey (USGS) indicate that large amounts of the world's oil and gas reserves are located north of the Arctic Circle [1]. Consequently, the oil and gas industry continue to explore and search for oil reserves further north. This expansion into colder and harsher climates presents challenges concerning design rules and design qualification procedures. Therefore, new knowledge regarding material behaviour at low temperatures is needed.

A crucial step in gaining knowledge is of course good and reliable experimental data. At room temperature, non-contact measuring devices, such as digital image correlation (DIC) or point tracking, are widely utilized to obtain local stress-strain data from experiments on polymers [2–9]. However, when a temperature chamber is introduced to conduct experiments at high [10–16] or low temperatures [17–26], many researchers rely on mechanical measuring devices such as extensometers and/or machine displacement. The disadvantage of using mechanical measuring devices, as opposed to optical devices, is that the strains will be obtained as average values over a large section of the specimen. This is especially problematic in uniaxial tension tests where

the material necks and the strains localize, but it is also the case in uniaxial compression when, or if, barreling occurs. Another limitation imposed by conventional temperature chambers is that they inhibit the use of a thermal camera to record self-heating in the test specimen during deformation. The ability to measure the surface temperature of the test specimen is vital to separate the competing contributions from strain rate, which tends to stiffen the material, and self-heating, which leads to thermal softening.

Material modelling of polymers has been an active research area for many years. Most available material models can be broken down into two parts (Figure 1.1): (1) a (visco)elastic-viscoplastic part where viscoplasticity is governed by, e.g., the transition state theory proposed by Eyring [27] and later modified by Ree and Eyring [28], the conformational change theory presented by Robertson [29], or the model given by Argon [30] accounting for the intermolecular shear resistance, and (2) an entropic spring derived from non-Gaussian (e.g. Langevin) chain statistics, for instance the three chain model by Wang and Guth [31] and the more recent eight chain model by Arruda and Boyce [32]. Haward and Thackray [33] were the first to propose this split into an

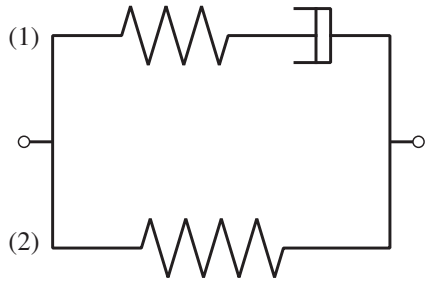

Figure 1.1: A typical rheological model showing (1) the elastic-viscoplastic part and (2) the orientational hardening part.

intermolecular part and an entropic part. Their model was extended to a three dimensional (3D) formulation by Boyce et al. [34]. The Boyce, Parks and Argon (BPA) model [34] also included strain softening and pressure sensitivity. Alternative methods to include strain hardening were incorporated in the Eindhoven Glassy Polymer (EGP) model [35, 36], where a Neo-Hookean spring was used as a backstress. Hoy and Robbins [37] proposed to scale the hardening modulus of the backstress by the flow stress, while Govaert et al. [38] advocated the use of a backstress in addition to viscous strain hardening modelled by either a stress-scaling of the hardening modulus as proposed by Hoy and Robbins [37], or a non-constant deformation dependent activation volume as in the work by Wendlandt et al. [39]. The latter approach, along with an alternative of making the reference plastic strain rate non-constant, was evaluated in detail by Senden et al. [40].

The Ree-Eyring [28] model is adopted in this study. In the Ree-Eyring model molecules slide with respect to each other by passing through a so-called transition state or an activated state. Finally, by overcoming an energy barrier which depends on temperature and the applied stress a chain segment may move from one site to another [41], see Figure 1.2. Using an Arrhenius law the frequency of a chain segment moving from site A to site B, or from site B to site A, by thermal

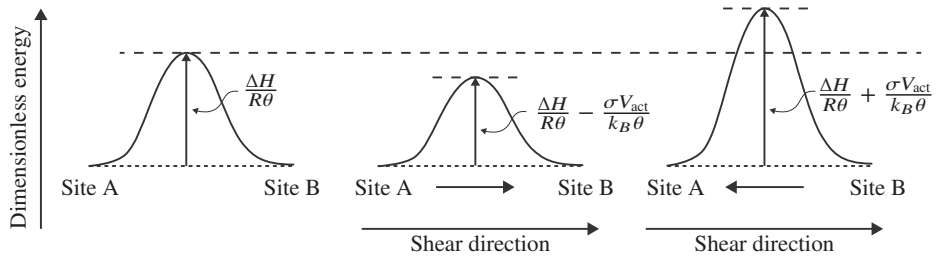

Figure 1.2: Illustration of the principle of the Ree-Eyring model. Adapted from Halary et al. [41].

activation without any applied stresses is given as

$$v_{\text{A}\to\text{B}} = v_{\text{B}\to\text{A}} = v_0 \exp\left(-\frac{\Delta H}{R\theta}\right) \tag{1.1}$$

where ΔH is the activation enthalpy in Joule per mole, v_0 is a pre-exponential factor, R is the universal gas constant and θ is the absolute temperature. As evident from Figure 1.2, the required energy to move a chain segment under the application of a stress is decreased in the direction of the stress, and increased in the opposite direction. The associated frequencies are then given as

$$v_{\text{A}\to\text{B}} = v_0 \exp\left[-\left(\frac{\Delta H}{R\theta} - \frac{\sigma V_{\text{act}}}{k_B\theta}\right)\right] \quad \text{and} \quad v_{\text{B}\to\text{A}} = v_0 \exp\left[-\left(\frac{\Delta H}{R\theta} + \frac{\sigma V_{\text{act}}}{k_B\theta}\right)\right] \tag{1.2}$$

where σ is the stress, V_{act} is the activation volume and k_B is Boltzmann's constant. The total frequency of a chain segment moving from site A then becomes

$$v_{\text{A}} = v_{\text{A}\to\text{B}} - v_{\text{B}\to\text{A}} = v_0 \exp\left(\frac{-\Delta H}{R\theta}\right)\left[\exp\left(\frac{\sigma V_{\text{act}}}{k_B\theta}\right) - \exp\left(\frac{-\sigma V_{\text{act}}}{k_B\theta}\right)\right] \tag{1.3}$$

or

$$v_{\text{A}} = 2v_0 \exp\left(\frac{-\Delta H}{R\theta}\right)\sinh\left(\frac{\sigma V_{\text{act}}}{k_B\theta}\right) \tag{1.4}$$

Assuming that the strain rate, $\dot{\varepsilon}$, is a linear function of the frequency we arrive at

$$\dot{\varepsilon} = \dot{\varepsilon}_0 \exp\left(\frac{-\Delta H}{R\theta}\right)\sinh\left(\frac{\sigma V_{\text{act}}}{k_B\theta}\right) \tag{1.5}$$

which is similar to the expression used in Parts 2 and 3 of this work.

Due to the strong influence of temperature and strain rate on the mechanical behaviour of polymeric materials, thermomechanical coupling is essential to accurately describe, and decouple, the competition between hardening due to increasing strain rate, and softening due to self-heating. There are many examples of thermomechanical models. Arruda et al. [10] and Boyce et al. [42] obtained good results with an elastic-thermoviscoplastic model where the elasticity was described by a Hookean (Hencky) spring and the thermoviscoplasticity was governed by non-Newtonian flow with strain hardening from an entropic backstress. Richeton et al. [43] used a similar approach, but

extended the model to span the glass transition temperature. The isothermal elastic-viscoplastic model developed by Polanco-Loria et al. [44] was recently extended by Garcia-Gonzalez et al. [45] to include thermomechanical coupling by introducing thermal expansion and thermal softening through a yield stress dependent on the homologous temperature. Anand et al. [46] and Ames et al. [47] presented a rather complex thermomechanical model to describe large deformations of amorphous polymers. The proposed model was successfully applied to complex loading modes such as loading/unloading and torsion. This model was further developed to span the glass transition temperature by Srivastava et al. [15].

In the study performed by Adams and Farris [48] it was found that approximately 50 to 80% of the mechanical work was converted into heat, a result that was corroborated by Boyce et al. [42]. However, in our study it will be shown that the total mechanical work has to contribute to heat generation. In order to achieve this without having to introduce isotropic hardening, entropic springs are used. Consequently, the free energy functions are cast in the same form as proposed by Miehe [49] and comprise three parts: an isochoric contribution, a purely thermal contribution and a volumetric contribution.

1.2 Objectives and scope

The objectives of the work in this thesis were to (1) establish an experimental set-up allowing for non-contact optical devices to measure the local stress-strain data from experiments at low temperatures and at different strain rates. Due to the link between self-heating and softening in polymeric materials, it was also desirable to instrument the experiments with a device able to measure the change of surface temperature of the test sample, e.g. an infrared thermal camera. (2) Establish an experimental database for two semi-crystalline materials relevant for use in cold conditions, and (3) to develop and implement a new constitutive model incorporating the effects of temperature and strain rate on the mechanical behaviour of the materials in the commercial finite element (FE) program Abaqus.

The scope was defined together with the partners in the Arctic Materials II programme: The investigated temperatures should lie above the glass transition temperatures of the two materials: a cross-linked low density polyethylene (XLPE) [50] used as, e.g., electrical insulation in high-voltage cables, and a rubber-modified polypropylene (PP) [51] used as for instance thermal insulation of offshore pipelines. In addition, the range of investigated strain rates should correspond to those obtained in for example reeling/unreeling of a pipeline or a cable. Consequently, it was determined to investigate temperatures from $T = -30$ °C to room temperature and nominal strain rates in the range $\dot{e} \in [0.01, 1.0]$ s^{-1}.

1.3 Summary

The works in this PhD thesis have been published in peer-reviewed international journals (Parts 1 and 2) or is in preparation for submission to an international peer-reviewed journal (Part 3). The three journal articles are summarized below.

1.3.1 Part 1

Johnsen, J., Grytten, F., Hopperstad, O. S., and Clausen, A. H. (2016). *Experimental set-up for determination of the large-strain tensile behaviour of polymers at low temperatures*. Polymer Testing, 53, 305–313.

The first article in this thesis presents the experimental set-up which was used to determine the material behaviour at low temperatures. Over the years, many studies have been performed on the mechanical behaviour of polymers at elevated temperatures, e.g., [10–16]. On the other hand, fewer studies have been devoted to the behaviour at low temperatures – especially for large strains. The early work by Bauwens and Bauwens-Crowet with co-workers [17–20] focused on the relation between yield stress and temperature, while more recent studies such as Şerban et al. [6], Brown et al. [25] and Cao et al. [23] conducted uniaxial tension tests using incremental extensometers to determine the stress-strain curves. This brings us to the crux of the problem: when a temperature chamber is involved in the mechanical testing, researchers often rely on mechanical measuring devices such as an extensometer and/or machine displacement to estimate the longitudinal strains. Some studies even assume incompressibility in order to calculate the current area of the cross-section. Since the true stress-strain behaviour is of utmost importance as input to subsequent numerical simulations with the finite element method, we have suggested a novel experimental method to obtain local strain measurements in the necked region of the tensile specimen.

In our approach we have replaced the conventional temperature chamber, usually equipped with only one window, with a transparent polycarbonate (PC) temperature chamber, see Figures 1.3 and 1.4. The transparency of the chamber allows for multiple digital cameras to monitor the specimen

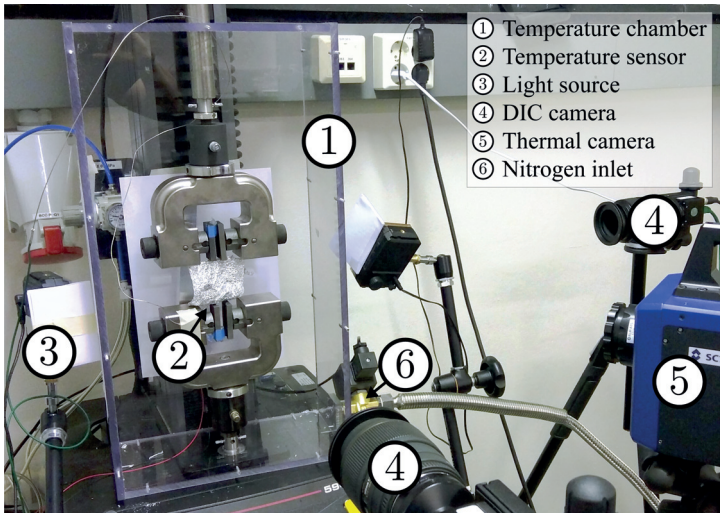

Figure 1.3: Picture showing the experimental set-up. Note that neither the front window nor the tensile specimen is mounted.

during deformation – enabling measurement of the longitudinal strain and both transverse strain components. Knowing all three coordinate strains, also the volumetric strain is easily found. A slit was added in the front window of the chamber to obtain a free line-of-sight between the test specimen and an infrared thermal camera. The desired temperature inside the chamber was maintained by a thermocouple temperature sensor controlling the influx of liquid nitrogen, while fans blowing air over the outside of the chamber walls were used to prevent icing.

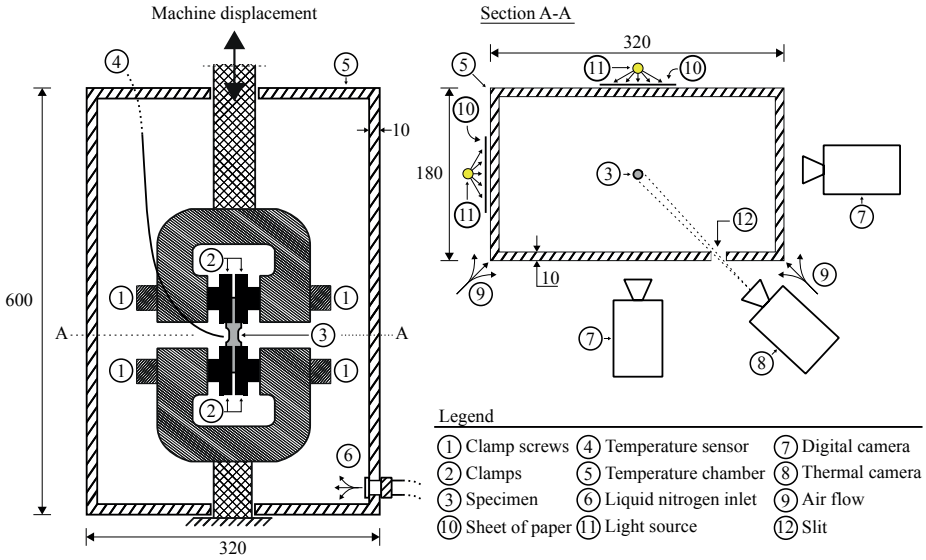

Figure 1.4: Illustration of the experimental set-up. The back-lighted sheets of paper were used to obtain good contrast between the specimen and the surroundings. All measures are in mm.

A prerequisite for using digital image correlation (DIC) to acquire local measurement of the strains on the surface of the test specimen is a high contrast (e.g. black and white) speckle pattern. Preliminary tests with a black and white speckle pattern applied with spray-paint revealed that the spray-paint became brittle and cracked during deformation. The spray-paint speckle pattern was thus replaced by a low temperature white grease (Molykote 33 Medium [52]) with a black powder added for contrast, see Figure 1.5.

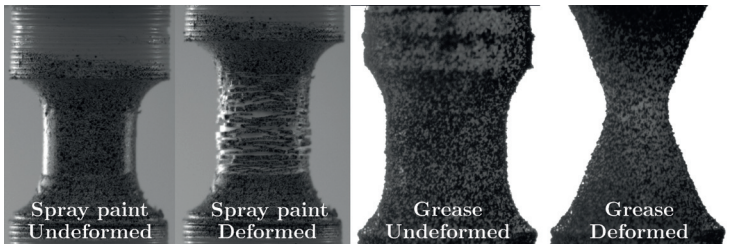

Figure 1.5: Image series illustrating the superior performance of grease compared to the conventional spray-paint speckle at −30 °C.

First we conducted an investigation to determine if 2×2D DIC could be used instead of 3D DIC. A quasi-static uniaxial tension test was conducted at room temperature and the strains obtained from 2D DIC were compared to those from 3D DIC. The difference between 2D and 3D DIC was found to be negligible and thus 2×2D DIC was used, a result that greatly reduces the complexity involved in post-processing of the digital images from experiments. To validate that replacing the black and white spray-paint speckle pattern with grease and that the introduction of the transparent PC temperature chamber did not introduce any errors in the DIC calculations, three benchmark tests on a rubber-modified polypropylene (PP) material were performed at room temperature: (1) a tensile test where we used the regular spray-paint speckle pattern, (2) a test with the spray-paint speckle behind a PC window, and (3) a tensile test where the spray-paint was replaced with the grease/black powder speckle pattern. The stress-strain curves along with the volumetric strain obtained from the three configurations were then compared. The comparison showed that the difference between the three configurations was small – making the experimental set-up a viable alternative to conventional methods.

Quasi-static stress-strain curves together with the volumetric strains were then presented for uniaxial tension tests performed on cross-linked low density polyethylene (XLPE) at four different temperatures: $T = 25$ °C, $T = 0$ °C, $T = -15$ °C and $T = -30$ °C. Both Young's modulus, E, and the flow stress, σ_{20}, were found to increase exponentially with decreasing temperature. In terms of the volumetric strain, the XLPE material was found to be close to incompressible at room temperature, while changing to become compressible at the lower temperatures. The temperature chamber presented in Part 1 was used in a more comprehensive experimental campaign on PP and XLPE in Part 2.

1.3.2 Part 2

Johnsen, J., Grytten, F., Hopperstad, O. S., and Clausen, A. H. (2017). *Influence of strain rate and temperature on the mechanical behaviour of rubber-modified polypropylene and cross-linked polyethylene*. Mechanics of Materials, 114, 40–56.

Experimental results obtained from uniaxial tension and compression tests on rubber-modified polypropylene (PP) and cross-linked low density polyethylene (XLPE) were presented in this study. Utilizing the experimental set-up outlined in Part 1 (Section 1.3.1), uniaxial tension and compression experiments were conducted at four temperatures: $T = 25$ °C, $T = 0$ °C, $T = -15$ °C and $T = -30$ °C and four initial nominal strain rates: $\dot{e} = 0.01$ s^{-1}, $\dot{e} = 0.1$ s^{-1} and $\dot{e} = 1.0$ s^{-1}. Cylindrical test specimens were used in both the tension and compression experiments, see Figure 1.6. Young's modulus of the XLPE material was found to be dependent on strain rate, in addition to the temperature dependence established in Part 1. For the PP material, Young's modulus was not as dependent on strain rate, but showed a strong dependence on temperature. The following phenomenological expression was demonstrated to capture the temperature dependence of Young's modulus:

$$E(\theta) = E_0 \exp\left[-a\left(\theta - \theta_0\right)\right] \tag{1.6}$$

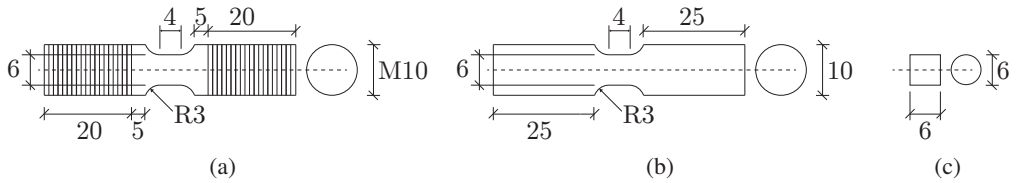

Figure 1.6: Schematics of (a) tensile test specimen for the PP material, (b) tensile test specimen for the XLPE material, and (c) compression test specimen for both materials. All measures are in mm.

where E_0 is Young's modulus at the reference temperature θ_0, θ is the current absolute temperature, and a is a parameter governing the temperature sensitivity. The flow stress, calculated as the Cauchy stress at a longitudinal strain of 15%, was found to be dependent on temperature and strain rate in a similar manner as Young's modulus. The Ree-Eyring [28] flow model including both the main α relaxation and the secondary β relaxation was successfully used to describe how the flow stress was affected by strain rate and temperature, see Figure 1.7.

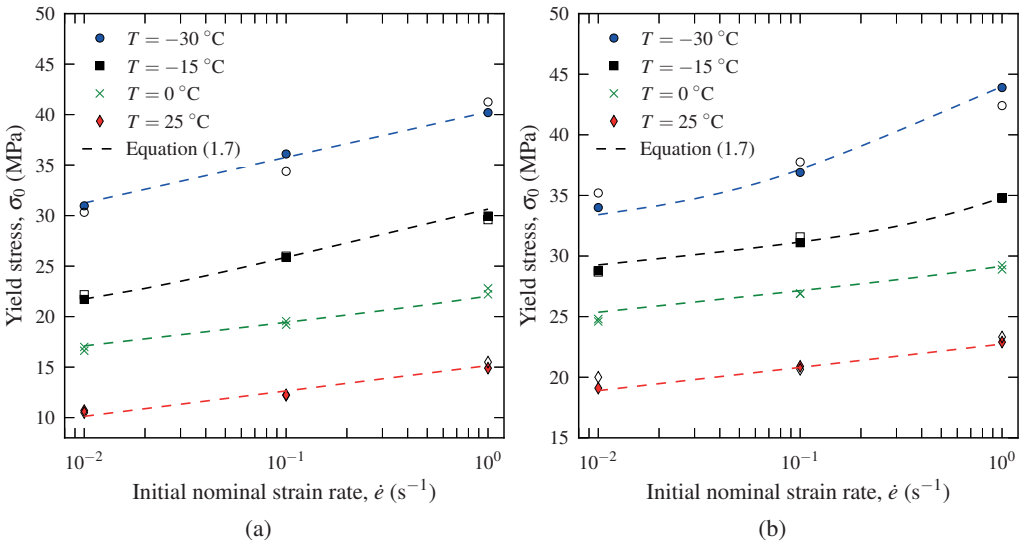

Figure 1.7: Influence of temperature and strain rate on the yield stress of (a) the XLPE material and (b) the PP material.

Assuming that the contribution from each relaxation process is additive [40], the equivalent viscous stress may be expressed as:

$$\bar{\sigma}(\dot{p},\theta) = \sum_{x=\alpha,\beta} \frac{k_B\theta}{V_x} \operatorname{arcsinh}\left(\frac{\dot{p}}{\dot{p}_{0,x}} \exp\left[\frac{\Delta H_x}{R\theta}\right]\right) \tag{1.7}$$

where k_B is Boltzmann's constant, θ is the absolute temperature, V_x are the activation volumes, $\dot{p}$

is the equivalent plastic strain rate, $\dot{p}_{0,x}$ are the reference equivalent plastic strain rates and R is the universal gas constant.

The compression tests revealed that the XLPE material was close to pressure insensitive, where the pressure sensitivity was defined as $\alpha_{\mathrm{p}} = \sigma_{\mathrm{C}}/\sigma_{\mathrm{T}}$ with σ_{C} and σ_{T} being the yield stress in compression and tension, respectively. For the PP material, however, the pressure sensitivity was found to be large – ranging from 1.22 to 1.71. The pressure dependency of the PP material was attributed to the voids formed due to cavitation in the rubbery phase during tension, resulting in large volumetric strains. Scanning electron microscopy (SEM) micrographs were presented to give a qualitative explanation of the difference between the XLPE and PP materials. The micrographs showed that the XLPE material was without voids and contained few particles, while the micrographs from the PP material demonstrated that it contained many voids, which became elongated during deformation and ultimately started to close.

Another observation was that the locking stretch, defined as the point at which there was an abrupt change in strain hardening, increased at elevated strain rates. This was explained by self-heating in the materials at elevated strain rates, which in effect increases the chain mobility. In the isothermal uniaxial tension tests, i.e., the tests performed at the lowest strain rate, the locking stretch was seen to decrease as a function of initial temperature in the PP material, while the effect of initial temperature on the locking stretch in the XLPE material was less important. This is believed to be an effect of the physical cross-links in the XLPE material as opposed to the entanglements in the PP material.

Substantial self-heating was observed in both materials, ranging from 20 to 30 °C in the XLPE material and from 40 to 50 °C in the PP material at the highest strain rate. At the highest strain rate, the temperature was also observed to increase continuously with deformation, indicating close to adiabatic conditions. At the intermediate strain rate, the duration of the test was sufficiently long to allow heat convection and heat conduction, causing the temperature in the materials to decrease at the end of the tensile test. Isothermal conditions were met for all tensile tests conducted at the lowest strain rate.

Part 2 contains an extensive database of experimental results. One dimensional (1D) models were shown to be capable of describing the observed trends regarding the flow stress and Young's modulus. In Part 3 a three dimensional (3D) model will be used to describe the material behaviour of XLPE.

1.3.3 Part 3

Johnsen, J., Clausen, A. H., Grytten, F., Benallal, A. and Hopperstad, O. S. (2017) *Thermo-mechanical modelling of temperature and strain rate effects in semi-crystalline polymers*. To be submitted for possible journal publication.

The third, and last, study in this thesis focuses on modelling the mechanical behaviour of the cross-linked polyethylene (XLPE) material in uniaxial tension at the investigated temperatures

(T = 25 °C, T = 0 °C, T = −15 °C and T = −30 °C) and nominal strain rates ($\dot{e}$ = 0.01 s^{-1}, $\dot{e}$ = 0.1 s^{-1} and $\dot{e}$ = 1.0 s^{-1}). This material was chosen because the volume change was less severe compared to the polypropylene material, as reported in Part 2. A thermomechanical model is proposed to capture the effects of temperature and strain rate on the observed mechanical behaviour. The material model was implemented in the commercial finite element (FE) software Abaqus/Standard as a UMAT subroutine. Following the work of Miehe [53] and Sun [54], a numerical method to obtain the consistent tangent operator was employed. In addition, a sub-stepping procedure limiting the effective strain increment to be less than a user-specified value (e.g. strain-to-yield) was used to ensure convergence. The proposed model consists of two parts: (1) an intermolecular part comprised of an elastic Hencky spring [55] coupled with a plastic part governed by two Ree-Eyring [28] dashpots modeling the main α relaxation and the secondary β relaxation with the plastic flow assumed isochoric, and kinematic hardening described by a deviatoric Hencky spring, and (2) an eight chain spring [32] describing entropic strain hardening caused by alignment of the polymer chains during stretching.

All free energy functions were formulated in a similar manner as proposed by Miehe [49], i.e., we used entropic springs where the free energy function has been split into three parts: (1) an isochoric (deviatoric) part, (2) a purely thermal contribution, and (3) a volumetric part. Additionally, the locking stretch was allowed to evolve with deformation using a modified version of the expression proposed by Cho et al. [56]. The evolution of the locking stretch also affected the shear modulus associated with the eight chain spring by enforcing the product between the chain density per unit volume n and the number of rigid links between entanglements N to remain constant [10, 57]. In extension this means that the product between the shear modulus, or rubbery modulus, $\mu = nk_B\theta$, where k_B is Boltzmann's constant, and the number of rigid links N also has to remain constant [56].

Using the same expression for the temperature dependent shear modulus as in Part 2 (Equation (1.6)), the Cauchy stress vs. longitudinal logarithmic strain was successfully predicted by the numerical model. A qualitative agreement of the volumetric strain at the three lowest temperatures was also obtained, while the volumetric strain was overestimated at room temperature due to the assumption of a constant Poisson's ratio. The self-heating in the XLPE material was also predicted fairly well by the model, even though the temperature evolution was too rapid in the numerical model compared to the experimental findings. Force vs. global displacement was also well captured, with a near perfect match in the beginning before the numerical model started to diverge from the experiments, an observation which is believed to be caused by the asymptotic strain hardening introduced by the eight chain spring. The local strain rate in the FE model was also shown to be comparable to that obtained from experiments.

Other contributions

Contributions not included in this thesis.

The following studies have been conducted in parallel with the work on the thesis, but have not been included for various reasons.

- Holmen, J. K., Johnsen, J., Hopperstad, O. S., and Børvik, T. (2016). *Influence of fragmentation on the capacity of aluminum alloy plates subjected to ballistic impact*. European Journal of Mechanics, A/Solids, 55, 221–233. https://doi.org/10.1016/j.euromechsol.2015.09.009
- Johnsen, J., Holmen, J. K., Warren, T., and Børvik, T. (2017). *Cylindrical cavity expansion approximations using different constitutive models for the target material*. Accepted for publication in International Journal of Protective Structures.
- Johnsen, J., Grytten, F., Hopperstad, O. S., and Clausen, A. H. (2016). *Large strain tensile behaviour of rubber-modified polypropylene at low temperatures*. Presented at the 15th European Mechanics of Materials Conference, EMMC15, Brussel, Belgium.
- Johnsen, J., Grytten, F., Hopperstad, O. S., and Clausen, A. H. (2017). *Numerical simulation of cross-linked polyethylene at different ambient temperatures and strain rates*. Presented at the 9th National Conference on Computational Mechanics, MekIT'17, Trondheim, Norway.

1.4 Concluding remarks

This thesis deals with the effects of low temperature and varying strain rate on the mechanical behaviour of two commercially available polymers: a rubber-modified polypropylene (PP), and a cross-linked low density polyethylene (XLPE). The main scientific contributions are summarized in the following bullet-points:

- A novel experimental set-up was developed to enable material testing at low temperatures. The set-up allowed for digital cameras to monitor the test specimens during the experiments, thus facilitating optical measurement of local strains as opposed to relying on mechanical measurements such as extensometers and/or machine displacement. It was also possible to monitor self-heating of the test specimens using an infrared thermal camera.
- An extensive experimental database was established for the two materials. The experimental campaign consisted of uniaxial tension and compression tests conducted at four temperatures (25 °C, 0 °C, −15 °C and −30 °C) and three initial nominal strain rates (0.01 s^{-1}, 0.1 s^{-1} and 1.0 s^{-1}). 2×2D digital image correlation (DIC) was used to obtain local measurement of the strains in the tension experiments, while point tracking in combination with edge tracing was used to calculate the strains in the compression tests. The tension tests were also monitored by an infrared thermal camera recording the surface temperature of the

test specimens. Scanning electron microscopy (SEM) was used to obtain a qualitative understanding of the observed volumetric strains in both materials.

- A new thermomechanical constitutive model was developed and implemented in the commercial finite element program Abaqus/Standard through a user subroutine (UMAT). The constitutive model is comprised of two parts: Part A governing the thermoelastic and thermoviscoplastic response using modified entropic Hencky springs and two Ree-Eyring dashpots, and Part B describing the abrupt change in strain hardening due to the alignment of the polymer chains using a modified entropic eight chain spring. The new constitutive model was shown to adequately predict the stress-strain response, the volumetric strains, self-heating, force vs. displacement, local strain rate, and the overall deformed shape of the tensile specimen of the XLPE material.

1.5 Suggestions for further work

One obvious suggestion for further work is to do numerical modelling of the PP material. Due to the substantial volumetric strains and the evolution of the void shape, a porous plasticity approach should be adopted. We give the following suggestions:

- Extend the presented constitutive model to include plastic dilatation by e.g. the Gurson model [58], and an evolving void shape similar to the work by for example Kitamura [59].
- To calibrate the porous plasticity parameters in the Gurson model, unit cell simulations (see e.g. Steenbrink and Van der Giessen [60]) can be performed.
- Perform notched tensile tests on both materials to gain insight into the effect of stress triaxiality on e.g. yield, volumetric strain and fracture.
- In connection to the previous bullet-point, it would be interesting to look into modelling of ductile failure.
- Expand the investigated deformation modes to include for instance biaxial tension, bending and component tests. It would also be interesting to increase the range of investigated strain rates and/or temperatures, and especially to investigate strain rate effects under isothermal conditions. This would remove the convoluted interaction between hardening due to strain rate and softening due to temperature.
- It would also be interesting to use the established experimental set-up to investigate the material behaviour at elevated temperatures.
- An effort should be put into further increasing the understanding of strain hardening and heat generation in semi-crystalline polymers.

References

[1] Gautier, D. L., Bird, K. J., Charpentier, R. R., Grantz, A., Houseknecht, D. W., Klett, T. R., Moore, T. E., Pitman, J. K., Schenk, C. J., Schuenemeyer, J. H., Sørensen, K., Tennyson, M. E., Valin, Z. C., and Wandrey, C. J. "Assessment of Undiscovered Oil and Gas in the Arctic". *Science* 324 (2009), pp. 1175–1179. DOI: 10.1126/science.1169467.

[2] Grytten, F., Daiyan, H., Polanco-Loria, M., and Dumoulin, S. "Use of digital image correlation to measure large-strain tensile properties of ductile thermoplastics". *Polymer Testing* 28 (2009), pp. 653–660. DOI: 10.1016/j.polymertesting.2009.05.009.

[3] Delhaye, V., Clausen, A. H., Moussy, F., Othman, R., and Hopperstad, O. S. "Influence of stress state and strain rate on the behaviour of a rubber-particle reinforced polypropylene". *International Journal of Impact Engineering* 38 (2011), pp. 208–218. DOI: 10.1016/j.ijimpeng.2010.11.004.

[4] Jerabek, M., Major, Z., and Lang, R. W. "Strain determination of polymeric materials using digital image correlation". *Polymer Testing* 29 (2010), pp. 407–416. DOI: 10.1016/j.polymertesting.2010.01.005.

[5] Ognedal, A. S., Clausen, A. H., Polanco-Loria, M., Benallal, A., Raka, B., and Hopperstad, O. S. "Experimental and numerical study on the behaviour of PVC and HDPE in biaxial tension". *Mechanics of Materials* 54 (2012), pp. 18–31. DOI: 10.1016/j.mechmat.2012.05.010.

[6] Şerban, D. A., Weber, G., Marşavina, L., Silberschmidt, V. V., and Hufenbach, W. "Tensile properties of semi-crystalline thermoplastic polymers: Effects of temperature and strain rates". *Polymer Testing* 32 (2013), pp. 413–425. DOI: 10.1016/j.polymertesting.2012.12.002.

[7] Heinz, S. R. and Wiggins, J. S. "Uniaxial compression analysis of glassy polymer networks using digital image correlation". *Polymer Testing* 29 (2010), pp. 925–932. DOI: 10.1016/j.polymertesting.2010.08.001.

[8] Ponçot, M., Addiego, F., and Dahoun, A. "True intrinsic mechanical behaviour of semi-crystalline and amorphous polymers: Influences of volume deformation and cavities shape". *International Journal of Plasticity* 40 (2013), pp. 126–139. DOI: 10.1016/j.ijplas.2012.07.007.

[9] Addiego, F., Dahoun, A., G'Sell, C., and Hiver, J. M. "Characterization of volume strain at large deformation under uniaxial tension in high-density polyethylene". *Polymer* 47 (2006), pp. 4387–4399. DOI: 10.1016/j.polymer.2006.03.093.

[10] Arruda, E. M., Boyce, M. C., and Jayachandran, R. "Effects of strain rate, temperature and thermomechanical coupling on the finite strain deformation of glassy polymers". *Mechanics of Materials* 19 (1995), pp. 193–212. DOI: 10.1016/0167-6636(94)00034-E.

[11] Zaroulis, J. and Boyce, M. "Temperature, strain rate, and strain state dependence of the evolution in mechanical behaviour and structure of poly(ethylene terephthalate) with finite strain deformation". *Polymer* 38 (1997), pp. 1303–1315. DOI: 10.1016/S0032-3861(96)00632-5.

[12] van Breemen, L. C. A., Engels, T. A. P., Klompen, E. T. J., Senden, D. J. A., and Govaert, L. E. "Rate- and temperature-dependent strain softening in solid polymers". *Journal of Polymer Science, Part B: Polymer Physics* 50 (2012), pp. 1757–1771. DOI: 10.1002/polb.23199.

[13] Zaïri, F., Naït-Abdelaziz, M., Gloaguen, J. M., and Lefebvre, J. M. "Constitutive modelling of the large inelastic deformation behaviour of rubber-toughened poly(methyl methacrylate): effects of strain rate, temperature and rubber-phase volume fraction". *Modelling and Simulation in Materials Science and Engineering* 18 (2010), p. 055004. DOI: 10.1088/0965-0393/18/5/055004.

[14] Nasraoui, M., Forquin, P., Siad, L., and Rusinek, A. "Influence of strain rate, temperature and adiabatic heating on the mechanical behaviour of poly-methyl-methacrylate: Experimental and modelling analyses". *Materials and Design* 37 (2012), pp. 500–509. DOI: 10.1016/j.matdes.2011.11.032.

[15] Srivastava, V., Chester, S. A., Ames, N. M., and Anand, L. "A thermo-mechanically-coupled large-deformation theory for amorphous polymers in a temperature range which spans their glass transition". *International Journal of Plasticity* 26 (2010), pp. 1138–1182. DOI: 10.1016/j.ijplas.2010.01.004.

[16] Llana, P. and Boyce, M. "Finite strain behavior of poly(ethylene terephthalate) above the glass transition temperature". *Polymer* 40 (Nov. 1999), pp. 6729–6751. DOI: 10.1016/S0032-3861(98)00867-2.

[17] Bauwens-Crowet, C., Bauwens, J. C., and Homès, G. "Tensile yield-stress behavior of glassy polymers". *Journal of Polymer Science Part A-2: Polymer Physics* 7 (1969), pp. 735–742. DOI: 10.1002/pol.1969.160070411.

[18] Bauwens-Crowet, C., Bauwens, J. C., and Homès, G. "The temperature dependence of yield of polycarbonate in uniaxial compression and tensile tests". *Journal of Materials Science* 7 (1972), pp. 176–183. DOI: 10.1007/BF00554178.

[19] Bauwens-Crowet, C. "The compression yield behaviour of polymethyl methacrylate over a wide range of temperatures and strain-rates". *Journal of Materials Science* 8 (1973), pp. 968–979. DOI: 10.1007/BF00756628.

[20] Bauwens, J. C. "Relation between the compression yield stress and the mechanical loss peak of bisphenol-A-polycarbonate in the β transition range". *Journal of Materials Science* 7 (1972), pp. 577–584. DOI: 10.1007/BF00761956.

[21] Jordan, J. L., Casem, D. T., Bradley, J. M., Dwivedi, A. K., Brown, E. N., and Jordan, C. W. "Mechanical Properties of Low Density Polyethylene". *Journal of Dynamic Behavior of Materials* 2 (2016), pp. 411–420. DOI: 10.1007/s40870-016-0076-0.

[22] Jang, B. Z., Uhlmann, D. R., and Sande, J. B. V. "Ductile–brittle transition in polymers". *Journal of Applied Polymer Science* 29 (1984), pp. 3409–3420. DOI: 10.1002/app.1984.070291118.

[23] Cao, K., Wang, Y., and Wang, Y. "Effects of strain rate and temperature on the tension behavior of polycarbonate". *Materials and Design* 38 (2012), pp. 53–58. DOI: 10.1016/j.matdes.2012.02.007.

[24] Richeton, J., Ahzi, S., Vecchio, K., Jiang, F., and Adharapurapu, R. "Influence of temperature and strain rate on the mechanical behavior of three amorphous polymers: Characterization and modeling of the compressive yield stress". *International Journal of Solids and Structures* 43 (2006), pp. 2318–2335. DOI: 10.1016/j.ijsolstr.2005.06.040.

[25] Brown, E. N., Rae, P. J., and Orler, E. B. "The influence of temperature and strain rate on the constitutive and damage responses of polychlorotrifluoroethylene (PCTFE, Kel-F 81)". *Polymer* 47 (2006), pp. 7506–7518. DOI: 10.1016/j.polymer.2006.08.032.

[26] Brown, E. N., Willms, R. B., Gray, G. T., Rae, P. J., Cady, C. M., Vecchio, K. S., Flowers, J., and Martinez, M. Y. "Influence of molecular conformation on the constitutive response of polyethylene: A comparison of HDPE, UHMWPE, and PEX". *Experimental Mechanics* 47 (2007), pp. 381–393. DOI: 10.1007/s11340-007-9045-9.

[27] Eyring, H. "Viscosity, Plasticity, and Diffusion as Examples of Absolute Reaction Rates". *The Journal of Chemical Physics* 4 (1936), pp. 283–291. DOI: 10.1063/1.1749836.

[28] Ree, T. and Eyring, H. "Theory of non-Newtonian flow. I. Solid plastic system". *Journal of Applied Physics* 26 (1955), pp. 793–800. DOI: 10.1063/1.1722098.

[29] Robertson, R. E. "Theory for the Plasticity of Glassy Polymers". *The Journal of Chemical Physics* 44 (1966), p. 3950. DOI: 10.1063/1.1726558.

[30] Argon, A. S. "A theory for the low-temperature plastic deformation of glassy polymers". *Philosophical Magazine* 28 (1973), pp. 839–865. DOI: 10.1080/14786437308220987.

[31] Wang, M. C. and Guth, E. "Statistical Theory of Networks of Non-Gaussian Flexible Chains". *The Journal of Chemical Physics* 20 (1952), pp. 1144–1157. DOI: 10.1063/1.1700682.

[32] Arruda, E. M. and Boyce, M. C. "A three-dimensional constitutive model for the large stretch behavior of rubber elastic materials". *Journal of the Mechanics and Physics of Solids* 41 (1993), pp. 389–412. DOI: 10.1016/0022-5096(93)90013-6.

[33] Haward, R. and Thackray, G. "The use of a mathematical model to describe isothermal stress-strain curves in glassy thermoplastics". *Proceedings of the Royal Society of London* 302 (1968), pp. 453–472. DOI: 10.1098/rspa.1968.0029.

[34] Boyce, M. C., Parks, D. M., and Argon, A. S. "Large inelastic deformation of glassy polymers. Part I: Rate dependent constitutive model". *Mechanics of Materials* 7 (1988), pp. 15–33. DOI: 10.1016/0167-6636(88)90003-8.

[35] Govaert, L. E., Timmermans, P. H. M., and Brekelmans, W. "The Influence of Intrinsic Strain Softening on Strain Localization in Polycarbonate: Modeling and Experimental Validation". *Journal of Engineering Materials and Technology* 122 (2000), p. 177. DOI: 10.1115/1.482784.

[36] Klompen, E. T. J., Engels, T. A. P., Govaert, L. E., and Meijer, H. E. H. "Modeling of the postyield response of glassy polymers: Influence of thermomechanical history". *Macromolecules* 38 (2005), pp. 6997–7008. DOI: 10.1021/ma050498v.

[37] Hoy, R. S. and Robbins, M. O. "Strain Hardening of Polymer Glasses: Effect of Entanglement Density, Temperature, and Rate". *Journal of Polymer Science, Part B: Polymer Physics* 44 (2006), pp. 3487–3500. DOI: 10.1002/polb.21012.

[38] Govaert, L. E., Engels, T. A. P., Wendlandt, M., Tervoort, T. A., and Suter, U. W. "Does the Strain Hardening Modulus of Glassy Polymers Scale with the Flow Stress?" *Journal of Polymer Science Part B: Polymer physics* 46 (2008), pp. 2475–2481. DOI: 10.1002/polb.21579.

[39] Wendlandt, M., Tervoort, T. A., and Suter, U. W. "Non-linear, rate-dependent strain-hardening behavior of polymer glasses". *Polymer* 46 (2005), pp. 11786–11797. DOI: 10.1016/j.polymer.2005.08.079.

[40] Senden, D. J. A., van Dommelen, J. A. W., and Govaert, L. E. "Strain Hardening and Its Relation to Bauschinger Effects in Oriented Polymers". *Journal of Polymer Science Part B: Polymer Physics* 48 (2010), pp. 1483–1494. DOI: 10.1002/polb.22056.

[41] Halary, J. L., Laupretre, F., and Monnerie, L. "Polymer Materials: Macroscopic Properties and Molecular Interpretations". Hoboken, New Jersey: John Wiley & Sons Inc, 2011. Chap. 1, p. 17.

[42] Boyce, M. C., Montagut, E. L., and Argon, A. S. "The effects of thermomechanical coupling on the cold drawing process of glassy polymers". *Polymer Engineering & Science* 32 (1992), pp. 1073–1085. DOI: 10.1002/pen.760321605.

[43] Richeton, J., Ahzi, S., Vecchio, K. S., Jiang, F. C., and Makradi, A. "Modeling and validation of the large deformation inelastic response of amorphous polymers over a wide range of temperatures and strain rates". *International Journal of Solids and Structures* 44 (2007), pp. 7938–7954. DOI: 10.1016/j.ijsolstr.2007.05.018.

[44] Polanco-Loria, M., Clausen, A. H., Berstad, T., and Hopperstad, O. S. "Constitutive model for thermoplastics with structural applications". *International Journal of Impact Engineering* 37 (2010), pp. 1207–1219. DOI: 10.1016/j.ijimpeng.2010.06.006.

[45] Garcia-Gonzalez, D., Zaera, R., and Arias, A. "A hyperelastic-thermoviscoplastic constitutive model for semi-crystalline polymers: Application to PEEK under dynamic loading conditions". *International Journal of Plasticity* 88 (2017), pp. 27–52. DOI: 10.1016/j.ijplas.2016.09.011.

[46] Anand, L., Ames, N. M., Srivastava, V., and Chester, S. A. "A thermo-mechanically coupled theory for large deformations of amorphous polymers. Part I: Formulation". *International Journal of Plasticity* 25 (2009), pp. 1474–1494. DOI: 10.1016/j.ijplas.2008.11.004.

[47] Ames, N. M., Srivastava, V., Chester, S. A., and Anand, L. "A thermo-mechanically coupled theory for large deformations of amorphous polymers. Part II: Applications". *International Journal of Plasticity* 25 (2009), pp. 1495–1539. DOI: 10.1016/j.ijplas.2008.11.005.

[48] Adams, G. W. and Farris, R. J. "Latent Energy of Deformation of Bisphenol A Polycarbonate". *Journal of Polymer Science Part B: Polymer Physics* 26 (1988), pp. 433–445. DOI: 10.1002/polb.1988.090260216.

[49] Miehe, C. "Entropic thermoelasticity at finite strains. Aspects of the formulation and numerical implementation". *Computer Methods in Applied Mechanics and Engineering* 120 (1995), pp. 243–269. DOI: 10.1016/0045-7825(94)00057-T.

[50] *Borlink LS4201S*. http://www.borealisgroup.com/en/polyolefins/products/Borlink/Borlink-LS4201S/. Accessed:2016-1116.

[51] *Borcoat EA165E*. http://www.borealisgroup.com/en/polyolefins/products/Borcoat/Borcoat-EA165E/. Accessed:2016-1116.

[52] *Molykote 33 Extreme Low Temp. Bearing Grease, Medium*. https://www.dowcorning.com/applications/search/products/Details.aspx?prod=01889788&type=PROD. Accessed:2016-04-04.

[53] Miehe, C. "Numerical computation of algorithmic (consistent) tangent moduli in large-strain computational inelasticity". *Computer Methods in Applied Mechanics and Engineering* 134 (1996), pp. 223–240. DOI: 10.1016/0045-7825(96)01019-5.

[54] Sun, W., Chaikof, E. L., and Levenston, M. E. "Numerical approximation of tangent moduli for finite element implementations of nonlinear hyperelastic material models." *Journal of Biomechanical Engineering* 130 (2008), pp. 061003-1–061003-7. DOI: 10.1115/1.2979872.

[55] Anand, L. "On H. Hencky's Approximate Strain-Energy Function for Moderate Deformations". *Journal of Applied Mechanics* 46 (1979), p. 78. DOI: 10.1115/1.3424532.

[56] Cho, H., Rinaldi, R. G., and Boyce, M. C. "Constitutive modeling of the rate-dependent resilient and dissipative large deformation behavior of a segmented copolymer polyurea". *Soft Matter* 9 (2013), pp. 6319–6330. DOI: 10.1039/c3sm27125k.

[57] Boyce, M. C. "Large inelastic deformation of glassy polymers". PhD thesis. The Massachusetts Institute of Technology, 1986.

[58] Gurson, A. L. *Continuum Theory of Ductile Rupture by Void Nucleation and Growth: Part I–Yield Criteria and Flow Rules for Porous Ductile Media*. 1977. DOI: 10.1115/1.3443401.

[59] Kitamura, H., Tsukiyama, K., Kuroda, M., and Ishikawa, M. “Constitutive modeling for rubber-toughened polymers with evolutional anisotropy and volume expansion”. *Modelling and Simulation in Materials Science and Engineering* 16 (2008). DOI: 10.1088/0965-0393/16/2/025003.

[60] Steenbrink, A. and van der Giessen, E. “On cavitation, post-cavitation and yield in amorphous polymer–rubber blends”. *Journal of the Mechanics and Physics of Solids* 47 (1999), pp. 843–876. DOI: 10.1016/S0022-5096(98)00075-1.

Part 1

The content of this part was published in:

Johnsen, J., Grytten, F., Hopperstad, O. S., and Clausen, A. H. (2016). *Experimental set-up for determination of the large-strain tensile behaviour of polymers at low temperatures*. Polymer Testing, 53, 305–313.

https://doi.org/10.1016/j.polymertesting.2016.06.011

Abstract

In this study, we present a method to determine the large-strain tensile behaviour of polymers at low temperatures using a purpose-built temperature chamber made of polycarbonate (PC). This chamber allows for several cameras during testing. In our case, two digital cameras were utilized to monitor the two perpendicular surfaces of the test sample. Subsequently, the pictures were analysed with digital image correlation (DIC) software to determine the strain field on the surface of the specimen. In addition, a thermal camera was used to monitor self-heating during loading. It is demonstrated that the PC chamber does not influence the stress-strain curve as determined by DIC. Applying this set-up, a semi-crystalline cross-linked low-density polyethylene (XLPE) under quasi-static tensile loading has been successfully analysed using DIC at four different temperatures (25 °C, 0 °C, −15 °C, −30 °C). At the lower temperatures, the conventional method of applying a spray-paint speckle failed due to embrittlement and cracking of the spray-paint speckle when the tensile specimen deformed. An alternative method was developed utilizing white grease with a black powder added as contrast. The results show a strong increase in both the Young's modulus and the flow stress for decreasing temperatures within the experimental range. We also observe that although the XLPE material is practically incompressible at room temperature, the volumetric strains reach a value of about 0.1 at the lower temperatures.

Chapter 2

Experimental set-up for determination of the large-strain tensile behaviour of polymers at low temperatures

2.1 Introduction

Polymeric materials are used in a variety of applications in the oil industry, e.g. thermal insulation coatings of pipelines, pressure barriers, and insulation of umbilical cables. Estimates from The United States Geological Survey (USGS) indicate that large amounts of the world's undiscovered oil and gas resources are located north of the Arctic Circle [1]. Consequently, the material behaviour at low temperatures is of increasing interest for the oil industry. The effect of temperature on the material behaviour needs to be understood for different complex load cases, such as reeling/unreeling of pipelines, and impact on various structures and components involving polymeric materials. It is therefore necessary to obtain reliable material data even at lower temperatures, because a reduction in temperature tends to reduce the ductility. Relevant input, such as true stress-strain curves for large deformations, volumetric strain to incorporate damage, temperature to include material softening, and rate effects on flow stress, is needed for the material models implemented in finite element (FE) software to predict the material response as accurately as possible. It is therefore essential to obtain precise data at large deformations from experiments in order to analyse such complex load cases successfully.

Several studies have been conducted addressing the performance of polymeric materials at elevated temperatures [2–8]. Fewer studies have been carried out with emphasis on the material behaviour at low temperatures, in particular with attention to the material response at large strains. Bauwens and Bauwens-Crowet with co-workers [9–12] published a series of papers on the relation between yield stress and temperature. Jang et al. [13] investigated the ductile-brittle transition in polypropylene and reported relevant stress-strain data. Şerban et al. [14], Brown et al. [15] and Cao et al. [16] conducted uniaxial tensile experiments on different polymers using an incremental extensometer. In addition, Richeton et al. [17] determined true stress-strain compression data for three different

materials at −40 °C using a deflectometer. Common for all the mentioned studies investigating the material response at low temperatures is that they have used a non-transparent temperature chamber, relying on mechanical measuring devices to calculate the strains instead of optical alternatives, like for example digital image correlation (DIC).

A typical feature with uniaxial tension and compression tests on polymers is that the stress and strain fields remain homogeneous only for small deformations. Localization occurs at the onset of necking in a tension test, meaning that the stress and strain fields become heterogeneous. After this stage, extensometer data are no longer useful and DIC, or another method for local measurement of the deformation in the neck, is needed to obtain the true stress-strain relationship. Another argument for instrumenting material tests on polymers with cameras for subsequent DIC analysis, is that such materials are susceptible to volume change during plastic deformation. Hence, the transverse strains have to be measured in order to calculate the true stress. It follows that DIC is an essential tool to extract accurate data from mechanical tests of polymers [14, 18–22].

Given that the material is isotropic, one can make due with only one DIC camera, while transversely anisotropic materials call for determination of both transverse strain components, and two cameras are required. Strong curvature of the deformed section would also normally call for two cameras and stereo (3D) DIC [23–25]. This issue is considered in Section 2.3.1.

In the present work, a temperature chamber was made of transparent polycarbonate (PC) to allow two digital cameras and a thermal camera to monitor the tensile specimens during experiments. The two digital cameras were mounted in two perpendicular directions, while a rectangular slit was added in one of the temperature chamber walls to obtain a free line-of-sight between the thermal camera and the test sample. The images obtained from the two digital cameras were analysed using DIC to obtain the strain fields on the two surfaces of the sample. As shown in the tests at low temperatures reported by Ilseng et al. [26], the usual spray-paint speckle, which is required for DIC analysis after the test, became brittle and cracked under deformation at low temperatures, rendering DIC analysis impossible. To remedy this a low temperature white grease (Molykote 33 Medium [27]) was applied evenly onto the specimen surface, and the speckle was added in the form of a black powder with a grain size between 75 µm and 125 µm.

2.2 Material and method

2.2.1 Material

The material, an extruded cross-linked low-density polyethylene (XLPE), was supplied by Nexans Norway as 128 mm long cable segments with an external diameter of 73 mm and a thickness of 21 mm. It was produced by Borealis under the product name Borlink LS4201S [28], a semi-crystalline thermoset polymer intended for use as electrical insulation of high-voltage cables, e.g. electric cables connecting the offshore platform to an onshore power plant.

2.2.2 Tensile specimen

The tensile specimen, see Figure 2.1, was designed by Andersen [29]. For evaluation of the

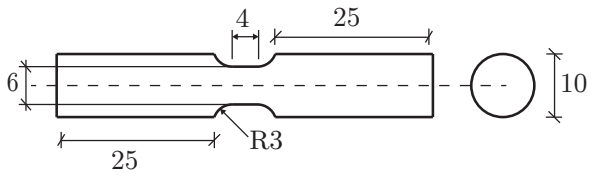

Figure 2.1: Tensile specimen used in the experiments. All measures in mm.

true stress-strain response at large deformations the circular cross-section is favourable to the rectangular specimen proposed in ISO 527-2:2012 [30] since (i) it removes the stress concentrations imposed by the comparatively stiff corners, (ii) the overall shape of the most strained cross-section is better maintained throughout the test, and (iii) it facilitates estimation of a Bridgman-corrected equivalent stress provided that the deformed contour can be tracked from the digital images. Another important aspect of the specimen design is the relatively short gauge length. This increases the resolution of the images used in the DIC analysis by allowing the digital cameras to capture a smaller area, thus facilitating accurate measurements of logarithmic strains approaching a magnitude of 2.0.

The specimens were machined in a turning lathe from sections cut in the longitudinal direction of an extruded cable insulation with dimensions 128 mm $\times$ 73 mm $\times$ 21 mm (length $\times$ diameter $\times$ thickness). To ensure that the DIC cameras monitored the same material orientations in each experiment, the thickness direction of the extruded cable insulation was marked on the tensile specimens. The perpendicular direction thus corresponds to the hoop direction of the cable insulation.

2.2.3 Temperature chamber

Regular temperature chambers are often fitted with only one window, see e.g. [31, 32]. This complicates the use of two digital cameras to monitor the specimen during experiments for later DIC analysis since the cameras must be mounted close together, see e.g. Grytten et al. [18]. Additionally, it is not feasible to obtain a free line-of-sight between the test sample and a thermal camera, making it impossible to measure any self-heating using infrared devices. Our temperature chamber however, shown in Figure 2.2, allows for this. The chamber was built of 10 mm thick plates made of transparent polycarbonate, produced by SABIC Innovative Plastics under the product name Lexan Exell D [33]. The material and solution are similar to the one used by Børvik et al. [34]. The transparency of the chamber in Figure 2.2 allowed several digital cameras to monitor the specimen. A rectangular slit was added in the front window of the temperature chamber to obtain a free line-of-sight between a thermal camera and the tensile specimen. The

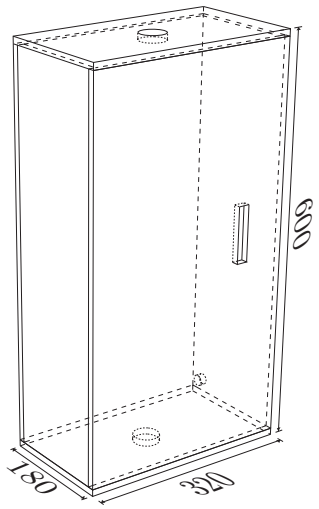

Figure 2.2: Temperature chamber used in the experiments. All measures in mm.

temperature in the chamber was governed by a thermocouple temperature sensor controlling the flow of liquid nitrogen through the small hole in one of the narrow side walls of the chamber. To ensure that the desired temperature was obtained at the most critical cross-section of the tensile specimen, the sensor was mounted close to the gauge section.

Circular holes were added in the top and in the bottom of the chamber to allow mounting of the test specimen in the tensile rig without impairing the seal of the chamber.

2.2.4 Experimental set-up

The test set-up is illustrated in Figures 2.3 and 2.4. In addition to the temperature chamber and an

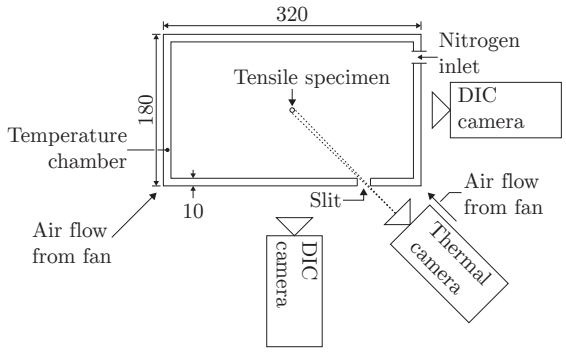

Figure 2.3: Section view of the set-up used in the experiments. All measures in mm. The distance to the three cameras is not drawn in scale.

Instron 5944 testing machine with a 2 kN load cell, it involves two Prosilica GC2450 cameras equipped with Sigma 105 mm and Nikon 105 mm macrolenses. Both cameras were positioned at a distance of approximately 25-35 cm from the tensile specimen, giving a resolution of roughly 60 pixels/mm. The two cameras were used to measure the transverse strain in both the thickness

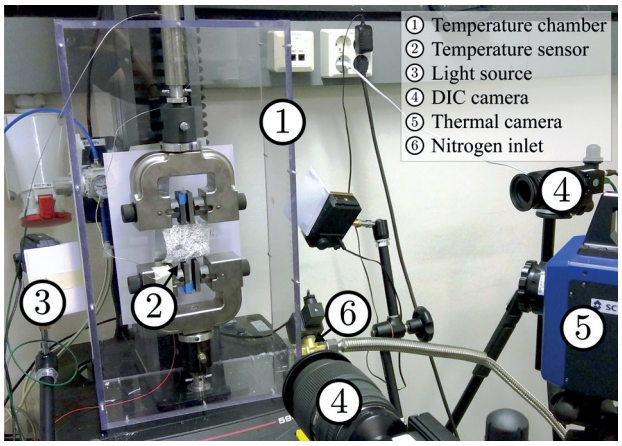

Figure 2.4: Picture showing the experimental set-up. Note that neither the front window nor the tensile specimen is mounted.

direction and the hoop direction of the cable insulation, in addition to the longitudinal strain. Moreover, a FLIR SC 7500 thermal camera was used to measure any possible self-heating in the specimen during the test. It also served to check that the surface temperature of the sample was the same as the gas temperature in the chamber.

Traditionally, a spray paint is used to apply a random black and white speckle which deforms along with the specimen. This deformation is monitored by the DIC cameras and transformed into strain by correlating the current deformed speckle to a reference. However, when the temperature drops, the spray paint becomes brittle and cracks even at relatively small strains, as illustrated in Figure 2.5. To prevent this, the spray paint was replaced by white grease, with black powder added to follow the deformation, see Figure 2.5. The black powder had a grain size from 75 µm to 125 µm. This set-up showed no signs of cracking, even at large strains.

In the preliminary experiments there were also problems with icing due to condensation on the outside of the chamber. The solution was to mount fans in the positions indicated in Figure 2.3. The continuous flow of air over the transparent walls of the chamber successfully prevented condensation and icing.

The tensile tests were carried out at four different temperatures; 25 °C, 0 °C, −15 °C and −30 °C; with two repetitions per test configuration. All experiments were conducted at an initial nominal strain rate of 10^{-2} s^{-1}, translating to a cross-head velocity of 2.4 mm/min.

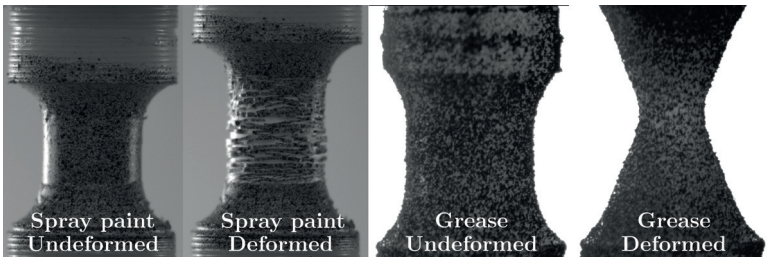

Figure 2.5: Image series illustrating the superior performance of grease compared to the conventional spray-paint speckle at −30 °C.

2.2.5 Thermal conditioning

A thermal analysis was performed in Abaqus [35] to estimate the required cooling time for the specimens before they reached the lowest temperature of −30 °C. The laser flash method [36] was used to determine the thermal conductivity k and the specific heat capacity C_p needed as input to the analysis. Five cylindrical samples with a diameter of 12.7 mm and a thickness of 0.5 mm were tested at three temperatures: 25 °C, 35 °C and 50 °C. Due to limitations in the testing apparatus, it was not possible to perform tests below room temperature. As seen in Figure 2.6, the thermal

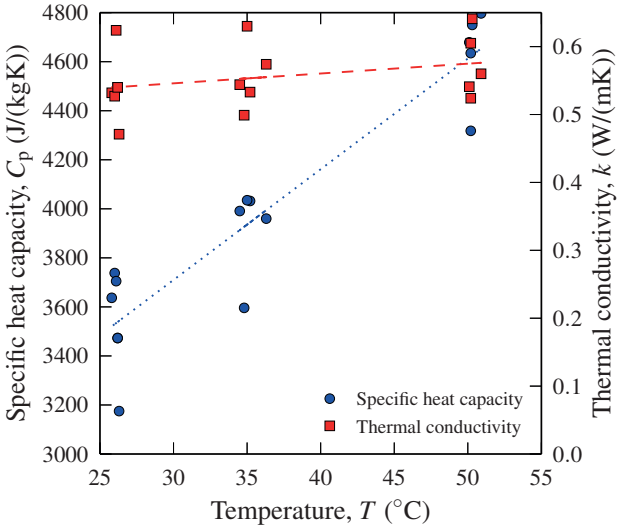

Figure 2.6: Specific heat capacity C_p and thermal conductivity k plotted against temperature.

conductivity is more or less constant, although with some scatter, while the specific heat capacity varies linearly with temperature. The mean value of the test results at room temperature was used as input to the thermal analysis. It is noted that it is conservative with respect to cooling time to apply a high value of C_p in the numerical simulation.

The coefficient of heat convection to air h_c was estimated by first heating a small cylindrical sample

with dimensions 20 mm × 5 mm (diameter × height) in boiling water, followed by monitoring the temperature decrease in the specimen using an infrared thermometer. From the recorded temperature history the heat convection to air was found to be about 21 W/(m^{2}K).

A 3D model of the tensile specimen was made in Abaqus, consisting of 51728 DC3D8 elements. Input parameters used in the Abaqus analysis are given in Table 2.1. The interior of the specimen

Table 2.1: Input parameters used in thermal analysis.

Specific heat capacity, C_p (J/(kg·K))	Thermal conductivity, k (W/(m·K))	Heat convection to air, h_c (W/(m^2·K))	Density, ρ (kg/m^3)
3546	0.56	21.0	922

was given an initial temperature of 25 °C, while at the exterior a thermal boundary condition of −30 °C was applied as a surface film. Analysis results showed that a preconditioning time of 30 min was sufficient to cool the specimen. Thus, each sample was put in the chamber 30 min before it was tested.

2.2.6 Determination of true stress and logarithmic strain

True stress, σ, is defined as

$$\sigma = \frac{F}{A} \tag{2.1}$$

where F is the applied force and A is the current cross-section area. The current cross-section area is calculated from the assumption that the transverse stretches in the thickness direction and in the hoop direction of the cable insulation represent the stretches along the minor and major axis of an elliptical cross-section, i.e.:

$$A = \pi \lambda_T \lambda_\perp r_0^2 \tag{2.2}$$

where $\lambda_T = r_T/r_0$ is the stretch in the thickness direction, $\lambda_\perp = r_\perp/r_0$ is the stretch in the hoop direction and r_0 is the initial radius of the undeformed specimen in the gauge area. The transverse stretches in both the thickness direction and the hoop direction are calculated as the average value over the cross-section in the neck.

The images from the tensile tests were post-processed using an in-house DIC software [29] written in MATLAB [37]. From this software we obtain the deformation gradient $\mathbf{F}$, which enables the calculation of the stretch tensor $\mathbf{U}$ from the polar decomposition $\mathbf{F} = \mathbf{RU}$. Now we can calculate the logarithmic strain tensor by taking the logarithm of the stretch tensor, viz.

$$\boldsymbol{\varepsilon} = \ln(\mathbf{U}) = \mathbf{N} \ln\left(\hat{\mathbf{U}}\right) \mathbf{N}^T \tag{2.3}$$

where $\mathbf{N}$ contains the eigenvectors of $\mathbf{U}$ and $\hat{\mathbf{U}}$ is the eigentensor. Note that for uniaxial tension $\mathbf{U} = \hat{\mathbf{U}}$ such that

$$\boldsymbol{\varepsilon} = \begin{bmatrix} \varepsilon_{\mathrm{L}} & 0 & 0 \\ 0 & \varepsilon_{\mathrm{T}} & 0 \\ 0 & 0 & \varepsilon_{\perp} \end{bmatrix} = \begin{bmatrix} \ln(\lambda_{\mathrm{L}}) & 0 & 0 \\ 0 & \ln(\lambda_{\mathrm{T}}) & 0 \\ 0 & 0 & \ln(\lambda_{\perp}) \end{bmatrix} \tag{2.4}$$

where $\lambda_{\mathrm{L}} = L/L_0$ is the longitudinal stretch.

The logarithmic volumetric strain is defined as the trace of the logarithmic strain tensor. However, as the logarithmic strain tensor estimated here represents an average over the gauge volume, it has been found necessary to correct the volumetric strain for the non-uniformity of the strain field. An appropriate correction was proposed by Andersen [29], which takes the heterogeneity of the longitudinal strain in the neck into account. The corrected volumetric strain reads

$$\begin{aligned} \varepsilon_{\mathrm{V,corr}} = \ln\left(\frac{V}{V_0}\right) &= \ln\left[\lambda_{\mathrm{L}}\lambda_{\mathrm{T}}\lambda_{\perp} \cdot \left(1 + \frac{\kappa R}{4}\right)\right] \\ &= \mathrm{tr}(\boldsymbol{\varepsilon}) + \ln\left(1 + \frac{\kappa R}{4}\right) \end{aligned} \tag{2.5}$$

where κ is the external curvature of the neck, and R is the current radius in the neck. The current values of κ and R are found from the digital images taken during the tests. This correction removes the unphysical negative volumetric strain in the beginning of the tension test, as shown in Section 2.3.3.

2.3 Results and discussion

2.3.1 Evaluation of experimental set-up

When the tensile specimen deforms, and eventually necks, the surface of the sample translates and rotates in the out-of-plane direction. A quasi-static tensile test was conducted at room temperature to compare the calculated strains from 2D DIC and 3D DIC. An in-house DIC software [29] applying a higher-order element for description of the deformation field, was employed in the 2D case. The analysis with 3D DIC was carried out using the in-house DIC software eCorr [38].

Based on the DIC analysis we obtain the displacement field $\mathbf{u}$, enabling the calculation of the deformation gradient $\mathbf{F}$. From the deformation gradient the strains are calculated following the procedure outlined in Section 2.2.6. The interested reader is referred to Fagerholt et al. [39, 40] for a thorough explanation of how the displacement field $\mathbf{u}$ is found from the digital images.

The representative strain was calculated from the average value of the longitudinal stretch for the elements highlighted in Figure 2.7.

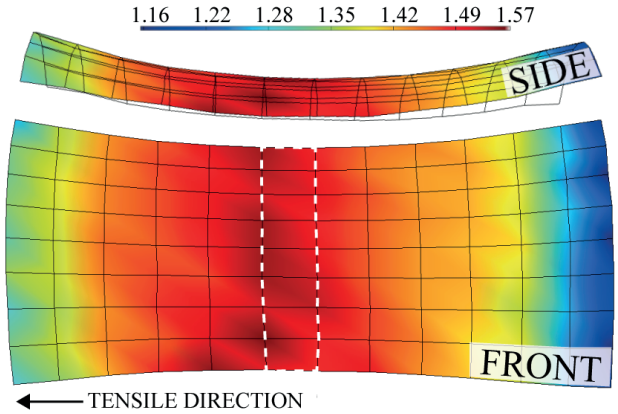

Figure 2.7: Front and side view of the 3D DIC mesh at a maximal stretch in the neck of about 1.55. The elements used in the strain calculations are highlighted by the white box.

Figure 2.8 shows that the difference between 2D (both cameras) and 3D DIC remains below 1.0% during the experiment, meaning that the error introduced in 2D DIC by the out-of-plane translation of the specimen during deformation is acceptable. Therefore 2D DIC was chosen for

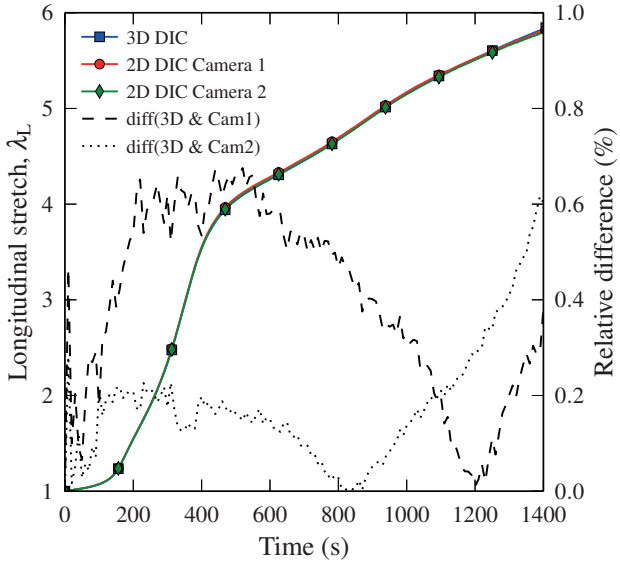

Figure 2.8: Comparison of longitudinal stretch for XLPE calculated by 3D and 2D DIC. The dashed lines give the relative percentage difference between 3D DIC and 2D DIC for camera 1 and camera 2.

the subsequent data processing.

To verify that there was no influence on the DIC results neither by the replacement of spray-paint with grease nor by introducing the polycarbonate window between the cameras and the sample, three tests were conducted at room temperature on a rubber modified polypropylene (PP) material:

First a test with a traditional spray-paint speckle, then a test with the spray-paint speckle behind a polycarbonate window, and finally a test where the spray-paint speckle was replaced with white grease and black powder. Using the transverse strains and the relation $\lambda_i = \exp(\varepsilon_i)$, the true stress was calculated following the procedure given in Section 2.2.6. The DIC analyses of the three tests revealed only negligible differences, illustrated by the three stress-strain curves in Figure 2.9a and the three curves representing the trace of the logarithmic strain tensor versus the logarithmic longitudinal strain in Figure 2.9b.

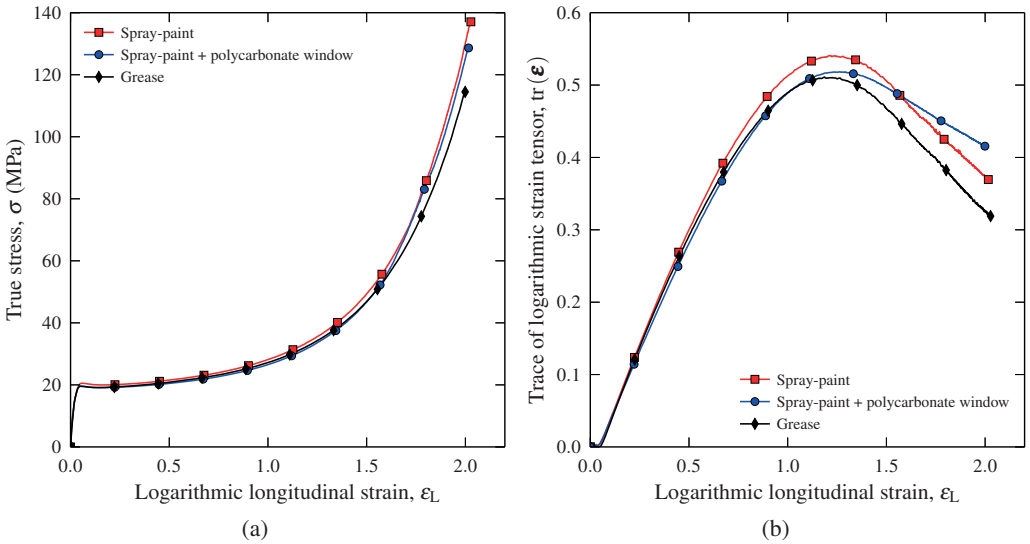

Figure 2.9: (a) True stress vs. logarithmic strain for the three benchmark tests performed on a polypropylene copolymer material. (b) Trace of the logarithmic strain tensor vs. logarithmic longitudinal strain for the three benchmark tests performed on a polypropylene copolymer material.

2.3.2 Stress-strain behaviour at different temperatures

The transverse strains, ε_t, as a function of longitudinal strain at room temperature are shown in Figure 2.10 for the XLPE material, where ε_t is either equal to ε_T or $\varepsilon_\perp$. Both transverse strains have a close to linear relation with the longitudinal strain, but with different slopes. This quasi-linear relation is also reflected in the moderate variation of the transverse strain ratios $r = \varepsilon_\perp/\varepsilon_T$ shown in the same figure, which lies between approximately 1.1 and 1.0 for the four investigated temperatures. These results demonstrate the transverse anisotropy of XLPE and the necessity of using two cameras to capture this effect. The stress-strain curves for XLPE at the four investigated temperatures are presented in Figure 2.11, where the true stress is calculated with Equations (2.1) and (2.2). It appears that Young's modulus and the flow stress increase with decreasing temperature. Another observation from Figure 2.11 is that the ductility of the material

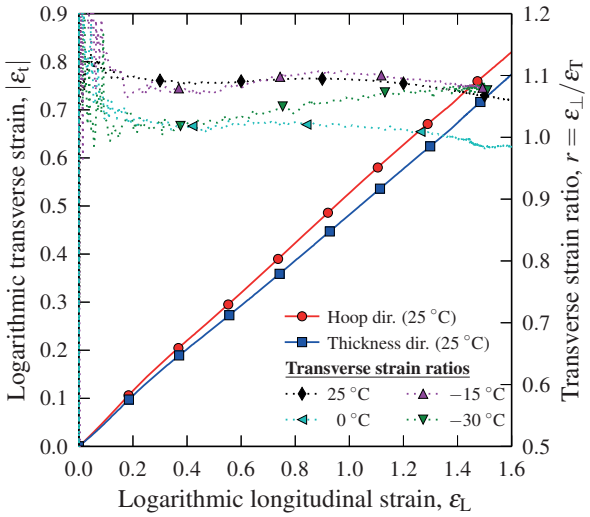

Figure 2.10: Logarithmic transverse strain for XLPE in the hoop (⊥) and in the thickness direction (T) at room temperature, and the transverse strain ratios for all investigated temperatures plotted against logarithmic longitudinal strain.

is more or less independent of temperature in the experimental range, making it well suited for low temperature applications. The uniaxial tension tests performed at −15 °C and −30 °C have a fracture strain of about 1.4, while the fracture strain in the tests carried out at 0 °C and 25 °C is roughly 1.6, i.e., 14% increase compared to the two lower temperatures. It is however noted that the network hardening occurring at strains larger than approximately 1.3 is less prominent at the two lowest temperatures, and that the initial strain hardening clearly has increased compared to the two highest temperatures.

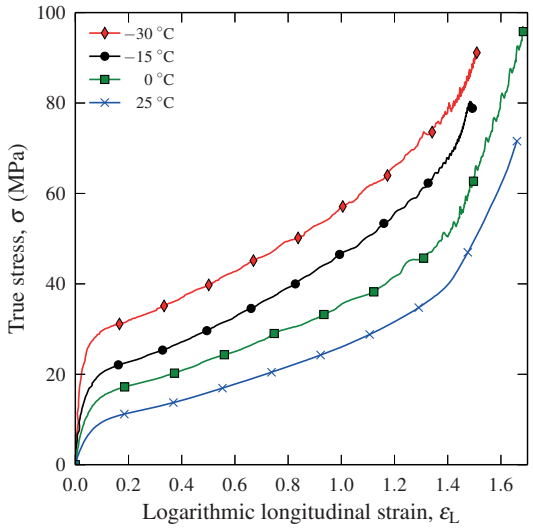

Figure 2.11: True stress vs. logarithmic longitudinal strain for XLPE at different temperatures.

Both the flow stress, σ_{20}, defined as the stress magnitude at a longitudinal strain of 0.2 (= 20%), and the initial stiffness, E, can be represented through the exponential relations

$$E(\theta) = E_0 \exp(a/\theta) \tag{2.6}$$

$$\sigma_{20}(\theta) = C \exp(b/\theta) \tag{2.7}$$

where a, b, E_0 and C are material parameters and θ is the absolute temperature. Figure 2.12 shows the calculated Young's modulus and flow stress versus temperature as well as the least square fits of Equations (2.6) and (2.7). Note that these expressions are valid only for the investigated temperature range.

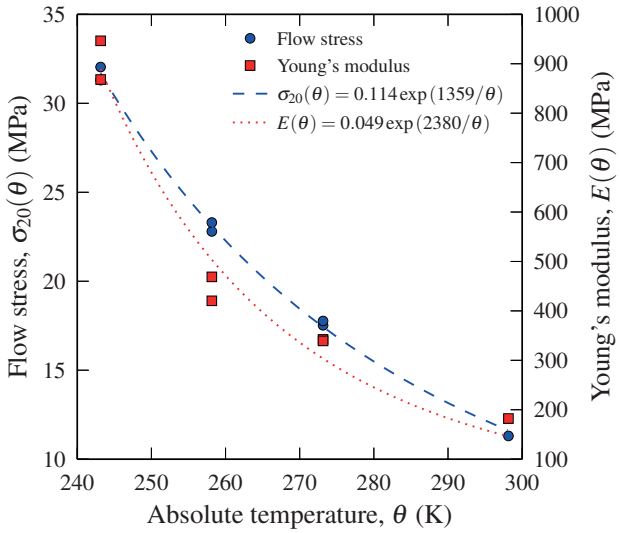

Figure 2.12: Evolution of flow stress and Young's modulus as a function of temperature for XLPE.

2.3.3 Volumetric strains at different temperatures

The logarithmic volumetric strain for XLPE calculated as the trace of the logarithmic strain tensor is given in Figure 2.13a, while the corrected volumetric strain calculated according to Equation (2.5) is given in Figure 2.13b. Since the grease was applied by hand, it was impossible to distribute it evenly over the gauge section. This made it difficult to approximate the curvature, κ, by tracing the edges of the specimen, which is needed in Equation (2.5). As an alternative method, we chose to fit a second-order polynomial to the element boundaries of the DIC mesh, and to calculate the curvature by taking the second-order derivative of this polynomial. Since the curvature is zero in the cold drawing phase at the end of the test (Figure 2.14), this approximation will not affect the final volumetric strain, but it removes the unphysical negative volumetric strain seen in Figure 2.13a. This approximation of the curvature might be the explanation for the minor difference between the volumetric strain at small ε_L for the test performed at −15 °C and the tests

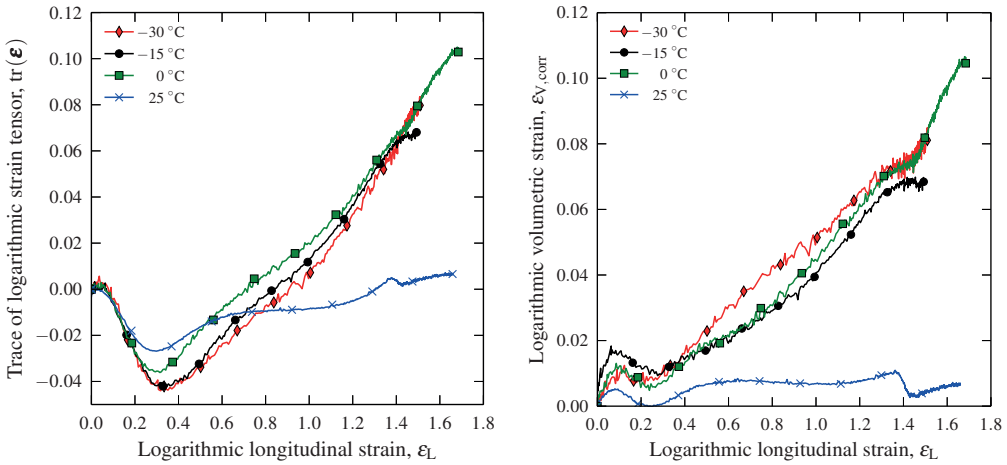

Figure 2.13: (a) Trace of the logarithmic strain tensor vs. logarithmic longitudinal strain for XLPE. (b) Corrected logarithmic volumetric strain using Equation (2.5) vs. logarithmic longitudinal strain for XLPE.

at 0 °C and −30 °C in Figure 2.13b. Nevertheless, in both figures we see that the volumetric strain increases for the lower temperatures compared to the response at room temperature where the volumetric strain is close to 0 at all deformation levels. Since there was no stress whitening during deformation, and that this material is tailored to include as few free particles as possible, it is not obvious that the increase in volumetric strain is caused by material damage. However, how much of this volumetric strain that is recoverable has not been investigated. Therefore, it would be

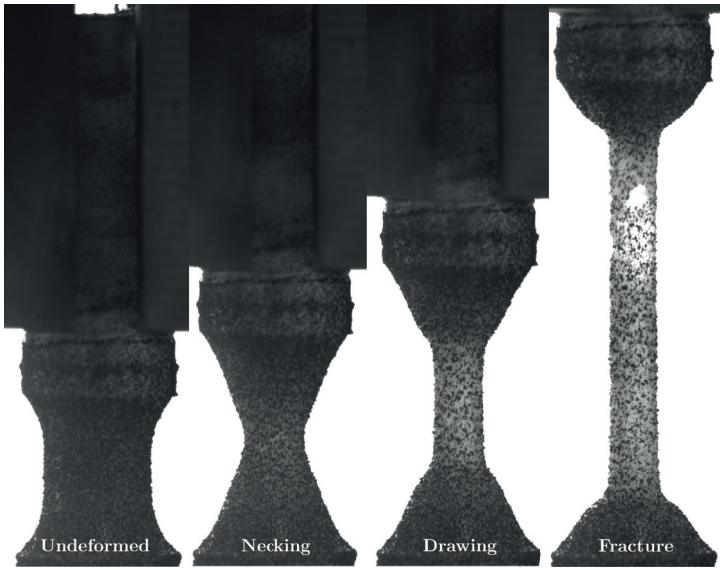

Figure 2.14: Time lapse showing the deformation history of the tensile specimen.

interesting to perform loading/unloading tests at lower temperatures in further work.

2.3.4 Self-heating at different temperatures

The temperature data recorded by the thermal camera showed no significant self-heating of the specimen at the applied nominal strain rate of 10^{-2} s^{-1}, indicating isothermal loading conditions. However, if the experiments had been conducted at higher strain rates, there would most likely have been a substantial temperature increase in the specimen. This experimental set-up could provide important input to any numerical model incorporating thermal softening.

2.4 Concluding remarks

A non-contact optical method for determining the large-strain tensile behaviour of polymers at low temperatures has been presented. The method successfully enables multiple DIC camera instrumentation during experiments, as well as the possibility to monitor self-heating in the specimen using a thermal camera. Since any temperature increase in the material due to self-heating introduces material softening, the ability to measure this using for instance a thermal camera is highly relevant for the development of material models to be used in numerical simulations.

The experimental set-up enables calculation of the true stress vs. logarithmic strain curve and the volumetric strain at low temperatures. Although the XLPE material exhibits rather small volumetric strain, this is not necessarily the case for all polymeric materials. In addition to this, the ability to monitor self-heating underlines the relevance of the presented experimental set-up, especially when considering how important volumetric strain and self-heating is in material models that include damage and thermal softening.

The investigated material (XLPE) exhibits an exponential increase in both the initial stiffness and the flow stress when the temperature is reduced within the experimental range. In addition, the reduction of temperature changes the material from nearly incompressible at room temperature to compressible at lower temperatures.

Acknowledgements

The authors wish to thank the Research Council of Norway for funding through the Petromaks 2 Programme, Contract No.228513/E30. The financial support from ENI, Statoil, Lundin, Total, Scana Steel Stavanger, JFE Steel Corporation, Posco, Kobe Steel, SSAB, Bredero Shaw, Borealis, Trelleborg, Nexans, Aker Solutions, FMC Kongsberg Subsea, Marine Aluminium, Hydro and Sapa are also acknowledged. Special thanks is given to Nexans Norway and Borealis for providing the material. Mr. Trond Auestad and Mr. Tore Wisth are acknowledged for their invaluable help in developing the experimental set-up and performing the experiments.

References

[1] Gautier, D. L., Bird, K. J., Charpentier, R. R., Grantz, A., Houseknecht, D. W., Klett, T. R., Moore, T. E., Pitman, J. K., Schenk, C. J., Schuenemeyer, J. H., Sørensen, K., Tennyson, M. E., Valin, Z. C., and Wandrey, C. J. "Assessment of Undiscovered Oil and Gas in the Arctic". *Science* 324 (2009), pp. 1175–1179. DOI: 10.1126/science.1169467.

[2] Arruda, E. M., Boyce, M. C., and Jayachandran, R. "Effects of strain rate, temperature and thermomechanical coupling on the finite strain deformation of glassy polymers". *Mechanics of Materials* 19 (1995), pp. 193–212. DOI: 10.1016/0167-6636(94)00034-E.

[3] Zaroulis, J. and Boyce, M. "Temperature, strain rate, and strain state dependence of the evolution in mechanical behaviour and structure of poly(ethylene terephthalate) with finite strain deformation". *Polymer* 38 (1997), pp. 1303–1315. DOI: 10.1016/S0032-3861(96)00632-5.

[4] van Breemen, L. C. A., Engels, T. A. P., Klompen, E. T. J., Senden, D. J. A., and Govaert, L. E. "Rate- and temperature-dependent strain softening in solid polymers". *Journal of Polymer Science, Part B: Polymer Physics* 50 (2012), pp. 1757–1771. DOI: 10.1002/polb.23199.

[5] Zaïri, F., Naït-Abdelaziz, M., Gloaguen, J. M., and Lefebvre, J. M. "Constitutive modelling of the large inelastic deformation behaviour of rubber-toughened poly(methyl methacrylate): effects of strain rate, temperature and rubber-phase volume fraction". *Modelling and Simulation in Materials Science and Engineering* 18 (2010), p. 055004. DOI: 10.1088/0965-0393/18/5/055004.

[6] Nasraoui, M., Forquin, P., Siad, L., and Rusinek, A. "Influence of strain rate, temperature and adiabatic heating on the mechanical behaviour of poly-methyl-methacrylate: Experimental and modelling analyses". *Materials and Design* 37 (2012), pp. 500–509. DOI: 10.1016/j.matdes.2011.11.032.

[7] Srivastava, V., Chester, S. A., Ames, N. M., and Anand, L. "A thermo-mechanically-coupled large-deformation theory for amorphous polymers in a temperature range which spans their glass transition". *International Journal of Plasticity* 26 (2010), pp. 1138–1182. DOI: 10.1016/j.ijplas.2010.01.004.

[8] Llana, P. and Boyce, M. "Finite strain behavior of poly(ethylene terephthalate) above the glass transition temperature". *Polymer* 40 (Nov. 1999), pp. 6729–6751. DOI: 10.1016/S0032-3861(98)00867-2.

[9] Bauwens-Crowet, C., Bauwens, J. C., and Homès, G. "Tensile yield-stress behavior of glassy polymers". *Journal of Polymer Science Part A-2: Polymer Physics* 7 (1969), pp. 735–742. DOI: 10.1002/pol.1969.160070411.

[10] Bauwens-Crowet, C., Bauwens, J. C., and Homès, G. "The temperature dependence of yield of polycarbonate in uniaxial compression and tensile tests". *Journal of Materials Science* 7 (1972), pp. 176–183. DOI: 10.1007/BF00554178.

[11] Bauwens, J. C. "Relation between the compression yield stress and the mechanical loss peak of bisphenol-A-polycarbonate in the β transition range". *Journal of Materials Science* 7 (1972), pp. 577–584. DOI: 10.1007/BF00761956.

[12] Bauwens-Crowet, C. "The compression yield behaviour of polymethyl methacrylate over a wide range of temperatures and strain-rates". *Journal of Materials Science* 8 (1973), pp. 968–979. DOI: 10.1007/BF00756628.

[13] Jang, B. Z., Uhlmann, D. R., and Sande, J. B. V. "Ductile–brittle transition in polymers". *Journal of Applied Polymer Science* 29 (1984), pp. 3409–3420. DOI: 10.1002/app.1984.070291118.

[14] Şerban, D. A., Weber, G., Marşavina, L., Silberschmidt, V. V., and Hufenbach, W. "Tensile properties of semi-crystalline thermoplastic polymers: Effects of temperature and strain rates". *Polymer Testing* 32 (2013), pp. 413–425. DOI: 10.1016/j.polymertesting.2012.12.002.

[15] Brown, E. N., Rae, P. J., and Orler, E. B. "The influence of temperature and strain rate on the constitutive and damage responses of polychlorotrifluoroethylene (PCTFE, Kel-F 81)". *Polymer* 47 (2006), pp. 7506–7518. DOI: 10.1016/j.polymer.2006.08.032.

[16] Cao, K., Wang, Y., and Wang, Y. "Effects of strain rate and temperature on the tension behavior of polycarbonate". *Materials and Design* 38 (2012), pp. 53–58. DOI: 10.1016/j.matdes.2012.02.007.

[17] Richeton, J., Ahzi, S., Vecchio, K., Jiang, F., and Adharapurapu, R. "Influence of temperature and strain rate on the mechanical behavior of three amorphous polymers: Characterization and modeling of the compressive yield stress". *International Journal of Solids and Structures* 43 (2006), pp. 2318–2335. DOI: 10.1016/j.ijsolstr.2005.06.040.

[18] Grytten, F., Daiyan, H., Polanco-Loria, M., and Dumoulin, S. "Use of digital image correlation to measure large-strain tensile properties of ductile thermoplastics". *Polymer Testing* 28 (2009), pp. 653–660. DOI: 10.1016/j.polymertesting.2009.05.009.

[19] Delhaye, V., Clausen, A. H., Moussy, F., Othman, R., and Hopperstad, O. S. "Influence of stress state and strain rate on the behaviour of a rubber-particle reinforced polypropylene". *International Journal of Impact Engineering* 38 (2011), pp. 208–218. DOI: 10.1016/j.ijimpeng.2010.11.004.

[20] Ognedal, A. S., Clausen, A. H., Polanco-Loria, M., Benallal, A., Raka, B., and Hopperstad, O. S. "Experimental and numerical study on the behaviour of PVC and HDPE in biaxial tension". *Mechanics of Materials* 54 (2012), pp. 18–31. DOI: 10.1016/j.mechmat.2012.05.010.

[21] Jerabek, M., Major, Z., and Lang, R. W. "Strain determination of polymeric materials using digital image correlation". *Polymer Testing* 29 (2010), pp. 407–416. DOI: 10.1016/j.polymertesting.2010.01.005.

[22] Heinz, S. R. and Wiggins, J. S. "Uniaxial compression analysis of glassy polymer networks using digital image correlation". *Polymer Testing* 29 (2010), pp. 925–932. DOI: 10.1016/j.polymertesting.2010.08.001.

[23] Besnard, G., Hild, F., Lagrange, J.-M., Martinuzzi, P., and Roux, S. "Analysis of necking in high speed experiments by stereocorrelation". *International Journal of Impact Engineering* 49 (2012), pp. 179–191. DOI: 10.1016/j.ijimpeng.2012.03.005.

[24] Gilat, A., Schmidt, T. E., and Walker, A. L. "Full Field Strain Measurement in Compression and Tensile Split Hopkinson Bar Experiments". *Experimental Mechanics* 49 (2 2009), pp. 291–302. DOI: 10.1007/s11340-008-9157-x.

[25] Sutton, M. A., Yan, J. H., Tiwari, V., Schreier, H. W., and Orteu, J. J. "The effect of out-of-plane motion on 2D and 3D digital image correlation measurements". *Optics and Lasers in Engineering* 46 (2008), pp. 746–757. DOI: 10.1016/j.optlaseng.2008.05.005.

[26] Ilseng, A., Skallerud, B. H., and Clausen, A. H. "Tension behaviour of HNBR and FKM elastomers for a wide range of temperatures". *Polymer Testing* 49 (2016), pp. 128–136. DOI: 10.1016/j.polymertesting.2015.11.017.

[27] *Molykote 33 Extreme Low Temp. Bearing Grease, Medium*. https://www.dowcorning.com/applications/search/products/Details.aspx?prod=01889788&type=PROD. Accessed:2016-04-04.

[28] *Borlink LS4201S*. http://www.borealisgroup.com/en/polyolefins/products/Borlink/Borlink-LS4201S/. Accessed:2016-1116.

[29] Andersen, M. "An experimental and numerical study of thermoplastics at large deformations". PhD thesis. Norwegian University of Science and Technology, NTNU, 2016.

[30] ISO527-2:2012. *Plastics - Determination of tensile properties - Part 2: Test conditions for moulding and extrusion plastics*. Feb. 2012.

[31] *Zwick, Temperature chambers*. https://www.zwick.com/en/systems-for-climate-and-temperature-testing/temperature-chamber-80-to-250-c. Accessed:2017-01-17.

[32] Zhang, H., Yao, Y., Zhu, D., Mobasher, B., and Huang, L. "Tensile mechanical properties of basalt fiber reinforced polymer composite under varying strain rates and temperatures". *Polymer Testing* 51 (2016), pp. 29–39. DOI: 10.1016/j.polymertesting.2016.02.006.

[33] *Lexan Exell D*. http://sfs.sabic.eu/product/lexan-solid-sheet/uv-protected/. Accessed:2016-03-21.

[34] Børvik, T., Lange, H., Marken, L. A., Langseth, M., Hopperstad, O. S., Aursand, M., and Rørvik, G. "Pipe fittings in duplex stainless steel with deviation in quality caused by sigma phase precipitation". *Materials Science and Engineering A* 527 (2010), pp. 6945–6955. DOI: 10.1016/j.msea.2010.06.087.

[35] Abaqus. *6.13-1*. Dassault Systemes, 2013.

[36] ISO22007-4:2008. *Plastics - Determination of thermal conductivity and thermal diffusivity - Part 4: Laser flash method*. Dec. 2008.

[37] MATLAB. *Version 8.3.0.532 (R2014a)*. Natick, Massachusetts, 2014.

[38] Aune, V., Fagerholt, E., Hauge, K. O., Langseth, M., and Børvik, T. "Experimental study on the response of thin aluminium and steel plates subjected to airblast loading". *International Journal of Impact Engineering* 90 (2016), pp. 106–121. DOI: 10.1016/j.ijimpeng.2015.11.017.

[39] Fagerholt, E., Børvik, T., and Hopperstad, O. S. "Measuring discontinuous displacement fields in cracked specimens using digital image correlation with mesh adaptation and crack-path optimization". *Optics and Lasers in Engineering* 51 (2013), pp. 299–310. DOI: 10.1016/j.optlaseng.2012.09.010.

[40] Fagerholt, E., Dørum, C., Børvik, T., Laukli, H. I., and Hopperstad, O. S. "Experimental and numerical investigation of fracture in a cast aluminium alloy". *International Journal of Solids and Structures* 47 (2010), pp. 3352–3365. DOI: 10.1016/j.ijsolstr.2010.08.013.

Part 2

The content of this part was published in:

Johnsen, J., Grytten, F., Hopperstad, O. S., and Clausen, A. H. (2017). *Influence of strain rate and temperature on the mechanical behaviour of rubber-modified polypropylene and cross-linked polyethylene*. Mechanics of Materials, 114, 40–56.

https://doi.org/10.1016/j.mechmat.2017.07.003

Abstract

In the present work, we investigate the effects of strain rate ($\dot{e}$ = 0.01 s^{-1}, 0.1 s^{-1}, and 1.0 s^{-1}) and low temperature (T = −30 °C, −15 °C, 0 °C, and 25 °C) on the mechanical behaviour in tension and compression of two materials: a rubber-modified polypropylene copolymer (PP) and a cross-linked low-density polyethylene (XLPE). Local stress-strain data for large deformations are obtained using digital image correlation (DIC) in the uniaxial tension tests and point tracking in the compression tests. Since both materials exhibit slight transverse anisotropy, two digital cameras are used to capture the strains on two perpendicular surfaces. Self-heating resulting from the elevated strain rates is monitored using an infrared (IR) camera. To enable the application of multiple digital cameras and an IR camera, a purpose-built transparent polycarbonate temperature chamber is used to create a cold environment for the tests. The mechanical behaviour of both materials, including the true stress-strain response and the volume change, is shown to be dependent on the temperature and strain rate. The dependence of the yield stress on the temperature and strain rate follows the Ree-Eyring flow theory for both materials, whereas Young's modulus increases with decreasing temperature for PP and XLPE and with increasing strain rate for XLPE. Furthermore, a scanning electron microscope (SEM) study was performed on both materials to get a qualitative understanding of the volumetric strains.

Chapter 3

Influence of strain rate and temperature on the mechanical behaviour of rubber-modified polypropylene and cross-linked polyethylene

3.1 Introduction

In recent years, there has been increased interest in using polymeric materials in structural applications. The automotive industry, for example, is using polymeric materials in their pedestrian safety devices as sacrificial components that are designed to dissipate energy during impacts. An important point in this context is that material characterization and impact tests are performed close to room temperature, thus failing to account for changes in material behaviour as the temperature decreases. At low temperatures, polymeric materials tend to be both stiffer and more brittle, which could have severe consequences in a collision between a car and a pedestrian. Considering the cost of conducting prototype testing, it is clear that increased knowledge regarding the material behaviour at different temperatures is highly relevant.

The oil and gas industry is also interested in polymeric materials. As they continue to explore and search for oil and gas in harsher climates, new classification rules for materials are needed. There is an increasing need to understand how polymers behave at low temperatures due to this industry's expansion into the arctic region. There are various relevant structural applications for polymers in the oil industry, ranging from polymeric shock absorbers in load-bearing structures to gaskets used in pressurized components. In particular, for the two materials considered in this work, cross-linked low-density polyethylene (XLPE) is used as electrical insulation in high-voltage cables and as a liner material in flexible risers, while one application for rubber-modified polypropylene (PP) is thermal insulation of pipelines. As in the automotive industry, prototype testing is expensive; therefore, there is a demand for validated material models in finite element codes to reduce the number of experiments necessary to qualify a given material.

Reliable and good experimental data are a prerequisite for developing and improving phenomeno-

logical material models. At room temperature, the use of non-contact measuring devices to extract local stress-strain data from mechanical tests on polymeric materials has become widespread [1–3]. Digital image correlation (DIC) is an important tool because it enables local measurements of the strains (both longitudinal and transverse) in the neck of a tension test, which differs from an extensometer that provides average strains over a section. Therefore, by using DIC, local measurements of the volumetric strain are obtainable – a quantity that is useful for determining the plastic potential and for including damage modelling. However, when a temperature chamber is introduced, either to increase or decrease the temperature, the view of the specimen is obstructed. Most commercially available temperature chambers have only one window. This limits the number of possible digital cameras in the experimental set-up to one, thereby making the monitoring technique suitable only for isotropic materials. Consequently, many researchers use mechanical measuring devices such as extensometers or machine displacement to obtain stress-strain data when using a temperature chamber. Such instrumentation protocols will only reveal the average strain over the gauge length. Nevertheless, using these measurement techniques, a number of studies [4–9] have investigated the effects of increased temperature and strain rate on the material behaviour. In all these studies, the typical polymer behaviour is observed, i.e., increasing the strain rate increases the yield stress, whereas increasing the temperature decreases the yield stress. However, only the study by Arruda et al. [4] was conducted using an infrared (IR) sensor to measure self-heating at elevated strain rates, while none of the studies [4–9] report the volumetric strain. Similar studies considering the material behaviour at low temperatures [10–14] report the same trend – decreasing the temperature and increasing the strain rate increases the yield stress. As for the studies at elevated temperatures, the strain calculation relies on mechanical measurement techniques. Neither self-heating nor change in volume is reported in any of these studies.

Previous studies have been conducted on materials comparable to the two materials of interest in our study. For instance, Ponçot et al. [15] studied the volumetric strain at different strain rates in a polypropylene/ethylene-propylene rubber using a VideoTraction system. Their results are similar to the results obtained for the rubber-modified polypropylene material investigated in our study. Using a linear variable differential transformer to measure the cross-head displacement, Jordan et al. [16] conducted compression tests on low density polyethylene (LDPE) at four different temperatures and eight strain rates. Considering the effect on the yield stress, they found that an order of magnitude change in strain rate is approximately equal to a 10 degree change in temperature. An extensive study on a cross-linked polyethylene (PEX) was conducted by Brown et al. [17] utilizing a displacement extensometer. In their study, compression tests were conducted at temperatures ranging from -75 °C to 100 °C, and strain rates from 10^{-4} s^{-1} to 2650 s^{-1}. Addiego et al. [18] characterized the volumetric strain in HDPE through uniaxial tension and loading/unloading experiments at room temperature and strain rates from 10^{-4} s^{-1} to $5 \cdot 10^{-3}$ s^{-1}, using the same VideoTraction system as Ponçot et al. [15].

Conventional temperature chambers also exclude the possibility of using an IR camera because a free line-of-sight between the specimen and the IR camera is required. Since polymers become softer at elevated temperatures, monitoring self-heating during a test is essential to successfully separate the effects of strengthening due to rate sensitivity and softening due to

increasing temperature. An experimental set-up that circumvents the limitations imposed by using a conventional temperature chamber was presented by Johnsen et al. [19]. Here, a transparent polycarbonate (PC) temperature chamber was used, facilitating the use of multiple digital cameras to monitor the specimen during deformation. In addition, a slit was added in one of the chamber walls to obtain a free line-of-sight between an IR camera and the test specimen.

This polycarbonate temperature chamber was used in the present work, where the Cauchy stress, the logarithmic strain tensor and self-heating were obtained from uniaxial tension tests performed on two different materials: a rubber-modified polypropylene and a cross-linked low-density polyethylene. The tests were performed at four temperatures (−30 °C, −15 °C, 0 °C and 25 °C) and three nominal strain rates (0.01 s^{-1}, 0.1 s^{-1} and 1.0 s^{-1}), and all experiments were monitored by two digital cameras and a thermal camera. The two digital cameras were used to obtain local measurements of the longitudinal and transverse strains on two perpendicular surfaces of the axisymmetric tensile specimen, allowing us to calculate the Cauchy stress and the volumetric strain during the entire deformation process. The strains, along with the thermal history, were extracted at the point of initial necking, thus providing us with the temperature change as a function of logarithmic longitudinal strain. These are all vital quantities in material model calibration. The volumetric strain may be used in damage modelling, the thermal history may be linked to strain softening, and the variation of temperature and strain rate may provide the temperature and rate sensitivity, e.g. through the Ree-Eyring model [20]. To obtain a qualitative understanding of the volume change, some scanning electron microscopy (SEM) micrographs are also presented herein.

Furthermore, uniaxial compression tests were performed at the same temperatures and strain rates to investigate the pressure sensitivity of the two materials. The combined information from the uniaxial tension and compression tests allows us to study any pressure sensitivity of the materials, a phenomenon that is caused by the reduced molecular mobility under compression compared to that under tension [21]. Another source for this pressure sensitivity may be the existence, or nucleation, of voids in the material [22]. Stretching the material will cause the voids to grow, thus reducing the density of the bulk material, whereas compressing the material will have the opposite effect. Consequently, this leads to different material response in the two deformation modes.

3.2 Materials and methods

3.2.1 Materials

Two materials produced by Borealis were investigated: a rubber-modified polypropylene (PP) with the product name EA165E [23] and a cross-linked low-density polyethylene (XLPE) with the product name LS4201S [24]. The polypropylene material was received directly from Borealis as an extruded pipe with dimensions of 1000 mm × 250 mm × 22 mm (length × diameter × thickness), whereas the XLPE material was received from Nexans Norway as high-voltage cable segments in which the copper conductor had been removed. The dimensions of the cable insulation were 128 mm × 73 mm × 22.5 mm (length × diameter × thickness).

The physical properties of both materials are presented in Table 3.1. The densities were found

Table 3.1: Material properties for the PP and XLPE materials. All parameters are given for room temperature.

Material	Density, ρ (kg/m^3)	Specific heat capacity, C_p (J/(kg·K))	Thermal conductivity, k (W/(m·K))	Heat convection to air, h_c (W/(m^2·K))
XLPE	922	3546	0.56	21
PP	900	2756	0.31	18

from the datasheets supplied with the materials, whereas the specific heat capacity C_p and the thermal conductivity k were determined using the laser flash method [25]. Five circular samples with dimensions of 12.7 mm × 0.5 mm (diameter × thickness) of each material were heated to three temperatures: 25 °C, 35 °C, and 50 °C. Subsequently, the specific heat capacity and thermal conductivity were measured at each temperature level. The specific heat capacity increased almost linearly with temperature, whereas the thermal conductivity exhibited little variation. The values presented in Table 3.1 are the values obtained at room temperature. Heat convection to air, h_c, was determined by heating a small cylindrical sample with dimensions of 20 mm × 5 mm (diameter × height) in boiling water. The temperature decay was monitored using an infrared thermometer, and the heat convection to air was then calculated from the temperature-time history.

3.2.2 Test specimens

Axisymmetric specimens were used for both the tensile tests and the compression tests on the PP and XLPE materials. However, since the XLPE is softer than the PP, it was not possible to machine threads into the grips of the XLPE tensile specimens. The test specimens are illustrated in Figure 3.1.

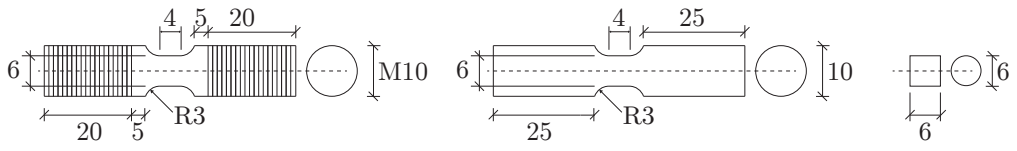

Figure 3.1: Schematics of (a) tensile test specimen for the PP material, (b) tensile test specimen for the XLPE material, and (c) compression test specimen for both materials. All measures are in mm.

All specimens were machined in a turning lathe from sections cut from the longitudinal direction of the extruded PP pipe and the extruded XLPE cable insulation. The radial direction was marked on the test specimens such that it could be distinguished from the hoop direction when the specimen was mounted in the test rig, see Figure 3.2.

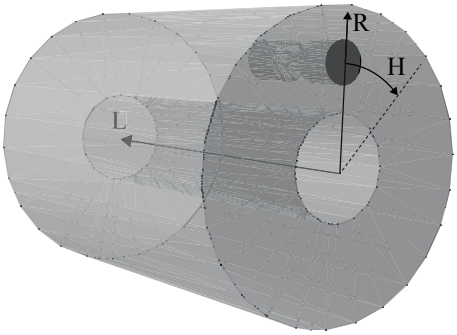

Figure 3.2: Illustration of the different directions used for the tension and compression specimens, where L, R, and H are the longitudinal, radial and hoop directions, respectively.

3.2.3 Experimental set-up and program

All experiments were performed in an Instron 5944 testing machine with a 2 kN load cell. A key component in the experimental set-up, see Figure 3.3, was a transparent polycarbonate (PC)

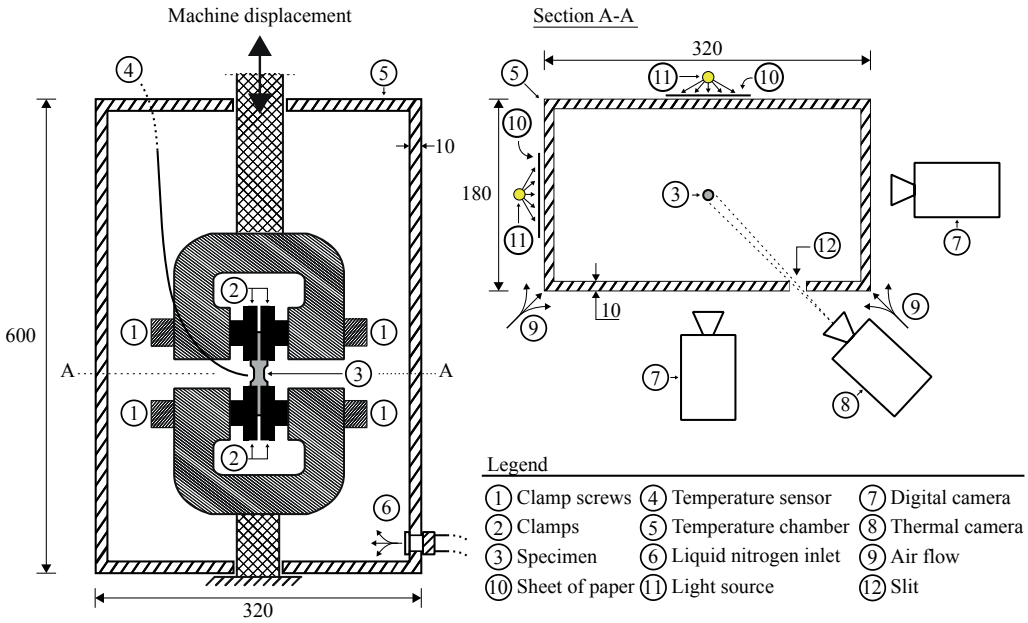

Figure 3.3: Illustration of the experimental set-up. The back-lighted sheets of paper were used to obtain good contrast between the specimen and the surroundings. All measures are in mm.

chamber, which allowed for non-contact optical devices to monitor local deformations during testing. Two Prosilica GC2450 digital cameras equipped with Sigma 105 mm and Nikon 105 mm lenses were used in this study. Both cameras were mounted between 25 cm and 35 cm from the

tensile specimen, equating to a resolution of approximately 60 pixels/mm. For the compression tests, the cameras were mounted approximately 10 cm away from the specimens, yielding a resolution of approximately 190 pixels/mm. Due to slight transverse anisotropy, see Figure 3.4, the two digital cameras, mounted perpendicular to each other, were used to monitor the surfaces

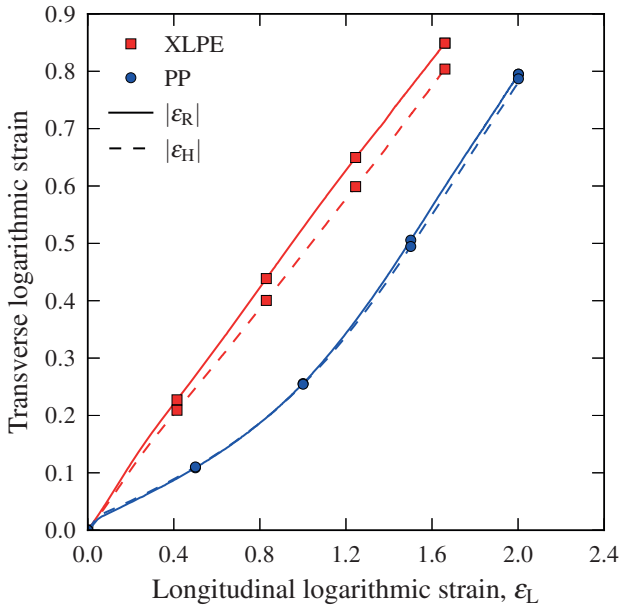

Figure 3.4: Absolute logarithmic transverse strains in the radial ($|\varepsilon_R|$) and the hoop ($|\varepsilon_H|$) directions as functions of logarithmic longitudinal strain (ε_L) for both materials. All curves are from tension experiments at room temperature and the lowest strain rate.

normal to the radial and hoop directions of the specimens, see Figures 3.2 and 3.3. Consequently, it was possible to obtain the longitudinal strain and the transverse strain in the radial and hoop directions of the extruded PP pipe and the XLPE cable insulation. In addition, a FLIR SC 7500 thermal camera, measuring temperatures down to −20 °C, was used to monitor self-heating in the test specimens during all uniaxial tension tests. A slit was added in the front window of the chamber (as indicated in Figure 3.3) to obtain a free line-of-sight between the test specimen and the thermal camera. A thermocouple temperature sensor mounted close to the test specimen was used to control the flow of liquid nitrogen into the chamber, and fans continuously blew air over the chamber walls to prevent condensation. The test specimens were thermally conditioned at the desired temperature for a minimum of 30 minutes prior to testing. A detailed description of the temperature chamber along with the experimental set-up is given by Johnsen et al. [19].

In the uniaxial tension tests at room temperature, a black and white spray-paint speckle was applied on the specimen surface. However, at the lower temperatures, the spray-paint speckle cracked and was therefore replaced with white grease and black powder. The black and white speckle is needed to perform digital image correlation (DIC) analyses of the images after the experiment. All uniaxial tension tests were post-processed using the in-house DIC code μDIC [26]. In the

compression tests, point tracking (subsets) was used to follow two points on the specimen surface to calculate the longitudinal strain, whereas edge tracing was used to determine the transverse strains. Another in-house DIC code, eCorr [27], was used to track the points on the surface of the compression specimen, and MATLAB was used to trace the edges. To reduce friction between the test machine and the compression specimen, PTFE tape and oil were used at the two highest temperatures (25 °C and 0 °C). At the two lowest temperatures (−15 °C and −30 °C), however, the oil was replaced with grease. Note that the specimen moved horizontally during some compression tests at the lowest temperatures and highest strain rates. In these tests, the lubrication was completely removed, and then the test was repeated. Photos of representative tensile and compression specimens with black and white speckle and surface points are shown in Figure 3.5.

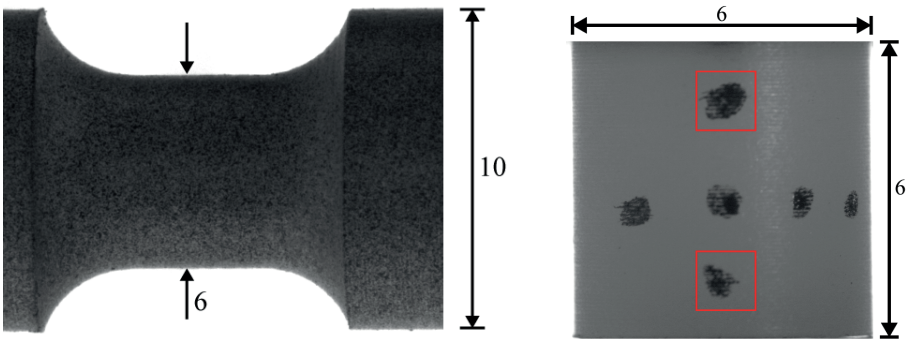

Figure 3.5: (a) Typical speckle pattern on a tensile specimen and (b) typical surface points on a compression specimen. The red squares indicate the two points that were used to calculate the longitudinal strain in the compression tests. All measures are in mm.

Uniaxial tension and compression tests were performed at four different temperatures T of 25 °C (room temperature), 0 °C, −15 °C, and −30 °C, and three different nominal strain rates $\dot{e}$ of 0.01 s^{-1}, 0.1 s^{-1}, and 1.0 s^{-1}, corresponding to cross-head velocities v of 0.04 mm/s, 0.4 mm/s and 4.0 mm/s in tension, and 0.06 mm/s, 0.6 mm/s and 6.0 mm/s in compression, respectively. The initial nominal strain rate was calculated as

$$\dot{e} = \frac{v}{L} \tag{3.1}$$

where v is the test machine's cross-head velocity and L is the length of the parallel section (gauge) of the test specimen. Figures 3.6a and 3.6b shows the local logarithmic strain rate ($\dot{\varepsilon}_{\mathrm{L}}$) in the section experiencing the first onset of necking as a function of longitudinal strain for both the XLPE and the PP material, respectively. Contrary to expectations the local logarithmic strain rate does not exceed the initial nominal strain rate. A possible explanation is that the effective length of the parallel section of the tensile specimen, L, is slightly higher than 4 mm, causing the strain rate to decrease. For each test configuration, a minimum of two replicate tests were performed. A third test was conducted if a significant deviation was observed in the force-displacement curves

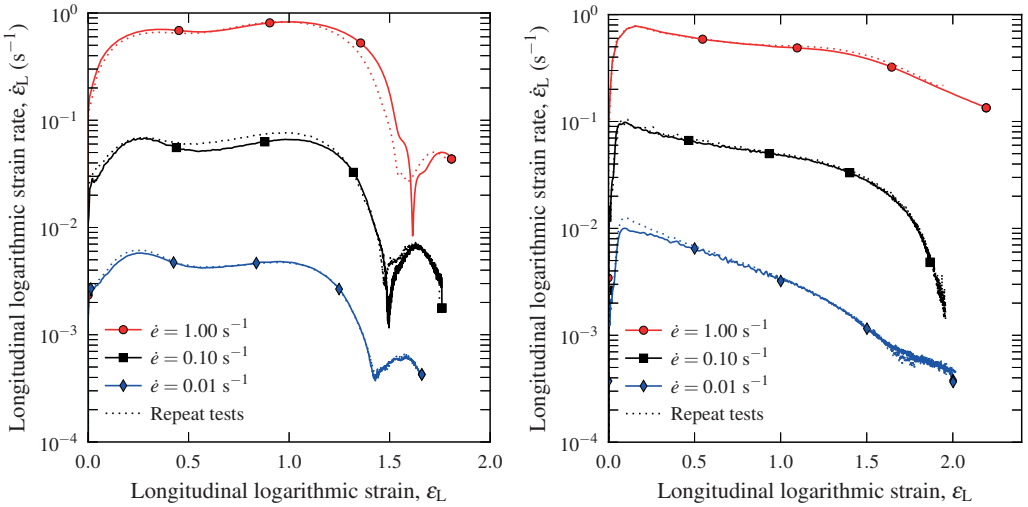

Figure 3.6: Longitudinal logarithmic strain rate ($\dot{\varepsilon}_L$) at room temperature for (a) the XLPE material and (b) the PP material as a function of longitudinal logarithmic strain.

between the two replicate tests. Although there was some variation in the fracture strain between the replicate tensile tests, there were only small differences in the stress-strain curve. In the replicate compression tests, there was some variation in the stress-strain curve after yielding but close to no variation in the magnitude of the yield stress. The clamping length of the specimens in the uniaxial tension tests was approximately 20 mm.

3.2.4 Calculation of Cauchy stress and logarithmic strain

Two digital cameras were used to monitor the deformation in the radial and hoop directions of the test specimen, with respect to the extruded PP pipe and XLPE cable insulation, see Figure 3.2. In the tension experiments, the section of initial necking was found on each surface, and the strain components were extracted at this section throughout the test. This ensured that the same point was tracked throughout the experiment, and that the strains from the two surfaces were obtained from the same point on the specimen. In the compression tests, the longitudinal strain was obtained from the distance between the highlighted points in Figure 3.5b, while the transverse strain on each surface was found by identifying the section of maximum diameter throughout the experiment. For both loading modes, the transverse stretches measured by each of the digital cameras were assumed to represent the stretches along the minor and major axes of an elliptical cross-section, enabling the calculation of the current cross-sectional area of the specimen as

$$A = \pi r_0^2 \cdot \frac{r_R}{r_0} \cdot \frac{r_H}{r_0} = \pi r_0^2 \lambda_R \lambda_H \tag{3.2}$$

where r_0 is the initial radius of the specimen; r_R and r_H are the radii in the radial and hoop directions, respectively; λ_R is the transverse stretch in the radial direction; and λ_H is the transverse stretch in the perpendicular hoop direction, see Figure 3.2. Using the transverse stretches from each camera, the volumetric strain is determined as

$$\varepsilon_V = \ln(\lambda_L \lambda_R \lambda_H) \tag{3.3}$$

where λ_L is the longitudinal stretch. The logarithmic strain components are calculated by taking the natural logarithm of the corresponding stretch component, i.e., $\varepsilon_i = \ln(\lambda_i)$. Note that we only obtain the strains on the surface of the specimen from the experiments. Thus, using Equation (3.3) to calculate the volumetric strain, we assume a homogeneous strain field over the cross-section. This assumption is only valid until the point of necking, where the strain field (and the stress field) becomes heterogeneous. The implications of this assumption are further discussed in Section 3.4. Using the expression for the area in Equation (3.2), the average Cauchy stress can be calculated as

$$\sigma = \frac{F}{A} \tag{3.4}$$

where F is the force measured by the testing machine.

Note that the yield stress (σ_0) throughout this study is taken to be equal to the flow stress at a longitudinal logarithmic strain of 0.15 (15%). A logarithmic strain of 0.15 was chosen because the material exhibits plastic flow at that point, while it is still close to the yield point. This definition of the yield stress applies for both tension and compression.

3.2.5 Calculation of self-heating

A MATLAB routine was established to obtain the temperature change on the surface of the tensile specimen at approximately the same position as the strains were extracted. Figure 3.7 shows a snapshot of the temperature field alongside the strain field for the PP material tested at room temperature and the highest strain rate. As indicated in the figure, the temperature gradient, ∇T, is calculated along a row of pixels (denoted row A in Figure 3.7) containing the top and bottom of the specimen, with air in-between. Since the temperature of the surrounding air is constant, an abrupt change in the temperature gradient will occur when transitioning from air to the specimen in the considered row of pixels. This allowed us to obtain the position of the top and bottom of the tensile specimen numerically, which again gave us the vertical coordinate, y_c, of the centre of the specimen during the experiment. The temperature is then extracted at the point (x_c, y_c) highlighted with a square in Figure 3.7, where x_c is the horizontal coordinate of the centre provided as user input. Note that the symbol T is used for all temperatures measured in degrees Celsius (°C) throughout the paper, while θ is applied for temperatures measured in Kelvin (K).

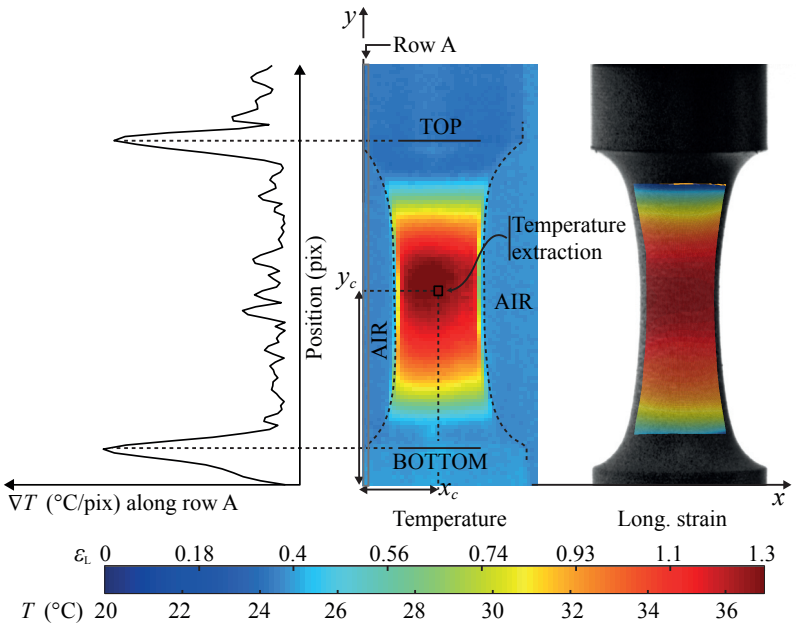

Figure 3.7: Temperature field from the IR camera alongside the longitudinal strain field from a tension test on PP at room temperature (T = 25 °C) and a strain rate $\dot{e}$ of 1.0 s^{-1}. The temperature gradient, ∇T, is calculated along row A to find the top and bottom of the specimen. The temperature was extracted at the position marked with a square. Dashed lines are guides to the eye showing the outline of the tensile specimen.

3.3 Results

3.3.1 Cross-linked low-density polyethylene (XLPE)

3.3.1.1 Uniaxial tension

Figure 3.8 presents the Cauchy stress plotted against the longitudinal logarithmic strain until fracture for uniaxial tension tests performed at four different temperatures (25 °C, 0 °C, −15 °C, and −30 °C) and three different initial nominal strain rates (0.01 s^{-1}, 0.1 s^{-1}, and 1.0 s^{-1}). Except for the lowest temperature, the stress-strain curves exhibit the same features: (1) a close to linear elastic behaviour up to the yield stress, (2) quasi-linear strain hardening, and (3) network hardening caused by the alignment of the polymer chains. At the lowest temperature, the network hardening is less prominent, and it appears to have completely vanished at the highest strain rate, as shown in Figure 3.8d.

By comparing Figures 3.8a through 3.8d, it is clearly observed that there is a strong increase in both the yield stress and the elastic stiffness as the temperature decreases. The yield stress at the lowest strain rate increases from approximately 10 MPa at room temperature (T = 25 °C) to approximately 30 MPa at the lowest temperature (T = −30 °C). As will be further discussed in

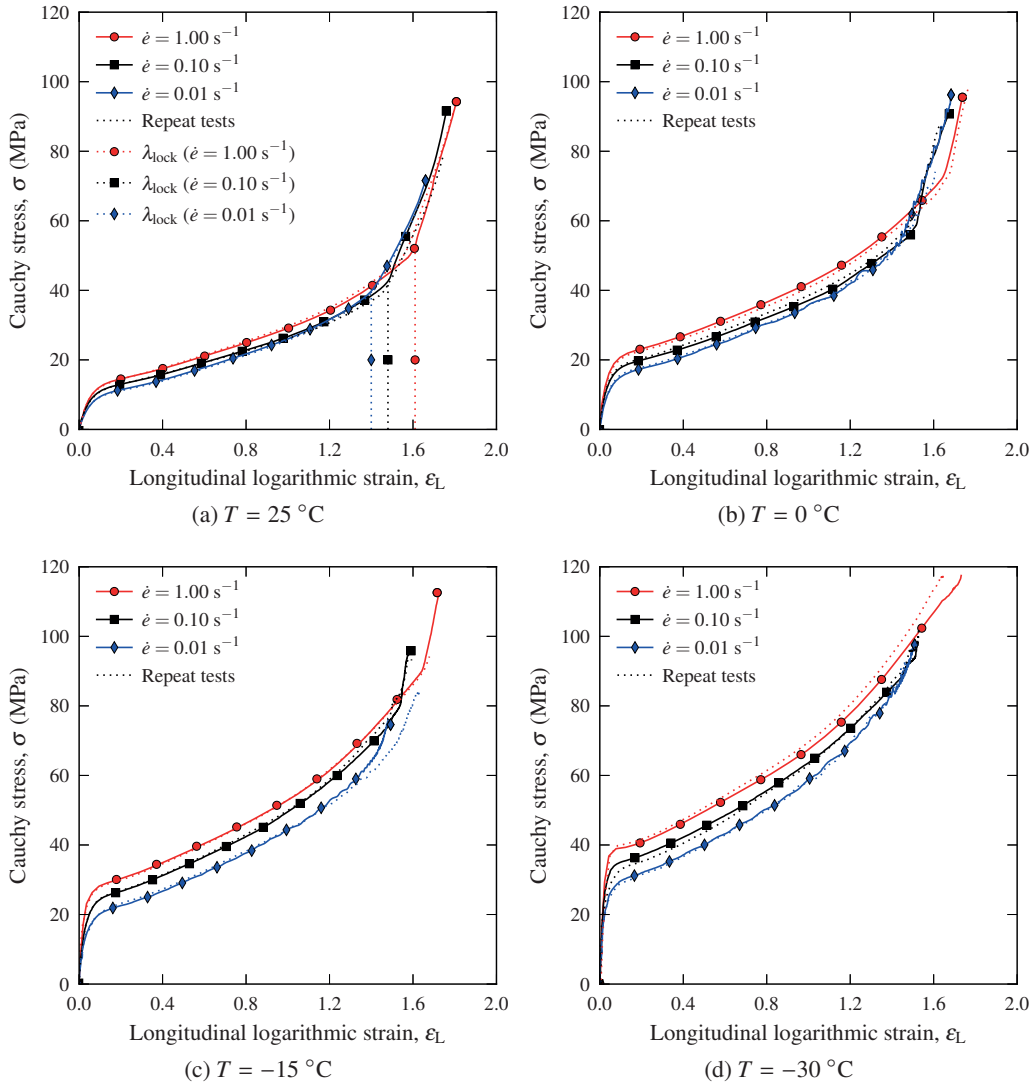

Figure 3.8: Cross-linked low-density polyethylene (XLPE): Cauchy stress vs. longitudinal logarithmic strain from uniaxial tension tests at three different nominal strain rates, $\dot{e} = 0.01\ s^{-1}$, $\dot{e} = 0.1\ s^{-1}$, and $\dot{e} = 1.0\ s^{-1}$, at four different temperatures, (a) $T = 25$ °C, (b) $T = 0$ °C, (c) $T = -15$ °C, and (d) $T = -30$ °C. Note that the repeat tests at the two highest strain rates in (a) were performed with only one digital camera.

Section 3.4, the dependence of the yield stress on strain rate and temperature obeys the Ree-Eyring flow theory [20]. The same trend is observed for the elastic stiffness: decreasing the temperature increases Young's modulus from approximately 200 MPa at room temperature to approximately 800 MPa at −30 °C. As for the yield stress, a dependence on strain rate is also evident for Young's modulus.

The locking stretch is taken as the stretch where the slope of the strain hardening curve increases

significantly, see Figure 3.8a. As shown in Figures 3.8a to 3.8c, the locking stretch increases with strain rate. This behaviour is believed to be caused by self-heating in the material at higher strain rates, which increases the chain mobility and extends the cold drawing domain. By inspecting the locking stretch in the experiments conducted at the lowest strain rate, which will later be shown to yield isothermal conditions, i.e., no self-heating, it is also observed that the locking stretch remains relatively constant down to a temperature of −15 °C. At the lowest temperature of −30 °C, no apparent locking stretch was detectable, see Figure 3.8d.

By applying Equation (3.3), the volumetric strains of XLPE at the investigated temperatures and strain rates are shown in Figure 3.9. Because of how the strain components are obtained from

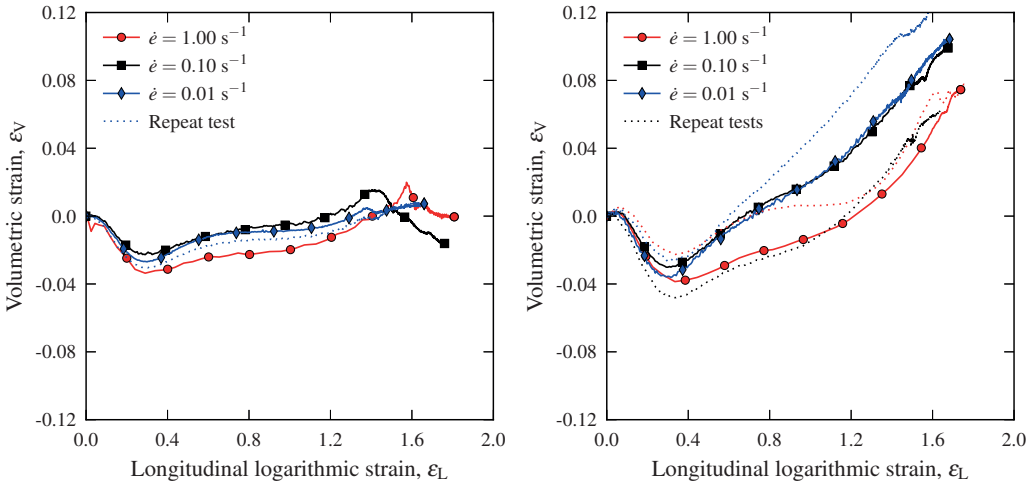

(a) $T = 25$ °C (b) $T = 0$ °C

Figure 3.9: Continues...

the experiments, an unphysical negative volumetric strain is observed at the beginning of each test. This discrepancy will be further discussed in Section 3.4. Nevertheless, Figure 3.9a shows that the polyethylene material is nearly incompressible for all the investigated strain rates at room temperature. This observation is further supported by the scanning electron microscopy (SEM) micrograph presented in Figure 3.10, where it is observed that the material contains few particles and, except for a few small cracks, is free of voids. At the three lowest temperatures, however, the volumetric strain increases to between 0.08 and 0.1. Note that the increasing negative volumetric strain at the beginning is due to the formation of a more pronounced neck, leading to a more heterogeneous strain field through the necked cross-section.

Figure 3.11 shows the self-heating in the XLPE material during deformation. At the lowest strain rate ($\dot{e} = 0.01\ s^{-1}$), we have isothermal conditions for all investigated temperatures. The reason for why there are no data points from the test performed at the lowest temperature ($T = -30$ °C) is that the infrared camera only records temperatures that are higher than −20 °C. At the intermediate

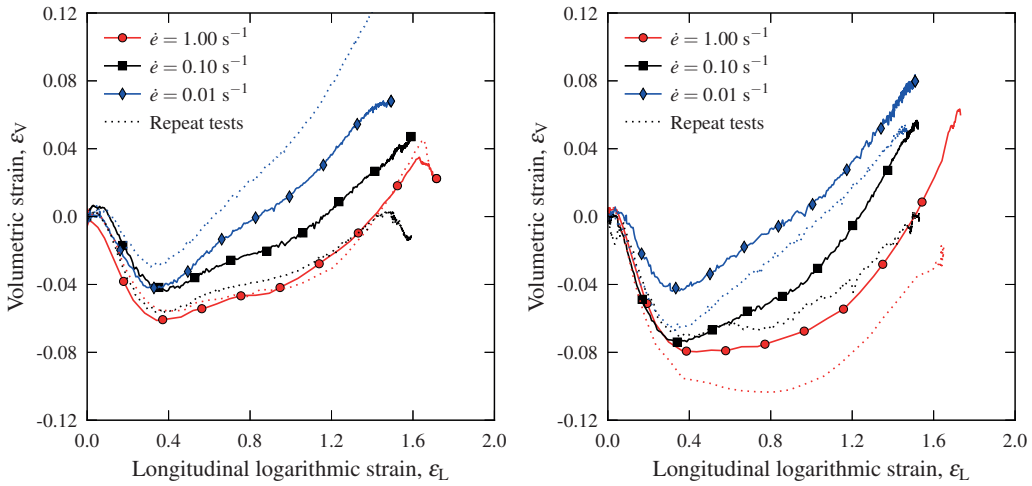

(c) $T = -15$ °C (d) $T = -30$ °C

Figure 3.9: Cross-linked low-density polyethylene (XLPE): Volumetric strain vs. longitudinal logarithmic strain from uniaxial tension tests at three different nominal strain rates, $\dot{e} = 0.01\ s^{-1}$, $\dot{e} = 0.1\ s^{-1}$, and $\dot{e} = 1.0\ s^{-1}$, at four different temperatures, (a) $T = 25$ °C, (b) $T = 0$ °C, (c) $T = -15$ °C, and (d) $T = -30$ °C.

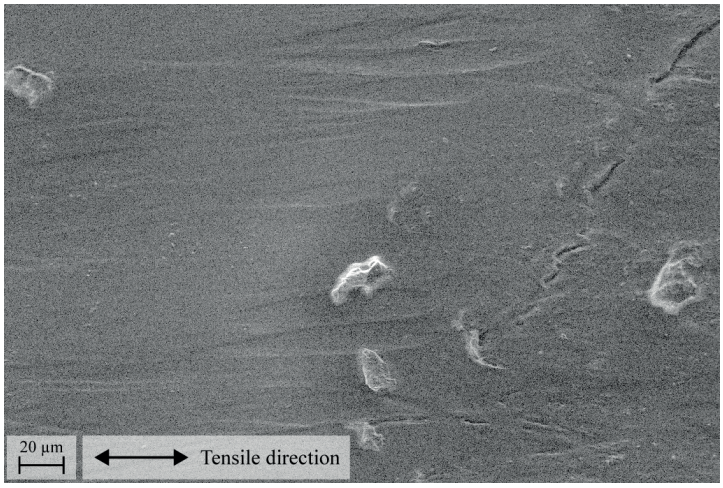

Figure 3.10: Cross-linked low-density polyethylene (XLPE): Scanning electron microscopy (SEM) micrograph of a tensile specimen loaded to a longitudinal strain of 1.1 and then unloaded.

strain rate ($\dot{e} = 0.1\ s^{-1}$), we observe a temperature increase due to self-heating of approximately 10 °C, whereas at the highest strain rate a temperature increase of approximately 20 °C to 30 °C is observed. The self-heating increases with reduced initial temperature.

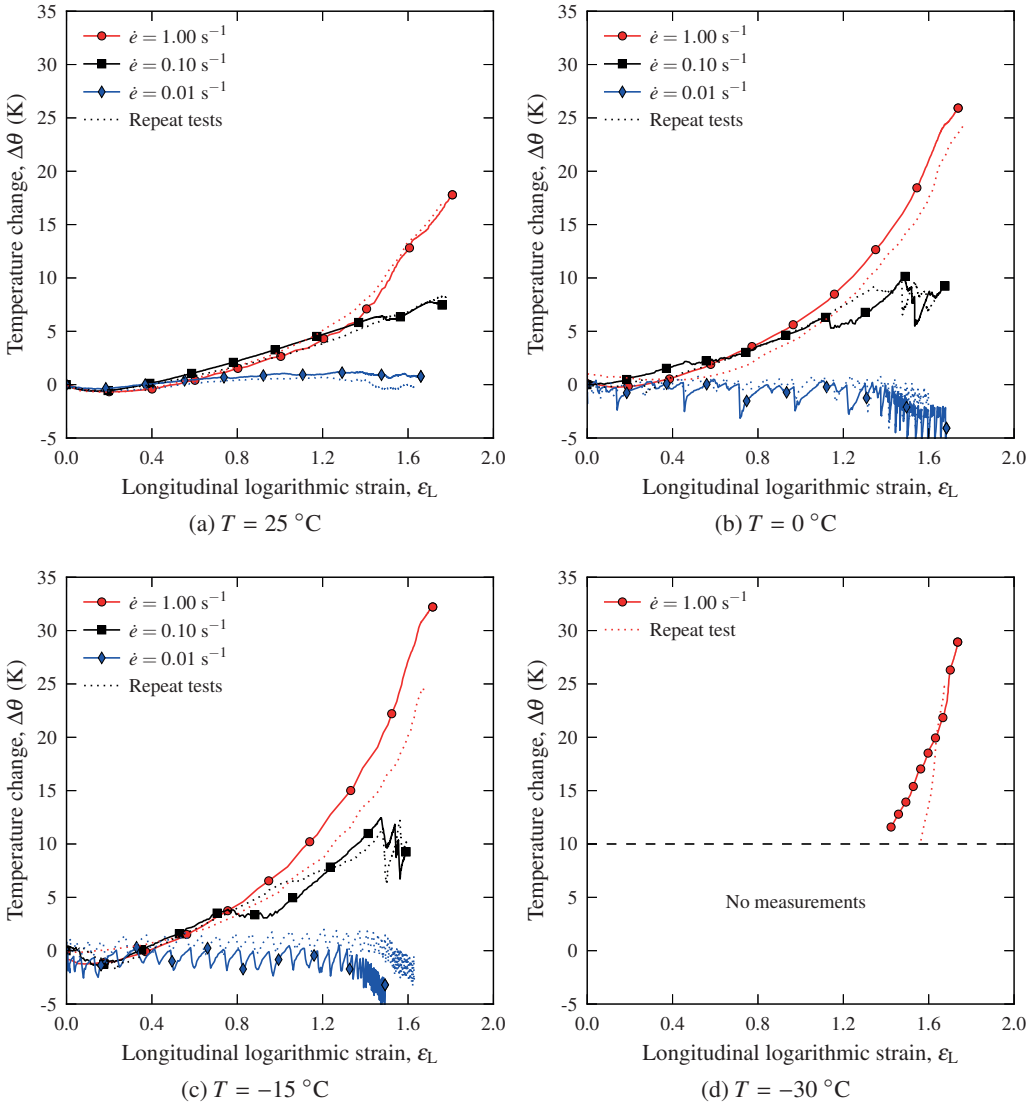

Figure 3.11: Cross-linked low-density polyethylene (XLPE): Self-heating vs. longitudinal logarithmic strain from uniaxial tension tests at three different nominal strain rates, $\dot{e} = 0.01\ \mathrm{s}^{-1}$, $\dot{e} = 0.1\ \mathrm{s}^{-1}$, and $\dot{e} = 1.0\ \mathrm{s}^{-1}$ at four different temperatures; (a) $T = 25$ °C, (b) $T = 0$ °C, (c) $T = -15$ °C, and (d) $T = -30$ °C.

3.3.1.2 Uniaxial compression

Uniaxial compression tests were performed at the same temperatures (25 °C, 0 °C, −15 °C, and −30 °C) and initial nominal strain rates (0.01 s^{-1}, 0.1 s^{-1}, and 1.0 s^{-1}) as the tension tests. A comparison of the Cauchy stress vs. logarithmic strain curves for uniaxial compression and tension at $T = 25$ °C is presented in Figure 3.12. As shown, the pressure sensitivity, defined as the ratio

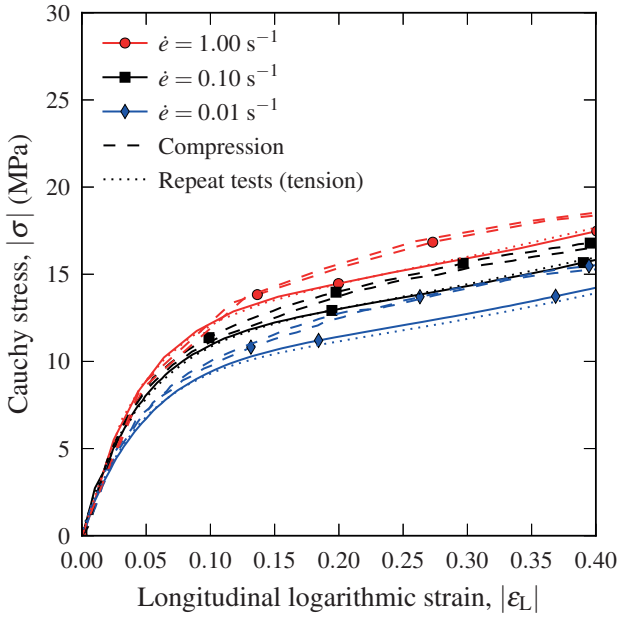

Figure 3.12: Cross-linked low-density polyethylene (XLPE): Comparison of Cauchy stress vs. longitudinal logarithmic strain curves in compression and tension at $T = 25$ °C. Note that two repeat tests are given for the compression stress-strain curves.

between the compressive and tensile yield stress, $\alpha_p = \sigma_C/\sigma_T$, is negligible for the polyethylene material. Conversely, the hardening is slightly higher in compression than in tension. However, note that barrelling occurred quite early in all the compression tests. Thus, the only purpose of the compression tests was to investigate the pressure sensitivity of the material in terms of the yield stress. A comparison of the compressive and tensile yield stress as functions of temperature and strain rate is shown in Figure 3.13. Similar to the observations from the uniaxial tension experiments, there is an increase in the compressive yield stress when decreasing the temperature and when increasing the strain rate.

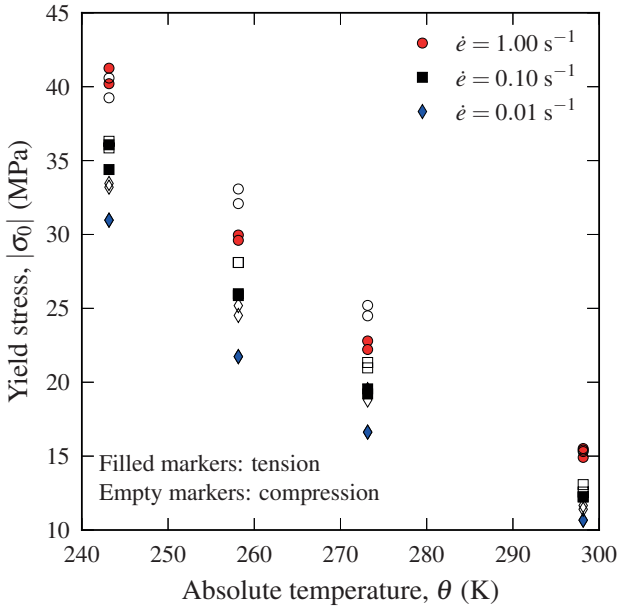

Figure 3.13: Cross-linked low-density polyethylene (XLPE): Comparison of the tensile and compressive yield stress as a function of temperature and strain rate.

The pressure sensitivity parameter $\alpha_\mathrm{p} = \sigma_\mathrm{C}/\sigma_\mathrm{T}$ is presented in Table 3.2 for all combinations of temperature and strain rate. Because α_p is consistently close to unity, the pressure sensitivity of the XLPE material is low.

Table 3.2: Pressure sensitivity parameter, $\alpha_\mathrm{p} = \sigma_\mathrm{C}/\sigma_\mathrm{T}$, for the XLPE material.

	$\dot{e}$ (s^{-1})		
T (°C)	0.01	0.1	1.0
25	1.08	1.02	0.98
0	1.13	1.09	1.08
−15	1.13	1.08	1.09
−30	1.08	1.02	0.98

3.3.2 Rubber-modified polypropylene (PP)

3.3.2.1 Uniaxial tension

The Cauchy stress vs. logarithmic strain curves from the tension tests of the polypropylene material are presented in Figure 3.14. Similar to the experiments conducted on the XLPE material, four temperatures (25 °C, 0 °C, −15 °C, and −30 °C) and three initial nominal strain rates (0.01 s^{-1}, 0.1 s^{-1}, and 1.0 s^{-1}) were investigated. The shape of the stress-strain curve for the two lowest

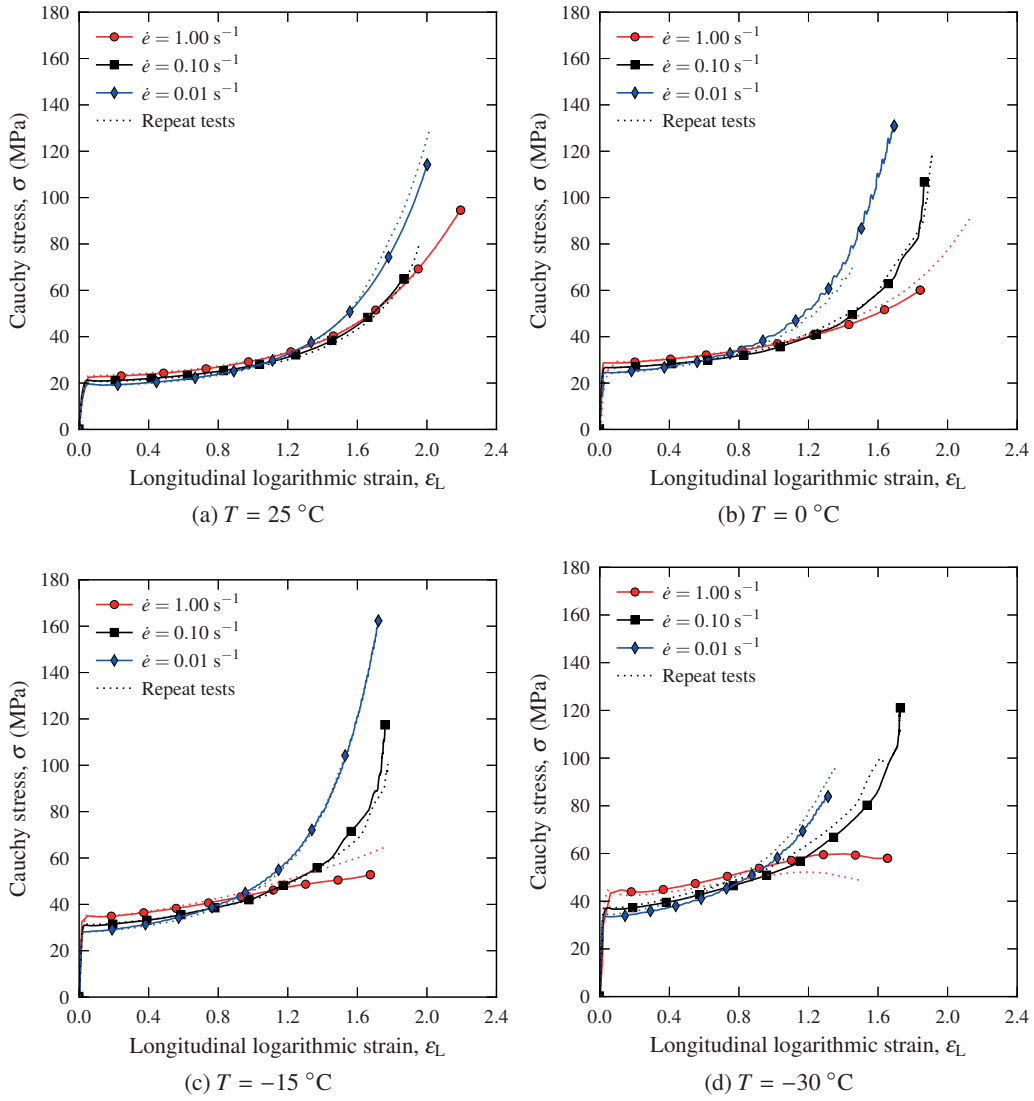

Figure 3.14: Rubber-modified polypropylene (PP): Cauchy stress vs. longitudinal logarithmic strain from uniaxial tension tests at three different nominal strain rates, $\dot{e} = 0.01\ \mathrm{s}^{-1}$, $\dot{e} = 0.1\ \mathrm{s}^{-1}$, and $\dot{e} = 1.0\ \mathrm{s}^{-1}$, at four different temperatures, (a) $T = 25\ ^\circ\mathrm{C}$, (b) $T = 0\ ^\circ\mathrm{C}$, (c) $T = -15\ ^\circ\mathrm{C}$, and (d) $T = -30\ ^\circ\mathrm{C}$.

strain rates is relatively the same for all temperatures: first a close to linear elastic behaviour up to a yield point, followed by strain hardening and ultimately asymptotic network hardening. At the highest strain rate and the three lowest temperatures, however, the material fractured before the locking stretch was reached.

In terms of the yield stress, the equivalence principle [28] holds, i.e., either reducing the temperature or increasing the strain rate increases the yield stress. At room temperature and for the lowest

strain rate, the yield stress is approximately 20 MPa, while it has increased to approximately 24 MPa for the highest strain rate. At the lowest temperature, the quasi-static yield stress is approximately 35 MPa and increases to approximately 45 MPa for the highest strain rate, indicating that the rate-sensitivity is slightly higher at lower temperatures. The elastic modulus, however, exhibits little dependence on the strain rate, but it changes drastically with temperature. At room temperature, Young's modulus is approximately 850 MPa, whereas it has increased to approximately 2600 MPa at the lowest temperature.

As shown in Figure 3.15, the volumetric strains for the polypropylene material are considerably

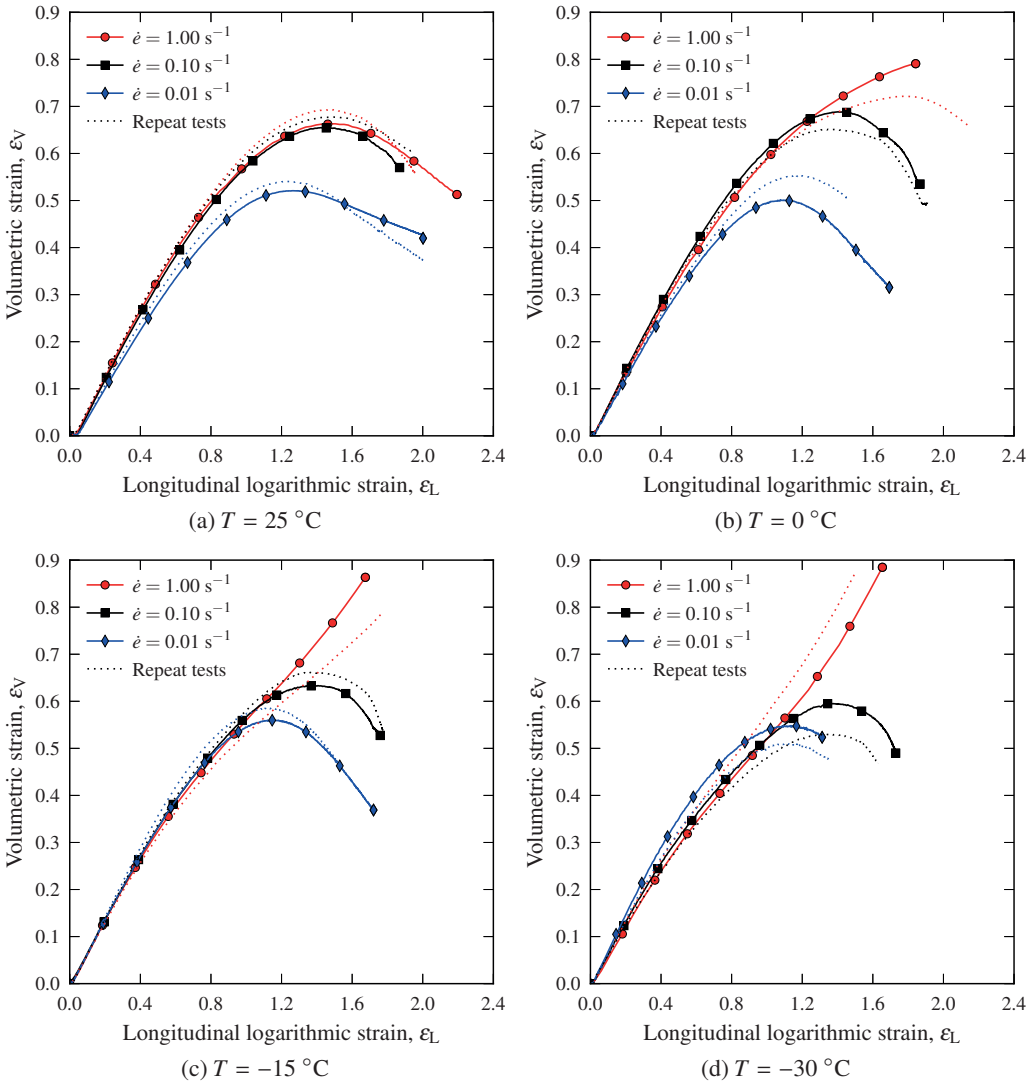

Figure 3.15: Rubber-modified polypropylene (PP): Volumetric strain vs. longitudinal logarithmic strain from uniaxial tension tests at three different nominal strain rates, $\dot{e} = 0.01\ \mathrm{s}^{-1}$, $\dot{e} = 0.1\ \mathrm{s}^{-1}$, and $\dot{e} = 1.0\ \mathrm{s}^{-1}$, at four different temperatures, (a) $T = 25\ ^\circ\mathrm{C}$, (b) $T = 0\ ^\circ\mathrm{C}$, (c) $T = -15\ ^\circ\mathrm{C}$, and (d) $T = -30\ ^\circ\mathrm{C}$.

larger than those for XLPE and attain values between 0.5 and 0.9. At the two lowest strain rates, the shape of the curve is the same for all temperatures: first a significant evolution of volumetric strain up to a peak value followed by decreasing volumetric strain. Ponçot et al. [15] reported a similar observation on a comparable material (polypropylene/ethylene-propylene rubber). This result is due to the formation of voids in the material, believed to be initiated by cavitation in the rubbery phase of the rubber-modified polypropylene. Since there are no particles in these voids, they are not restrained against collapsing, which explains the decreasing volumetric strains after the peak value is reached. To investigate this assumption, two specimens were loaded in uniaxial tension at room temperature and a strain rate of 0.01 s^{-1} and thereafter unloaded; one specimen was unloaded before the maximum volumetric strain was reached, and the other one was unloaded after the maximum volumetric strain. SEM micrographs of the two samples are presented in Figures 3.16a and 3.16b. It appears from Figure 3.16 that the voids become elongated and start to close after the maximum volumetric strain is reached. At the highest strain rate, however, it seems that the voids do not collapse at the three lowest temperatures, leading to a monotonically increasing volumetric strain up to fracture, as shown in Figures 3.15b to 3.15d.

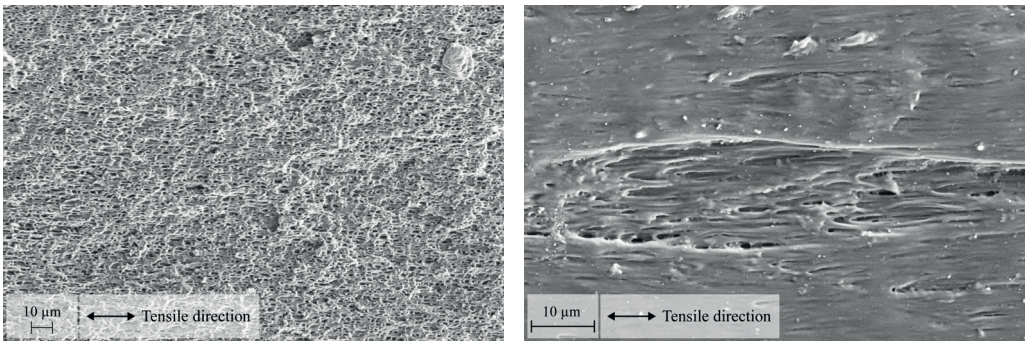

(a) (b)

Figure 3.16: Rubber-modified polypropylene (PP): Scanning electron microscopy (SEM) micrographs of tensile specimens unloaded (a) before and (b) after peak volumetric strain.

The self-heating during the tensile experiments is presented in Figure 3.17. At the lowest strain rate, isothermal conditions prevail at all temperatures. As previously mentioned, there are no data points for the temperature change in the material at the lowest temperature ($T = -30$ °C) and the lowest strain rate due to the infrared camera being limited to temperatures above −20 °C. At the intermediate strain rate ($\dot{e} = 0.10$ s^{-1}), a temperature increase between 15 °C and 30 °C is observed before the temperature begins to decrease in the material. This decrease in temperature is due to the formation of a stable neck leading to cold drawing. This provides the material with enough time to conduct heat within the specimen and to convect heat to the surroundings. Although we have cold drawing at the highest strain rate ($\dot{e} = 1.0$ s^{-1}) at room temperature, the duration of the test is too short to allow for heat conduction or convection. This leads to the continuously increasing temperature for the highest strain rate at all temperatures in Figure 3.17.

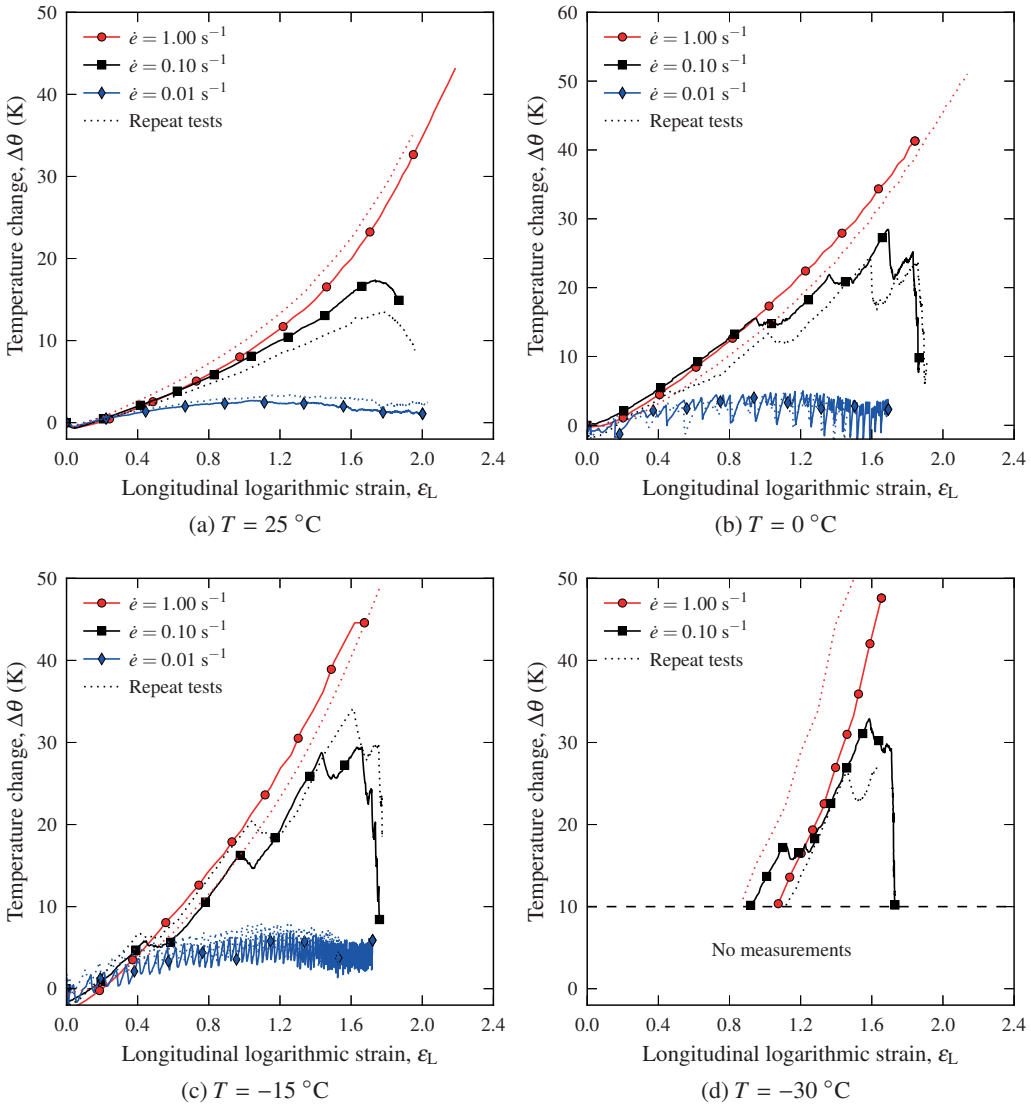

Figure 3.17: Rubber-modified polypropylene (PP): Self-heating vs. longitudinal logarithmic strain from uniaxial tension tests at three different nominal strain rates, $\dot{e} = 0.01\ \mathrm{s}^{-1}$, $\dot{e} = 0.1\ \mathrm{s}^{-1}$, and $\dot{e} = 1.0\ \mathrm{s}^{-1}$, at four different temperatures, (a) $T = 25\ ^\circ\mathrm{C}$, (b) $T = 0\ ^\circ\mathrm{C}$, (c) $T = -15\ ^\circ\mathrm{C}$, and (d) $T = -30\ ^\circ\mathrm{C}$.

In contrast to XLPE, the temperature increase is approximately the same for all temperatures, i.e., between 40 and 50 °C, when adiabatic heating conditions are met.

Another observation is that the self-heating introduces a softening in the material, as indicated by the crossing of the stress-strain curves observed, for instance in Figure 3.14a. The self-heating increases the locking stretch for higher strain rates. Unlike XLPE, however, the opposite effect is observed when decreasing the temperature at the lowest strain rate, i.e., there is a reduction of the

locking stretch for PP with decreasing temperature.

3.3.2.2 Uniaxial compression

Similar to the XLPE material, compression tests were performed for the PP material at four temperatures (25 °C, 0 °C, −15 °C, and −30 °C) and three initial nominal strain rates (0.01 s^{-1}, 0.1 s^{-1} and 1.0 s^{-1}). Figure 3.18 compares the stress-strain curves in uniaxial compression and tension

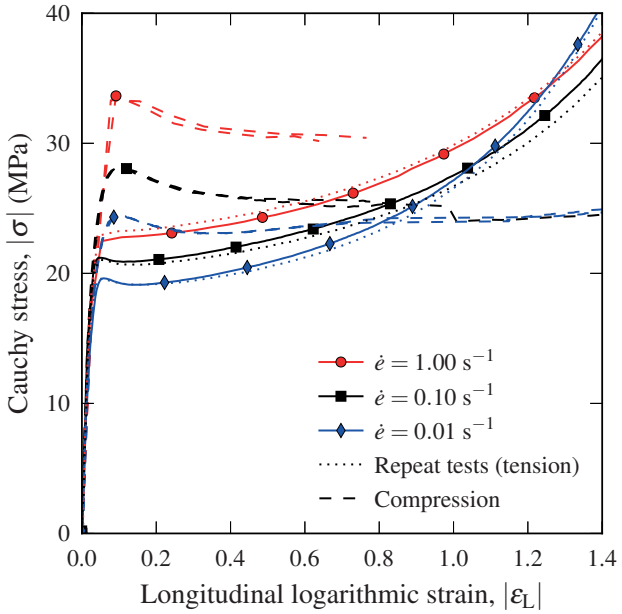

Figure 3.18: Rubber-modified polypropylene (PP): Comparison of Cauchy stress vs. longitudinal logarithmic strain curves in compression and tension at $T = 25$ °C. Note that two repeat tests are given for the compression stress-strain curves.

at room temperature. It is clearly observed from the difference in compressive and tensile yield stress that the pressure sensitivity of the PP material is strong. Similar to the compression tests performed on the XLPE material, the onset of barrelling occurred for quite small deformations. Consequently, the compression tests were only conducted to determine the yield stress. As in tension, it is observed that higher strain rates and lower temperatures increase the yield stress in compression. The yield stresses in compression and tension are plotted as functions of temperature in Figure 3.19 for all the investigated strain rates.

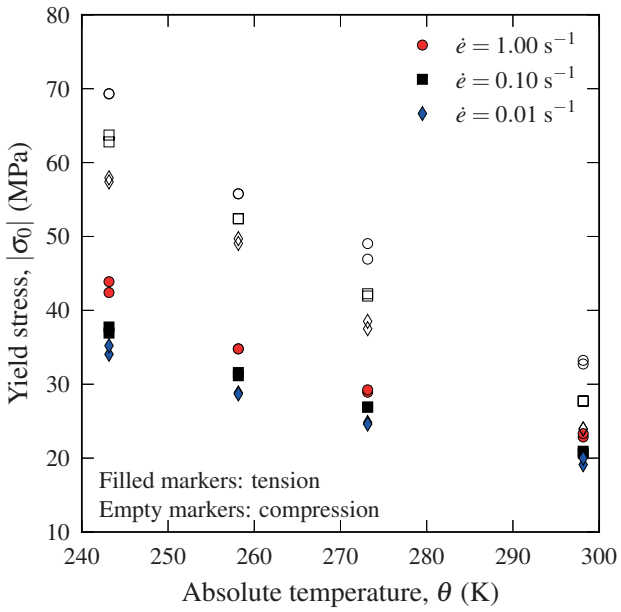

Figure 3.19: Rubber-modified polypropylene (PP): Comparison of the tensile and compressive yield stress as a function of temperature and strain rate.

The pressure sensitivity parameter $\alpha_\mathrm{p} = \sigma_\mathrm{C}/\sigma_\mathrm{T}$ is presented in Table 3.3 for all combinations of temperature and strain rate. In contrast to the XLPE material, the pressure sensitivity is very high for the rubber-modified polypropylene. It is also observed that the pressure sensitivity increases at low temperatures.

Table 3.3: Pressure sensitivity parameter, $\alpha_\mathrm{p} = \sigma_\mathrm{C}/\sigma_\mathrm{T}$, for the PP material.

	$\dot{e}$ (s^{-1})		
T (°C)	0.01	0.1	1.0
25	1.22	1.33	1.43
0	1.54	1.56	1.65
−15	1.71	1.67	1.60
−30	1.66	1.69	1.61

3.4 Discussion

3.4.1 Temperature measurements

An infrared camera was employed to measure self-heating during the tests, see Section 3.2.3. In all experiments an emissivity of 0.95 was used. As validation, a uniaxial tension test at room

temperature ($T = 25$ °C) and at the highest strain rate ($\dot{e} = 1.0$ s^{-1}) was performed on the XLPE material where the surface facing the thermal camera was coated with a black paint with an emissivity close to 1.0. The temperature as a function of longitudinal strain was then compared with a similar experiment where only a black and white speckle was applied. As evident from Figure 3.11a the difference between the measured self-heating for the two tests at the highest strain rate is minimal. Another possible issue is that the grease applied to the samples tested at low temperatures may affect thermal measurements. To validate the calculated self-heating from tests performed on materials coated with white grease, two tests at the highest strain rate were performed on the PP material at room temperature. In one of the tests a black and white spray paint speckle was applied, while in the other a white grease was used. The difference in self-heating, as shown in Figure 3.17a, was found to be negligible.

3.4.2 Young's modulus

Young's modulus as a function of temperature and strain rate is presented in Figures 3.20 and 3.21 for XLPE and PP, respectively. Young's modulus of the XLPE material was found through a linear fit of the stress-strain curve up to a longitudinal strain of $\varepsilon_L = 0.025$. For the PP material, Young's modulus was obtained by a linear fit of the stress-strain curve for $\sigma \in [0, 0.5\sigma_0]$, where σ_0 is the quasi-static yield stress at the investigated temperature. Due to noise in the strain values obtained from DIC, it was necessary to average the strain values over a larger area of the parallel section of the tensile specimen for the PP material. This can be done since the strain field remains homogeneous for the part of the stress-strain curve used to obtain Young's modulus.

For both materials, the elastic stiffness was found to be strongly dependent on the temperature. In XLPE, the elastic stiffness increases by a factor of four: from approximately 200 MPa at room temperature to 800 MPa at −30 °C. For the PP material, Young's modulus increases more than threefold: from approximately 850 MPa at room temperature to 2600 MPa at −30 °C. The temperature dependence within the experimental range is described using the same expression as Arruda et al. [4], i.e.

$$E(\theta) = E_0 \cdot \exp\left[-a\left(\theta - \theta_0\right)\right] \tag{3.5}$$

where θ_0 is the reference temperature, E_0 is Young's modulus at the reference temperature, a is a material parameter, and θ is the absolute temperature. The least squares fits of Equation (3.5) to the experimentally obtained Young's modulus for the materials at the lowest strain rate are shown in Figures 3.20 and 3.21, with $E_0 = 141$ MPa and $a = 0.03$ K^{-1} for the XLPE material, $E_0 = 842$ MPa and $a = 0.021$ K^{-1} for the PP material, and $\theta_0 = 298.15$ K (room temperature) for both materials.

Young's modulus was also found to be influenced by strain rate for the XLPE material, as shown in Figure 3.20. The trend of the elastic stiffness with respect to the rate sensitivity is not as clear for the PP material, as indicated in Figure 3.21. Since both Young's modulus and the yield stress is higher in PP compared to XLPE, this observation could be an artefact of the acceleration of the

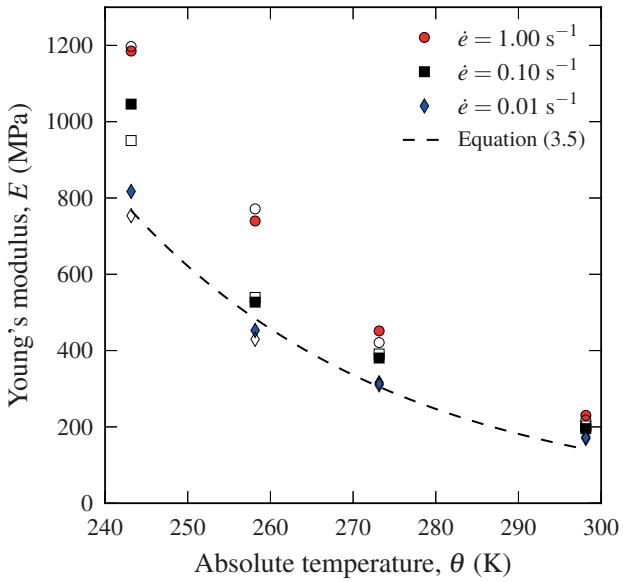

Figure 3.20: Cross-linked low-density polyethylene (XLPE): Influence of strain rate and temperature on Young's modulus. Equation (3.5) is fitted only to the Young's moduli at the lowest strain rate. The empty markers are from the repeat tests in Figure 3.8.

test machine, meaning that some time is needed before the cross-head reaches the desired velocity, or due to some slack in, e.g., the load cell or the grip. These factors, combined with a limited

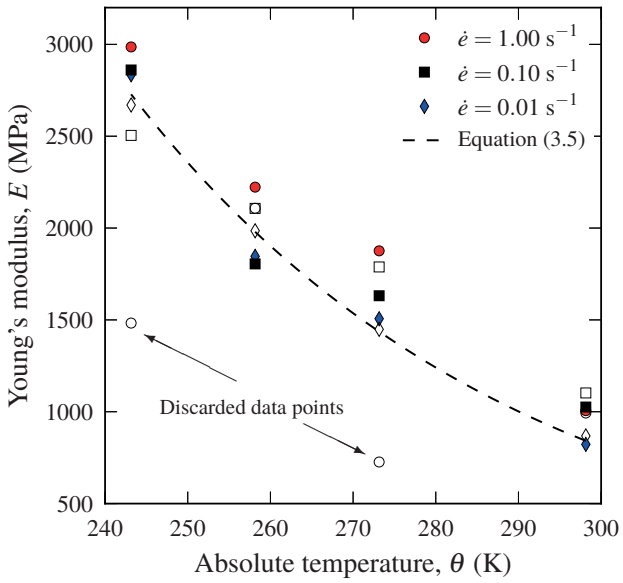

Figure 3.21: Rubber-modified polypropylene (PP): Influence of strain rate and temperature on Young's modulus. Equation (3.5) is fitted only to the Young's moduli at the lowest strain rate. The empty markers are from the repeat tests in Figure 3.14.

number of data points before yield for the two highest strain rates, could explain the discrepancies observed in Figure 3.21. Nevertheless, given that the most influential factor for both materials was the temperature, the strain rate dependence has been omitted in Equation (3.5).

3.4.3 Yield stress and pressure sensitivity

The Ree-Eyring flow theory [20] is frequently applied to model the influence of temperature and strain rate on the yield stress. Following the work of Senden et al. [29], a double Ree-Eyring model that includes both the main α relaxation and the secondary β relaxation is employed for evaluation and discussion of the experimental findings herein. Assuming that the contributions from each relaxation process are additive, the equivalent stress is given as

$$\bar{\sigma}(\dot{p}, \theta) = \sum_{x=\alpha,\beta} \frac{k_B \theta}{V_x} \operatorname{arcsinh}\left(\frac{\dot{p}}{\dot{p}_{0,x}} \exp\left[\frac{\Delta H_x}{R\theta}\right]\right) \tag{3.6}$$

Here, k_B is Boltzmann's constant, R is the gas constant, $\dot{p}$ is the equivalent plastic strain rate, θ is the absolute temperature, V_x ($x = \{\alpha, \beta\}$) is the activation volume, $\dot{p}_{0,x}$ is a local reference plastic strain rate, and ΔH_x is the activation enthalpy. For the purpose of obtaining the relation between the yield stress, temperature and strain rate, the equivalent stress $\bar{\sigma}$ is taken to be equal to the yield stress σ_0, and $\dot{p}$ is assumed to be equal to the initial nominal strain rate $\dot{e}$. The material parameters obtained from a least squares fit of Equation (3.6) to the experimental data are presented in Table 3.4. All material parameters from the least squares fit appear to be reasonable from a

Table 3.4: Material parameters of the Ree-Eyring model, Equation (3.6).

Material	k_B (J/K)	R (J/(mol·K))	V_α (nm^3)	$\dot{p}_{0,\alpha}$ (s^{-1})	ΔH_α (kJ/mol)	V_β (nm^3)	$\dot{p}_{0,\beta}$ (s^{-1})	ΔH_β (kJ/mol)
XLPE	$1.38 \cdot 10^{-23}$	8.314	3.77	$2.48 \cdot 10^{31}$	211.8	3.14	$6.07 \cdot 10^{37}$	194.8
PP	$1.38 \cdot 10^{-23}$	8.314	1.37	$3.09 \cdot 10^{17}$	86.4	4.95	$3.62 \cdot 10^{38}$	286.0

physical perspective: the activation volume is between 1 nm^3 and 5 nm^3, the activation enthalpy ranges from 100 kJ/mol to 300 kJ/mol, and the local reference plastic strain rate attains values between 10^{17} s^{-1} and 10^{38} s^{-1}. The orders of magnitude are comparable to those of parameters reported for other materials in the literature, e.g. [10, 29]. Addressing the yield stress in tension, it appears from Figures 3.22 and 3.23 that the model captures the temperature and strain rate dependence of both materials excellently. Thus, the double Ree-Eyring model appears to be a promising choice for a thermomechanical description of the flow process of the materials at hand.

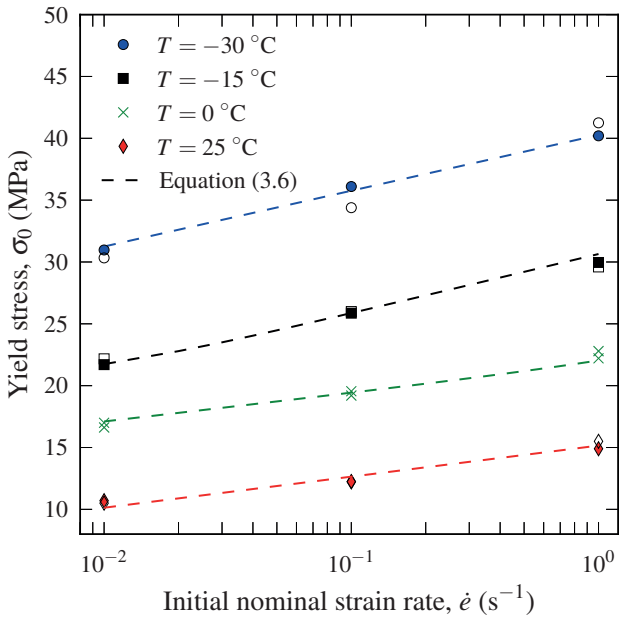

Figure 3.22: Cross-linked low-density polyethylene (XLPE): Influence of temperature and strain rate on the yield stress. The empty markers are from the repeat tests in Figure 3.8.

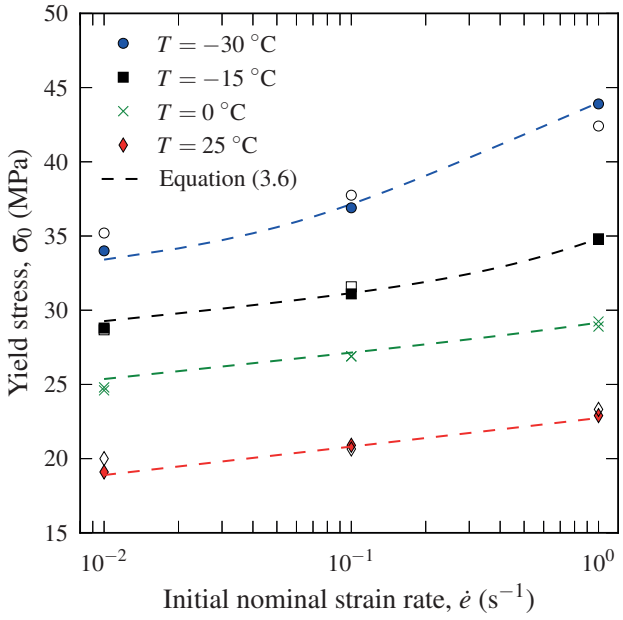

Figure 3.23: Rubber-modified polypropylene (PP): Influence of temperature and strain rate on the yield stress. The empty markers are from the repeat tests in Figure 3.14.

The pressure sensitivity parameter $\alpha_p = \sigma_C/\sigma_T$ is given in Tables 3.2 and 3.3 for the two materials. For the polyethylene material, which exhibits rather small volumetric strains, the pressure sensitivity is low, and α_p is close to unity. In contrast, the pressure sensitivity of the polypropylene material, which exhibits large volumetric strains, is high, and α_p ranges from 1.22 to 1.71. This result suggests that the lower yield stress in tension could be caused by the nucleation and growth of voids in the PP material. This assumption is supported by Lazzeri and Bucknall [21]. However, note that neither cavitation nor initial voids are prerequisites for a pressure-dependent material. In solid polymers, pressure dependence may arise from the fact that compression reduces the molecular mobility compared to tension, which increases the yield stress [21].

3.4.4 Volumetric strain

The negative volumetric strain observed for the polyethylene material, as shown in Figure 3.9, is due to the way in which it is calculated, i.e., we assume that the strain components calculated on the surface of the specimen are representative for the entire cross-section. This assumption is true only for homogeneous deformation, which occurs prior to necking. When the material necks, however, the strain components vary over the cross-section. The longitudinal strain component is largest in the centre of the specimen and smallest at the surface. This variation is not accounted for in our calculations and thus leads to an increasingly negative volumetric strain for test configurations where the external curvature of the neck, and thus the heterogeneity of the longitudinal strain, increases. This counter-intuitive and fictitious result can be remedied by accounting for the variation in the longitudinal strain over the cross-section, for instance, by assuming a parabolic distribution of the strain. Using this assumption, Andersen [26] obtained a formula for the corrected volumetric strain, viz.

$$\varepsilon_{V,corr} = \ln\left[\lambda_L \lambda_R \lambda_H \left(\frac{\kappa R}{4} + 1\right)\right] \tag{3.7}$$

where κ is the external curvature of the neck and R is the radius in the neck. This correction removes the observed unphysical negative volumetric strain, as shown in Johnsen et al. [19]. Both geometrical measures κ and R can in principle be extracted from the digital pictures. In our case, however, the use of grease and black powder on the surface of the tensile specimens prohibited determination of the external curvature; therefore, the volumetric strain was calculated according to Equation (3.3).

Both materials have a fairly high linear thermal expansion coefficient α_T, which ranges between $146 \cdot 10^{-6}$ K^{-1} and $180 \cdot 10^{-6}$ K^{-1} for polypropylene and from $180 \cdot 10^{-6}$ K^{-1} to $400 \cdot 10^{-6}$ K^{-1} for low-density polyethylene [30]. Thus, the substantial self-heating may provide a significant contribution to the observed dilatation. The thermal volumetric strain is defined as

$$\varepsilon_{V,thermal} = 3\alpha_T \Delta\theta \tag{3.8}$$

where $\Delta\theta$ is the temperature change. Assuming a thermal expansion coefficient of $180 \cdot 10^{-6}$ K^{-1}

and a temperature increase of 50 K in the PP material, the volumetric strain due to self-heating is determined to be 0.9%, which is negligible compared to the substantial volumetric strain from deformation. Considering XLPE, we assume a thermal expansion coefficient of $200 \cdot 10^{-6}$ K^{-1} and a temperature increase of 30 K. This assumption provides a thermal volumetric strain of 0.6%, which is approximately 30% of the maximum volumetric strain ($\approx 2\%$) at room temperature (Figure 3.9a).

3.4.5 Network hardening and locking stretch

An interesting observation for the PP material is that the characteristic network hardening, caused by the alignment of the polymer chains, does not occur for the highest strain rate ($\dot{e} = 1.0$ s^{-1}) at the two lowest temperatures ($T = -15$ °C and $T = -30$ °C). This result is due to the formation of an unstable neck, as shown by the Considère construction in Figure 3.24, which presents graphs of the functions $\sigma(\varepsilon_L)$ and $\Theta(\varepsilon_L)$, where $\Theta = d\sigma/d\varepsilon_L$ is the hardening modulus.

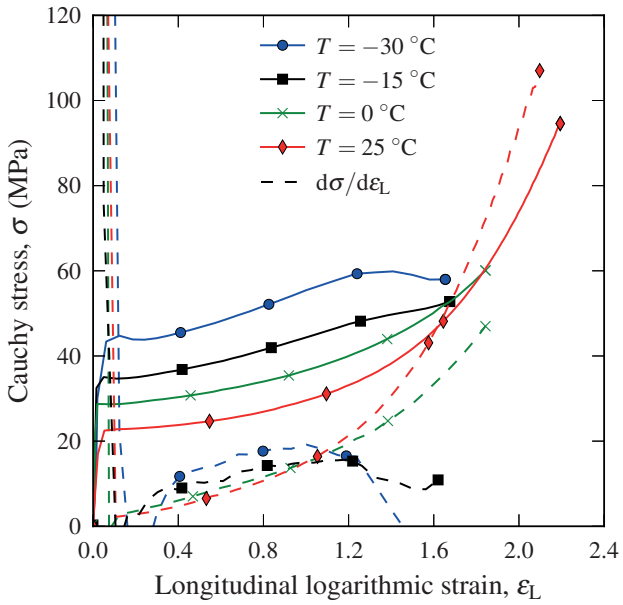

Figure 3.24: Rubber-modified polypropylene (PP): Considère construction for the uniaxial tension tests at all temperatures for the strain rate $\dot{e} = 1.0$ s^{-1}.

The function $\Theta(\varepsilon_L)$ is found by numerical differentiation of $\sigma(\varepsilon_L)$ and then smoothed. It is evident that the graph of $\Theta(\varepsilon_L)$ crosses the graph of $\sigma(\varepsilon_L)$ twice for the uniaxial tension test performed at room temperature, whereas for the three lower temperatures, there is only one intersection – indicating an unstable neck. An explanation for this result may be found by examining the volumetric strain vs. longitudinal strain curves in Figure 3.15. At room temperature, a peak value is reached before the volumetric strain decreases. This result indicates, as previously depicted in

Figure 3.16, that voids in the material grow up to a certain point before they are stabilized or start to collapse. At the lower temperatures, however, the voids only continue to grow up to fracture, which in effect inhibits the formation of a stable neck. This is also supported by the observed reduction in the overall ductility of the tensile specimen, as shown by the two photographs in Figure 3.25.

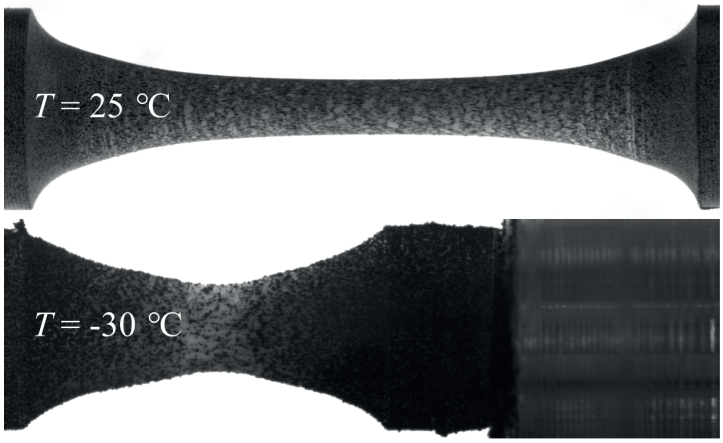

Figure 3.25: Rubber-modified polypropylene (PP): Comparison of deformed specimens just before fracture in uniaxial tension at $T = 25$ °C (room temperature) and $T = -30$ °C at a strain rate of $\dot{e} = 1.0\ \mathrm{s}^{-1}$.

The influence of rate and temperature on the locking stretch can be analyzed by application of the expression proposed by Arruda et al. [4], viz.

$$\mu(\theta)N(\theta) = \text{constant} \tag{3.9}$$

where $\mu(\theta)$ is the temperature-dependent shear modulus and $N(\theta)$ is the temperature-dependent number of statistical rigid links per chain. Equation (3.9) also conserves the number of rigid links (cross-links in the XLPE material and entanglements in the PP material), and hence preserves the mass of the system. The number of statistical rigid links per chain, N, is related to the locking stretch as $\lambda_{\text{lock}} = \sqrt{N}$. Young's modulus, and consequently the shear modulus, increases with decreasing temperature for both materials, as shown in Figures 3.20 and 3.21. Equation (3.9) then implies that the locking stretch increases with temperature. Investigating the locking stretch at increasing strain rates while keeping the temperature fixed, we see from Figures 3.8 and 3.14 that the implication of Equation (3.9) holds, i.e., the locking stretch increases at elevated strain rates due to self-heating in the material (Figures 3.11 and 3.17). Exceptions are PP at the highest strain rate, which fails to form a stable neck below a temperature of $T = 0$ °C, and XLPE at a temperature of −30 °C, where network hardening does not occur at the two highest strain rates.

Considering isothermal conditions ($\dot{e} = 0.01\ \mathrm{s}^{-1}$), the implications of Equation (3.9) hold for PP, where we find that the locking stretch decreases and Young's modulus increases when the temperature decreases. However, for XLPE, we find that Young's modulus increases for decreasing

temperatures, but a less significant effect is observed in terms of the locking stretch.

3.5 Conclusions

The following conclusions are drawn:

- The influence of strain rate and temperature on the mechanical behaviour of PP and XLPE in tension and compression was studied experimentally. We observed that the yield stress in tension relates to the temperature and strain rate through the Ree-Eyring flow theory and that Young's modulus follows an exponential relation with decreasing temperature within the experimental range. This finding holds for both materials.
- In terms of self-heating, a substantial temperature increase is observed in both materials at the elevated strain rates. At the highest strain rate ($\dot{e} = 1.0\ \mathrm{s}^{-1}$), a continuous temperature increase indicates that we have close to adiabatic conditions, whereas for the lowest strain rate ($\dot{e} = 0.01\ \mathrm{s}^{-1}$) isothermal conditions are met.
- The polypropylene material exhibits substantial volumetric strains, ranging from 0.6 to 0.9. This is believed to be caused by cavitation in the rubbery phase of the material. A change in the evolution of the volumetric strain is also observed at the highest strain rates when decreasing the temperature. At room temperature, the volumetric strain increases until it reaches a maximum value, after which it starts to decrease. SEM micrographs suggest that this behaviour is caused by the stabilization of the growing voids when the material hardens due to large strains, causing the voids to collapse. However, this does not occur at the lower temperatures, which could be caused by the loss of ductility, facilitating coalescence rather than void collapse. In the polyethylene material, the volumetric strain remains small at room temperature but increases when the temperature is lowered.
- Pressure sensitivity, defined as the ratio between the compressive and tensile yield stress ($\alpha_\mathrm{p} = \sigma_\mathrm{C}/\sigma_\mathrm{T}$), is found to be substantial for the PP material, ranging from a minimum value of 1.22 at room temperature and the lowest strain rate to 1.71 at a temperature of $-15\ ^\circ\mathrm{C}$ and the highest strain rate. This difference in yield stress in the two deformation modes is due to the formation of voids in tension, a phenomenon that does not occur in compression. In the XLPE material, however, where the volumetric strain remains small, the pressure sensitivity parameter is close to unity for all test configurations.

Acknowledgements

The authors wish to thank the Research Council of Norway for funding through the Petromaks 2 programme, Contract No. 228513/E30. The financial support from ENI, Statoil, Lundin, Total, Scana Steel Stavanger, JFE Steel Corporation, Posco, Kobe Steel, SSAB, Bredero Shaw, Borealis, Trelleborg, Nexans, Aker Solutions, FMC Kongsberg Subsea, Marine Aluminium, Hydro and

Sapa are also acknowledged. Special thanks is given to Nexans Norway and Borealis for providing the materials. Mr. Trond Auestad and Mr. Tore Wisth are acknowledged for their invaluable help in developing the experimental set-up and performing the experiments. Mr. Christian Oen Paulsen's help with the SEM micrographs is also greatly appreciated.

References

[1] Grytten, F., Daiyan, H., Polanco-Loria, M., and Dumoulin, S. "Use of digital image correlation to measure large-strain tensile properties of ductile thermoplastics". *Polymer Testing* 28 (2009), pp. 653–660. DOI: 10.1016/j.polymertesting.2009.05.009.

[2] Delhaye, V., Clausen, A. H., Moussy, F., Othman, R., and Hopperstad, O. S. "Influence of stress state and strain rate on the behaviour of a rubber-particle reinforced polypropylene". *International Journal of Impact Engineering* 38 (2011), pp. 208–218. DOI: 10.1016/j.ijimpeng.2010.11.004.

[3] Jerabek, M., Major, Z., and Lang, R. W. "Strain determination of polymeric materials using digital image correlation". *Polymer Testing* 29 (2010), pp. 407–416. DOI: 10.1016/j.polymertesting.2010.01.005.

[4] Arruda, E. M., Boyce, M. C., and Jayachandran, R. "Effects of strain rate, temperature and thermomechanical coupling on the finite strain deformation of glassy polymers". *Mechanics of Materials* 19 (1995), pp. 193–212. DOI: 10.1016/0167-6636(94)00034-E.

[5] Zaroulis, J. and Boyce, M. "Temperature, strain rate, and strain state dependence of the evolution in mechanical behaviour and structure of poly(ethylene terephthalate) with finite strain deformation". *Polymer* 38 (1997), pp. 1303–1315. DOI: 10.1016/S0032-3861(96)00632-5.

[6] van Breemen, L. C. A., Engels, T. A. P., Klompen, E. T. J., Senden, D. J. A., and Govaert, L. E. "Rate- and temperature-dependent strain softening in solid polymers". *Journal of Polymer Science, Part B: Polymer Physics* 50 (2012), pp. 1757–1771. DOI: 10.1002/polb.23199.

[7] Zaïri, F., Naït-Abdelaziz, M., Gloaguen, J. M., and Lefebvre, J. M. "Constitutive modelling of the large inelastic deformation behaviour of rubber-toughened poly(methyl methacrylate): effects of strain rate, temperature and rubber-phase volume fraction". *Modelling and Simulation in Materials Science and Engineering* 18 (2010), p. 055004. DOI: 10.1088/0965-0393/18/5/055004.

[8] Nasraoui, M., Forquin, P., Siad, L., and Rusinek, A. "Influence of strain rate, temperature and adiabatic heating on the mechanical behaviour of poly-methyl-methacrylate: Experimental and modelling analyses". *Materials and Design* 37 (2012), pp. 500–509. DOI: 10.1016/j.matdes.2011.11.032.

[9] Srivastava, V., Chester, S. A., Ames, N. M., and Anand, L. "A thermo-mechanically-coupled large-deformation theory for amorphous polymers in a temperature range which spans their glass transition". *International Journal of Plasticity* 26 (2010), pp. 1138–1182. DOI: 10.1016/j.ijplas.2010.01.004.

[10] Richeton, J., Ahzi, S., Vecchio, K., Jiang, F., and Adharapurapu, R. "Influence of temperature and strain rate on the mechanical behavior of three amorphous polymers: Characterization and modeling of the compressive yield stress". *International Journal of Solids and Structures* 43 (2006), pp. 2318–2335. DOI: 10.1016/j.ijsolstr.2005.06.040.

[11] Cao, K., Wang, Y., and Wang, Y. "Effects of strain rate and temperature on the tension behavior of polycarbonate". *Materials and Design* 38 (2012), pp. 53–58. DOI: 10.1016/j.matdes.2012.02.007.

[12] Brown, E. N., Rae, P. J., and Orler, E. B. "The influence of temperature and strain rate on the constitutive and damage responses of polychlorotrifluoroethylene (PCTFE, Kel-F 81)". *Polymer* 47 (2006), pp. 7506–7518. DOI: 10.1016/j.polymer.2006.08.032.

[13] Şerban, D. A., Weber, G., Marşavina, L., Silberschmidt, V. V., and Hufenbach, W. "Tensile properties of semi-crystalline thermoplastic polymers: Effects of temperature and strain rates". *Polymer Testing* 32 (2013), pp. 413–425. DOI: 10.1016/j.polymertesting.2012.12.002.

[14] Bauwens-Crowet, C. "The compression yield behaviour of polymethyl methacrylate over a wide range of temperatures and strain-rates". *Journal of Materials Science* 8 (1973), pp. 968–979. DOI: 10.1007/BF00756628.

[15] Ponçot, M., Addiego, F., and Dahoun, A. "True intrinsic mechanical behaviour of semi-crystalline and amorphous polymers: Influences of volume deformation and cavities shape". *International Journal of Plasticity* 40 (2013), pp. 126–139. DOI: 10.1016/j.ijplas.2012.07.007.

[16] Jordan, J. L., Casem, D. T., Bradley, J. M., Dwivedi, A. K., Brown, E. N., and Jordan, C. W. "Mechanical Properties of Low Density Polyethylene". *Journal of Dynamic Behavior of Materials* 2 (2016), pp. 411–420. DOI: 10.1007/s40870-016-0076-0.

[17] Brown, E. N., Willms, R. B., Gray, G. T., Rae, P. J., Cady, C. M., Vecchio, K. S., Flowers, J., and Martinez, M. Y. "Influence of molecular conformation on the constitutive response of polyethylene: A comparison of HDPE, UHMWPE, and PEX". *Experimental Mechanics* 47 (2007), pp. 381–393. DOI: 10.1007/s11340-007-9045-9.

[18] Addiego, F., Dahoun, A., G'Sell, C., and Hiver, J. M. "Characterization of volume strain at large deformation under uniaxial tension in high-density polyethylene". *Polymer* 47 (2006), pp. 4387–4399. DOI: 10.1016/j.polymer.2006.03.093.

[19] Johnsen, J., Grytten, F., Hopperstad, O. S., and Clausen, A. H. "Experimental set-up for determination of the large-strain tensile behaviour of polymers at low temperatures". *Polymer Testing* 53 (2016), pp. 305–313. DOI: 10.1016/j.polymertesting.2016.06.011.

[20] Ree, T. and Eyring, H. “Theory of non-Newtonian flow. I. Solid plastic system”. *Journal of Applied Physics* 26 (1955), pp. 793–800. DOI: 10.1063/1.1722098.

[21] Lazzeri, A. and Bucknall, C. B. “Dilatational bands in rubber-toughened polymers”. *Journal of Materials Science* 28 (1993), pp. 6799–6808. DOI: 10.1007/BF00356433.

[22] Steenbrink, A. and van der Giessen, E. “On cavitation, post-cavitation and yield in amorphous polymer–rubber blends”. *Journal of the Mechanics and Physics of Solids* 47 (1999), pp. 843–876. DOI: 10.1016/S0022-5096(98)00075-1.

[23] *Borcoat EA165E*. http://www.borealisgroup.com/en/polyolefins/products/Borcoat/Borcoat-EA165E/. Accessed:2016-1116.

[24] *Borlink LS4201S*. http://www.borealisgroup.com/en/polyolefins/products/Borlink/Borlink-LS4201S/. Accessed:2016-1116.

[25] ISO22007-4:2008. *Plastics - Determination of thermal conductivity and thermal diffusivity - Part 4: Laser flash method*. Dec. 2008.

[26] Andersen, M. “An experimental and numerical study of thermoplastics at large deformations”. PhD thesis. Norwegian University of Science and Technology, NTNU, 2016.

[27] Fagerholt, E., Børvik, T., and Hopperstad, O. S. “Measuring discontinuous displacement fields in cracked specimens using digital image correlation with mesh adaptation and crack-path optimization”. *Optics and Lasers in Engineering* 51 (2013), pp. 299–310. DOI: 10.1016/j.optlaseng.2012.09.010.

[28] Halary, J. L., Laupretre, F., and Monnerie, L. “Polymer Materials: Macroscopic Properties and Molecular Interpretations”. Hoboken, New Jersey: John Wiley & Sons Inc, 2011. Chap. 1, p. 17.

[29] Senden, D. J. A., Krop, S., van Dommelen, J. A. W., and Govaert, L. E. “Rate- and temperature-dependent strain hardening of polycarbonate”. *Journal of Polymer Science, Part B: Polymer Physics* 50 (2012), pp. 1680–1693. DOI: 10.1002/polb.23165.

[30] Callister Jr., W. D. and Rethwisch, D. G. “Materials Science and Engineering”. 8th ed. John Wiley & Sons, Inc., 2011. Chap. Appendix B, A19.

Part 3

The content of this part is to be submitted to a peer-reviewed international journal.

Johnsen, J., Clausen, A. H., Grytten, F., Benallal, A., and Hopperstad, O. S. (2017).
A thermoelastic-thermoviscoplastic constitutive model for semi-crystalline polymers.

Abstract

Tensile tests conducted at different temperatures and strain rates on a low density cross-linked polyethylene (XLPE) have shown that increasing the strain rate raises the yield stress in a similar manner as decreasing the temperature. The locking stretch also increases as a function of the strain rate, but not to the same extent by decreasing the temperature. The volumetric strain and self-heating of the specimens were also measured in the experimental campaign. In this study, a thermoelastic-thermoviscoplastic model is developed for XLPE in an attempt to describe the combined effects of temperature and strain rate on the stress-strain response. The proposed model consists of two parts. Part A models the thermoelastic and thermoviscoplastic response, and incorporates an elastic Hencky spring in series with two Ree-Eyring dashpots and an inelastic Hencky spring coupled in parallel. The two Ree-Eyring dashpots represent the effects of the main α relaxation and the secondary β relaxation processes on the plastic flow, while the inelastic Hencky spring introduces a backstress on the dashpots and describes the first stage of strain hardening. Part B consists of an eight chain spring capturing the entropic strain hardening due to alignment of the polymer chains during deformation. To capture the self-heating at elevated strain rates, also the elastic and inelastic Hencky springs of Part A are assumed to be entropic. The constitutive model was implemented in a nonlinear finite element (FE) code using a semi-implicit stress update algorithm combined with sub-stepping and a numerical scheme to calculate the consistent tangent operator. After calibration to available experimental data, FE simulations with the constitutive model are shown to successfully describe the stress-strain curves, the volumetric strain, the local strain rate and the self-heating observed in the tensile tests. In addition, the FE simulations adequately predict the global response of the tensile tests, such as the force-displacement curves, the deformed shape of the tensile specimen and local strain as a function of global displacement.

Is not included due to copyright

DEPARTMENT OF STRUCTURAL ENGINEERING
NORWEGIAN UNIVERSITY OF SCIENCE AND TECHNOLOGY

N–7491 TRONDHEIM, NORWAY
Telephone: +47 73 59 47 00 Telefax: +47 73 59 47 01

"Reliability Analysis of Structural Systems using Nonlinear Finite Element Methods",
C. A. Holm, 1990:23, ISBN 82-7119-178-0.

"Uniform Stratified Flow Interaction with a Submerged Horizontal Cylinder",
Ø. Arntsen, 1990:32, ISBN 82-7119-188-8.

"Large Displacement Analysis of Flexible and Rigid Systems Considering
Displacement-Dependent Loads and Nonlinear Constraints",
K. M. Mathisen, 1990:33, ISBN 82-7119-189-6.

"Solid Mechanics and Material Models including Large Deformations",
E. Levold, 1990:56, ISBN 82-7119-214-0, ISSN 0802-3271.

"Inelastic Deformation Capacity of Flexurally-Loaded Aluminium Alloy Structures",
T. Welo, 1990:62, ISBN 82-7119-220-5, ISSN 0802-3271.

"Visualization of Results from Mechanical Engineering Analysis",
K. Aamnes, 1990:63, ISBN 82-7119-221-3, ISSN 0802-3271.

"Object-Oriented Product Modeling for Structural Design",
S. I. Dale, 1991:6, ISBN 82-7119-258-2, ISSN 0802-3271.

"Parallel Techniques for Solving Finite Element Problems on Transputer Networks",
T. H. Hansen, 1991:19, ISBN 82-7119-273-6, ISSN 0802-3271.

"Statistical Description and Estimation of Ocean Drift Ice Environments",
R. Korsnes, 1991:24, ISBN 82-7119-278-7, ISSN 0802-3271.

“Properties of concrete related to fatigue damage: with emphasis on high strength concrete”,
G. Petkovic, 1991:35, ISBN 82-7119-290-6, ISSN 0802-3271.

"Turbidity Current Modelling",
B. Brørs, 1991:38, ISBN 82-7119-293-0, ISSN 0802-3271.

"Zero-Slump Concrete: Rheology, Degree of Compaction and Strength. Effects of Fillers as Part Cement-Replacement",
C. Sørensen, 1992:8, ISBN 82-7119-357-0, ISSN 0802-3271.

"Nonlinear Analysis of Reinforced Concrete Structures Exposed to Transient Loading",
K. V. Høiseth, 1992:15, ISBN 82-7119-364-3, ISSN 0802-3271.

"Finite Element Formulations and Solution Algorithms for Buckling and Collapse Analysis of Thin Shells",
R. O. Bjærum, 1992:30, ISBN 82-7119-380-5, ISSN 0802-3271.

"Response Statistics of Nonlinear Dynamic Systems",
J. M. Johnsen, 1992:42, ISBN 82-7119-393-7, ISSN 0802-3271.

"Digital Models in Engineering. A Study on why and how engineers build and operate digital models for decisison support",
J. Høyte, 1992:75, ISBN 82-7119-429-1, ISSN 0802-3271.

"Sparse Solution of Finite Element Equations",
A. C. Damhaug, 1992:76, ISBN 82-7119-430-5, ISSN 0802-3271.

"Some Aspects of Floating Ice Related to Sea Surface Operations in the Barents Sea",
S. Løset, 1992:95, ISBN 82-7119-452-6, ISSN 0802-3271.

"Modelling of Cyclic Plasticity with Application to Steel and Aluminium Structures",
O. S. Hopperstad, 1993:7, ISBN 82-7119-461-5, ISSN 0802-3271.

"The Free Formulation: Linear Theory and Extensions with Applications to Tetrahedral Elements
with Rotational Freedoms",
G. Skeie, 1993:17, ISBN 82-7119-472-0, ISSN 0802-3271.

"Høyfast betongs motstand mot piggdekkslitasje. Analyse av resultater fra prøving i Veisliter'n",
T. Tveter, 1993:62, ISBN 82-7119-522-0, ISSN 0802-3271.

"A Nonlinear Finite Element Based on Free Formulation Theory for Analysis of Sandwich Structures",
O. Aamlid, 1993:72, ISBN 82-7119-534-4, ISSN 0802-3271.

"The Effect of Curing Temperature and Silica Fume on Chloride Migration and Pore Structure of High Strength Concrete",
C. J. Hauck, 1993:90, ISBN 82-7119-553-0, ISSN 0802-3271.

"Failure of Concrete under Compressive Strain Gradients",
G. Markeset, 1993:110, ISBN 82-7119-575-1, ISSN 0802-3271.

"An experimental study of internal tidal amphidromes in Vestfjorden",
J. H. Nilsen, 1994:39, ISBN 82-7119-640-5, ISSN 0802-3271.

"Structural analysis of oil wells with emphasis on conductor design",
H. Larsen, 1994:46, ISBN 82-7119-648-0, ISSN 0802-3271.

"Adaptive methods for non-linear finite element analysis of shell structures",
K. M. Okstad, 1994:66, ISBN 82-7119-670-7, ISSN 0802-3271.

"On constitutive modelling in nonlinear analysis of concrete structures",
O. Fyrileiv, 1994:115, ISBN 82-7119-725-8, ISSN 0802-3271.

"Fluctuating wind load and response of a line-like engineering structure with emphasis on motion-induced wind forces",
J. Bogunovic Jakobsen, 1995:62, ISBN 82-7119-809-2, ISSN 0802-3271.

"An experimental study of beam-columns subjected to combined torsion, bending and axial actions",
A. Aalberg, 1995:66, ISBN 82-7119-813-0, ISSN 0802-3271.

"Scaling and cracking in unsealed freeze/thaw testing of Portland cement and silica fume concretes",
S. Jacobsen, 1995:101, ISBN 82-7119-851-3, ISSN 0802-3271.

"Damping of water waves by submerged vegetation. A case study of laminaria hyperborea",
A. M. Dubi, 1995:108, ISBN 82-7119-859-9, ISSN 0802-3271.

"The dynamics of a slope current in the Barents Sea",
Sheng Li, 1995:109, ISBN 82-7119-860-2, ISSN 0802-3271.

"Modellering av delmaterialenes betydning for betongens konsistens",
Ernst Mørtsell, 1996:12, ISBN 82-7119-894-7, ISSN 0802-3271.

"Bending of thin-walled aluminium extrusions",
Birgit Søvik Opheim, 1996:60, ISBN 82-7119-947-1, ISSN 0802-3271.

"Material modelling of aluminium for crashworthiness analysis",
Torodd Berstad, 1996:89, ISBN 82-7119-980-3, ISSN 0802-3271.

"Estimation of structural parameters from response measurements on submerged floating tunnels",
Rolf Magne Larssen, 1996:119, ISBN 82-471-0014-2, ISSN 0802-3271.

“Numerical modelling of plain and reinforced concrete by damage mechanics”,
Mario A. Polanco-Loria, 1997:20, ISBN 82-471-0049-5, ISSN 0802-3271.

“Nonlinear random vibrations - numerical analysis by path integration methods”,
Vibeke Moe, 1997:26, ISBN 82-471-0056-8, ISSN 0802-3271.

“Numerical prediction of vortex-induced vibration by the finite element method”,
Joar Martin Dalheim, 1997:63, ISBN 82-471-0096-7, ISSN 0802-3271.

“Time domain calculations of buffeting response for wind sensitive structures”,
Ketil Aas-Jakobsen, 1997:148, ISBN 82-471-0189-0, ISSN 0802-3271.

"A numerical study of flow about fixed and flexibly mounted circular cylinders",
Trond Stokka Meling, 1998:48, ISBN 82-471-0244-7, ISSN 0802-3271.

“Estimation of chloride penetration into concrete bridges in coastal areas”,
Per Egil Steen, 1998:89, ISBN 82-471-0290-0, ISSN 0802-3271.

“Stress-resultant material models for reinforced concrete plates and shells”,
Jan Arve Øverli, 1998:95, ISBN 82-471-0297-8, ISSN 0802-3271.

“Chloride binding in concrete. Effect of surrounding environment and concrete composition”,
Claus Kenneth Larsen, 1998:101, ISBN 82-471-0337-0, ISSN 0802-3271.

“Rotational capacity of aluminium alloy beams”,
Lars A. Moen, 1999:1, ISBN 82-471-0365-6, ISSN 0802-3271.

“Stretch Bending of Aluminium Extrusions”,
Arild H. Clausen, 1999:29, ISBN 82-471-0396-6, ISSN 0802-3271.

“Aluminium and Steel Beams under Concentrated Loading”,
Tore Tryland, 1999:30, ISBN 82-471-0397-4, ISSN 0802-3271.

"Engineering Models of Elastoplasticity and Fracture for Aluminium Alloys",
Odd-Geir Lademo, 1999:39, ISBN 82-471-0406-7, ISSN 0802-3271.

"Kapasitet og duktilitet av dybelforbindelser i trekonstruksjoner",
Jan Siem, 1999:46, ISBN 82-471-0414-8, ISSN 0802-3271.

“Etablering av distribuert ingeniørarbeid; Teknologiske og organisatoriske erfaringer fra en norsk ingeniørbedrift”,
Lars Line, 1999:52, ISBN 82-471-0420-2, ISSN 0802-3271.

“Estimation of Earthquake-Induced Response”,
Símon Ólafsson, 1999:73, ISBN 82-471-0443-1, ISSN 0802-3271.

“Coastal Concrete Bridges: Moisture State, Chloride Permeability and Aging Effects”
Ragnhild Holen Relling, 1999:74, ISBN 82-471-0445-8, ISSN 0802-3271.

”Capacity Assessment of Titanium Pipes Subjected to Bending and External Pressure”,
Arve Bjørset, 1999:100, ISBN 82-471-0473-3, ISSN 0802-3271.

“Validation of Numerical Collapse Behaviour of Thin-Walled Corrugated Panels”,
Håvar Ilstad, 1999:101, ISBN 82-471-0474-1, ISSN 0802-3271.

“Strength and Ductility of Welded Structures in Aluminium Alloys”,
Miroslaw Matusiak, 1999:113, ISBN 82-471-0487-3, ISSN 0802-3271.

“Thermal Dilation and Autogenous Deformation as Driving Forces to Self-Induced Stresses in High Performance Concrete”,
Øyvind Bjøntegaard, 1999:121, ISBN 82-7984-002-8, ISSN 0802-3271.

“Some Aspects of Ski Base Sliding Friction and Ski Base Structure”,
Dag Anders Moldestad, 1999:137, ISBN 82-7984-019-2, ISSN 0802-3271.

"Electrode reactions and corrosion resistance for steel in mortar and concrete",
Roy Antonsen, 2000:10, ISBN 82-7984-030-3, ISSN 0802-3271.

"Hydro-Physical Conditions in Kelp Forests and the Effect on Wave Damping and Dune Erosion. A case study on Laminaria Hyperborea",
Stig Magnar Løvås, 2000:28, ISBN 82-7984-050-8, ISSN 0802-3271.

"Random Vibration and the Path Integral Method",
Christian Skaug, 2000:39, ISBN 82-7984-061-3, ISSN 0802-3271.

"Buckling and geometrical nonlinear beam-type analyses of timber structures",
Trond Even Eggen, 2000:56, ISBN 82-7984-081-8, ISSN 0802-3271.

”Structural Crashworthiness of Aluminium Foam-Based Components”,
Arve Grønsund Hanssen, 2000:76, ISBN 82-7984-102-4, ISSN 0809-103X.

“Measurements and simulations of the consolidation in first-year sea ice ridges, and some aspects of mechanical behaviour”,
Knut V. Høyland, 2000:94, ISBN 82-7984-121-0, ISSN 0809-103X.

”Kinematics in Regular and Irregular Waves based on a Lagrangian Formulation”,
Svein Helge Gjøsund, 2000-86, ISBN 82-7984-112-1, ISSN 0809-103X.

”Self-Induced Cracking Problems in Hardening Concrete Structures”,
Daniela Bosnjak, 2000-121, ISBN 82-7984-151-2, ISSN 0809-103X.

"Ballistic Penetration and Perforation of Steel Plates",
Tore Børvik, 2000:124, ISBN 82-7984-154-7, ISSN 0809-103X.

"Freeze-Thaw resistance of Concrete. Effect of: Curing Conditions, Moisture Exchange and Materials",
Terje Finnerup Rønning, 2001:14, ISBN 82-7984-165-2, ISSN 0809-103X

"Structural behaviour of post tensioned concrete structures. Flat slab. Slabs on ground",
Steinar Trygstad, 2001:52, ISBN 82-471-5314-9, ISSN 0809-103X.

"Slipforming of Vertical Concrete Structures. Friction between concrete and slipform panel",
Kjell Tore Fosså, 2001:61, ISBN 82-471-5325-4, ISSN 0809-103X.

"Some numerical methods for the simulation of laminar and turbulent incompressible flows",
Jens Holmen, 2002:6, ISBN 82-471-5396-3, ISSN 0809-103X.

“Improved Fatigue Performance of Threaded Drillstring Connections by Cold Rolling”,
Steinar Kristoffersen, 2002:11, ISBN: 82-421-5402-1, ISSN 0809-103X.

"Deformations in Concrete Cantilever Bridges: Observations and Theoretical Modelling",
Peter F. Takâcs, 2002:23, ISBN 82-471-5415-3, ISSN 0809-103X.

"Stiffened aluminium plates subjected to impact loading",
Hilde Giæver Hildrum, 2002:69, ISBN 82-471-5467-6, ISSN 0809-103X.

"Full- and model scale study of wind effects on a medium-rise building in a built up area",
Jónas Thór Snæbjørnsson, 2002:95, ISBN82-471-5495-1, ISSN 0809-103X.

“Evaluation of Concepts for Loading of Hydrocarbons in Ice-infested water”,
Arnor Jensen, 2002:114, ISBN 82-417-5506-0, ISSN 0809-103X.

”Numerical and Physical Modelling of Oil Spreading in Broken Ice”,
Janne K. Økland Gjøsteen, 2002:130, ISBN 82-471-5523-0, ISSN 0809-103X.

”Diagnosis and protection of corroding steel in concrete”,
Franz Pruckner, 20002:140, ISBN 82-471-5555-4, ISSN 0809-103X.

“Tensile and Compressive Creep of Young Concrete: Testing and Modelling”,
Dawood Atrushi, 2003:17, ISBN 82-471-5565-6, ISSN 0809-103X.

“Rheology of Particle Suspensions. Fresh Concrete, Mortar and Cement Paste with Various Types of Lignosulfonates”,
Jon Elvar Wallevik, 2003:18, ISBN 82-471-5566-4, ISSN 0809-103X.

“Oblique Loading of Aluminium Crash Components”,
Aase Reyes, 2003:15, ISBN 82-471-5562-1, ISSN 0809-103X.

“Utilization of Ethiopian Natural Pozzolans”,
Surafel Ketema Desta, 2003:26, ISSN 82-471-5574-5, ISSN:0809-103X.

“Behaviour and strength prediction of reinforced concrete structures with discontinuity regions”, Helge Brå, 2004:11, ISBN 82-471-6222-9, ISSN 1503-8181.

“High-strength steel plates subjected to projectile impact. An experimental and numerical study”, Sumita Dey, 2004:38, ISBN 82-471-6282-2 (printed version), ISBN 82-471-6281-4 (electronic version), ISSN 1503-8181.

“Alkali-reactive and inert fillers in concrete. Rheology of fresh mixtures and expansive reactions.”
Bård M. Pedersen, 2004:92, ISBN 82-471-6401-9 (printed version), ISBN 82-471-6400-0 (electronic version), ISSN 1503-8181.

“On the Shear Capacity of Steel Girders with Large Web Openings”.
Nils Christian Hagen, 2005:9 ISBN 82-471-6878-2 (printed version), ISBN 82-471-6877-4 (electronic version), ISSN 1503-8181.

”Behaviour of aluminium extrusions subjected to axial loading”.
Østen Jensen, 2005:7, ISBN 82-471-6873-1 (printed version), ISBN 82-471-6872-3 (electronic version), ISSN 1503-8181.

”Thermal Aspects of corrosion of Steel in Concrete”.
Jan-Magnus Østvik, 2005:5, ISBN 82-471-6869-3 (printed version), ISBN 82-471-6868 (electronic version), ISSN 1503-8181.

”Mechanical and adaptive behaviour of bone in relation to hip replacement.” A study of bone remodelling and bone grafting.
Sébastien Muller, 2005:34, ISBN 82-471-6933-9 (printed version), ISBN 82-471-6932-0 (electronic version), ISSN 1503-8181.

“Analysis of geometrical nonlinearities with applications to timber structures”.
Lars Wollebæk, 2005:74, ISBN 82-471-7050-5 (printed version), ISBN 82-471-7019-1 (electronic version), ISSN 1503-8181.

“Pedestrian induced lateral vibrations of slender footbridges”,
Anders Rönnquist, 2005:102, ISBN 82-471-7082-5 (printed version), ISBN 82-471-7081-7 (electronic version), ISSN 1503-8181.

“Initial Strength Development of Fly Ash and Limestone Blended Cements at Various Temperatures Predicted by Ultrasonic Pulse Velocity”,
Tom Ivar Fredvik, 2005:112, ISBN 82-471-7105-8 (printed version), ISBN 82-471-7103-1 (electronic version), ISSN 1503-8181.

“Behaviour and modelling of thin-walled cast components”,
Cato Dørum, 2005:128, ISBN 82-471-7140-6 (printed version), ISBN 82-471-7139-2 (electronic version), ISSN 1503-8181.

“Behaviour and modelling of selfpiercing riveted connections”,
Raffaele Porcaro, 2005:165, ISBN 82-471-7219-4 (printed version), ISBN 82-471-7218-6 (electronic version), ISSN 1503-8181.

”Behaviour and Modelling og Aluminium Plates subjected to Compressive Load”,
Lars Rønning, 2005:154, ISBN 82-471-7169-1 (printed version), ISBN 82-471-7195-3 (electronic version), ISSN 1503-8181.

”Bumper beam-longitudinal system subjected to offset impact loading”,
Satyanarayana Kokkula, 2005:193, ISBN 82-471-7280-1 (printed version), ISBN 82-471-7279-8 (electronic version), ISSN 1503-8181.

“Control of Chloride Penetration into Concrete Structures at Early Age”,
Guofei Liu, 2006:46, ISBN 82-471-7838-9 (printed version), ISBN 82-471-7837-0 (electronic version), ISSN 1503-8181.

“Modelling of Welded Thin-Walled Aluminium Structures”,
Ting Wang, 2006:78, ISBN 82-471-7907-5 (printed version), ISBN 82-471-7906-7 (electronic version), ISSN 1503-8181.

”Time-variant reliability of dynamic systems by importance sampling and probabilistic analysis of ice loads”,
Anna Ivanova Olsen, 2006:139, ISBN 82-471-8041-3 (printed version), ISBN 82-471-8040-5 (electronic version), ISSN 1503-8181.

“Fatigue life prediction of an aluminium alloy automotive component using finite element analysis of surface topography”.
Sigmund Kyrre Ås, 2006:25, ISBN 82-471-7791-9 (printed version), ISBN 82-471-7791-9 (electronic version), ISSN 1503-8181.

”Constitutive models of elastoplasticity and fracture for aluminium alloys under strain path change”,
Dasharatha Achani, 2006:76, ISBN 82-471-7903-2 (printed version), ISBN 82-471-7902-4 (electronic version), ISSN 1503-8181.

“Simulations of 2D dynamic brittle fracture by the Element-free Galerkin method and linear fracture mechanics”,
Tommy Karlsson, 2006:125, ISBN 82-471-8011-1 (printed version), ISBN 82-471-8010-3 (electronic version), ISSN 1503-8181.

“Penetration and Perforation of Granite Targets by Hard Projectiles”,
Chong Chiang Seah, 2006:188, ISBN 82-471-8150-9 (printed version), ISBN 82-471-8149-5 (electronic version), ISSN 1503-8181.

“Deformations, strain capacity and cracking of concrete in plastic and early hardening phases”,
Tor Arne Hammer, 2007:234, ISBN 978-82-471-5191-4 (printed version), ISBN 978-82-471-5207-2 (electronic version), ISSN 1503-8181.

“Crashworthiness of dual-phase high-strength steel: Material and Component behaviour”, Venkatapathi Tarigopula, 2007:230, ISBN 82-471-5076-4 (printed version), ISBN 82-471-5093-1 (electronic version), ISSN 1503-8181.

“Fibre reinforcement in load carrying concrete structures”,
Åse Lyslo Døssland, 2008:50, ISBN 978-82-471-6910-0 (printed version), ISBN 978-82-471-6924-7 (electronic version), ISSN 1503-8181.

“Low-velocity penetration of aluminium plates”,
Frode Grytten, 2008:46, ISBN 978-82-471-6826-4 (printed version), ISBN 978-82-471-6843-1 (electronic version), ISSN 1503-8181.

“Robustness studies of structures subjected to large deformations”,
Ørjan Fyllingen, 2008:24, ISBN 978-82-471-6339-9 (printed version), ISBN 978-82-471-6342-9 (electronic version), ISSN 1503-8181.

“Constitutive modelling of morsellised bone”,
Knut Birger Lunde, 2008:92, ISBN 978-82-471-7829-4 (printed version), ISBN 978-82-471-7832-4 (electronic version), ISSN 1503-8181.

“Experimental Investigations of Wind Loading on a Suspension Bridge Girder”,
Bjørn Isaksen, 2008:131, ISBN 978-82-471-8656-5 (printed version), ISBN 978-82-471-8673-2 (electronic version), ISSN 1503-8181.

“Cracking Risk of Concrete Structures in The Hardening Phase”,
Guomin Ji, 2008:198, ISBN 978-82-471-1079-9 (printed version), ISBN 978-82-471-1080-5 (electronic version), ISSN 1503-8181.

“Modelling and numerical analysis of the porcine and human mitral apparatus”,
Victorien Emile Prot, 2008:249, ISBN 978-82-471-1192-5 (printed version), ISBN 978-82-471-1193-2 (electronic version), ISSN 1503-8181.

“Strength analysis of net structures”,
Heidi Moe, 2009:48, ISBN 978-82-471-1468-1 (printed version), ISBN 978-82-471-1469-8 (electronic version), ISSN1503-8181.

“Numerical analysis of ductile fracture in surface cracked shells”,
Espen Berg, 2009:80, ISBN 978-82-471-1537-4 (printed version), ISBN 978-82-471-1538-1 (electronic version), ISSN 1503-8181.

“Subject specific finite element analysis of bone – for evaluation of the healing of a leg lengthening and evaluation of femoral stem design”,
Sune Hansborg Pettersen, 2009:99, ISBN 978-82-471-1579-4 (printed version), ISBN 978-82-471-1580-0 (electronic version), ISSN 1503-8181.

“Evaluation of fracture parameters for notched multi-layered structures”,
Lingyun Shang, 2009:137, ISBN 978-82-471-1662-3 (printed version), ISBN 978-82-471-1663-0 (electronic version), ISSN 1503-8181.

“Modelling of Dynamic Material Behaviour and Fracture of Aluminium Alloys for Structural Applications”
Yan Chen, 2009:69, ISBN 978-82-471-1515-2 (printed version), ISBN 978-82 471-1516-9 (electronic version), ISSN 1503-8181.

“Nanomechanics of polymer and composite particles”
Jianying He 2009:213, ISBN 978-82-471-1828-3 (printed version), ISBN 978-82-471-1829-0 (electronic version), ISSN 1503-8181.

“Mechanical properties of clear wood from Norway spruce”
Kristian Berbom Dahl 2009:250, ISBN 978-82-471-1911-2 (printed version) ISBN 978-82-471-1912-9 (electronic version), ISSN 1503-8181.

“Modeling of the degradation of TiB_2 mechanical properties by residual stresses and liquid Al penetration along grain boundaries”
Micol Pezzotta 2009:254, ISBN 978-82-471-1923-5 (printed version) ISBN 978-82-471-1924-2 (electronic version) ISSN 1503-8181.

“Effect of welding residual stress on fracture”
Xiabo Ren 2010:77, ISBN 978-82-471-2115-3 (printed version) ISBN 978-82-471-2116-0 (electronic version), ISSN 1503-8181.

“Pan-based carbon fiber as anode material in cathodic protection system for concrete structures”
Mahdi Chini 2010:122, ISBN 978-82-471-2210-5 (printed version) ISBN 978-82-471-2213-6 (electronic version), ISSN 1503-8181.

“Structural Behaviour of deteriorated and retrofitted concrete structures”
Irina Vasililjeva Sæther 2010:171, ISBN 978-82-471-2315-7 (printed version) ISBN 978-82-471-2316-4 (electronic version) ISSN 1503-8181.

“Prediction of local snow loads on roofs”
Vivian Meløysund 2010:247, ISBN 978-82-471-2490-1 (printed version) ISBN 978-82-471-2491-8 (electronic version) ISSN 1503-8181.

“Behaviour and modelling of polymers for crash applications”
Virgile Delhaye 2010:251, ISBN 978-82-471-2501-4 (printed version) ISBN 978-82-471-2502-1 (electronic version) ISSN 1503-8181.

“Blended cement with reducted CO_2 emission – Utilizing the Fly Ash-Limestone Synergy”,
Klaartje De Weerdt 2011:32, ISBN 978-82-471-2584-7 (printed version) ISBN 978-82-471-2584-4 (electronic version) ISSN 1503-8181.

“Chloride induced reinforcement corrosion in concrete” Concept of critical chloride content – methods and mechanisms.
Ueli Angst 2011:113, ISBN 978-82-471-2769-9 (printed version) ISBN 978-82-471-2763-6 (electronic version) ISSN 1503-8181.

“A thermo-electric-Mechanical study of the carbon anode and contact interface for Energy savings in the production of aluminium”.
Dag Herman Andersen 2011:157, ISBN 978-82-471-2859-6 (printed version) ISBN 978-82-471-2860-2 (electronic version) ISSN 1503-8181.

“Structural Capacity of Anchorage Ties in Masonry Veneer Walls Subjected to Earthquake”. The implications of Eurocode 8 and Eurocode 6 on a typical Norwegain veneer wall.
Ahmed Mohamed Yousry Hamed 2011:181, ISBN 978-82-471-2911-1 (printed version) ISBN 978-82-471-2912-8 (electronic ver.) ISSN 1503-8181.

“Work-hardening behaviour in age-hardenable Al-Zn-Mg(-Cu) alloys”.
Ida Westermann , 2011:247, ISBN 978-82-471-3056-8 (printed ver.) ISBN 978-82-471-3057-5 (electronic ver.) ISSN 1503-8181.

“Behaviour and modelling of selfpiercing riveted connections using aluminium rivets”.
Nguyen-Hieu Hoang, 2011:266, ISBN 978-82-471-3097-1 (printed ver.) ISBN 978-82-471-3099-5 (electronic ver.) ISSN 1503-8181.

“Fibre reinforced concrete”.
Sindre Sandbakk, 2011:297, ISBN 978-82-471-3167-1 (printed ver.) ISBN 978-82-471-3168-8 (electronic ver) ISSN 1503:8181.

“Dynamic behaviour of cablesupported bridges subjected to strong natural wind”.
Ole Andre Øiseth, 2011:315, ISBN 978-82-471-3209-8 (printed ver.) ISBN 978-82-471-3210-4 (electronic ver.) ISSN 1503-8181.

“Constitutive modeling of solargrade silicon materials”
Julien Cochard, 2011:307, ISBN 978-82-471-3189-3 (printed ver). ISBN 978-82-471-3190-9 (electronic ver.) ISSN 1503-8181.

“Constitutive behavior and fracture of shape memory alloys”
Jim Stian Olsen, 2012:57, ISBN 978-82-471-3382-8 (printed ver.) ISBN 978-82-471-3383-5 (electronic ver.) ISSN 1503-8181.

“Field measurements in mechanical testing using close-range photogrammetry and digital image analysis”
Egil Fagerholt, 2012:95, ISBN 978-82-471-3466-5 (printed ver.) ISBN 978-82-471-3467-2 (electronic ver.) ISSN 1503-8181.

“Towards a better under standing of the ultimate behaviour of lightweight aggregate concrete in compression and bending”,
Håvard Nedrelid, 2012:123, ISBN 978-82-471-3527-3 (printed ver.) ISBN 978-82-471-3528-0 (electronic ver.) ISSN 1503-8181.

“Numerical simulations of blood flow in the left side of the heart”
Sigrid Kaarstad Dahl, 2012:135, ISBN 978-82-471-3553-2 (printed ver.) ISBN 978-82-471-3555-6 (electronic ver.) ISSN 1503-8181.

“Moisture induced stresses in glulam”
Vanessa Angst-Nicollier, 2012:139, ISBN 978-82-471-3562-4 (printed ver.) ISBN 978-82-471-3563-1 (electronic ver.) ISSN 1503-8181.

“Biomechanical aspects of distraction osteogensis”
Valentina La Russa, 2012:250, ISBN 978-82-471-3807-6 (printed ver.) ISBN 978-82-471-3808-3 (electronic ver.) ISSN 1503-8181.

“Ductile fracture in dual-phase steel. Theoretical, experimental and numerical study”
Gaute Gruben, 2012:257, ISBN 978-82-471-3822-9 (printed ver.) ISBN 978-82-471-3823-6 (electronic ver.) ISSN 1503-8181.

“Damping in Timber Structures”
Nathalie Labonnote, 2012:263, ISBN 978-82-471-3836-6 (printed ver.) ISBN 978-82-471-3837-3 (electronic ver.) ISSN 1503-8181.

“Biomechanical modeling of fetal veins: The umbilical vein and ductus venosus bifurcation”
Paul Roger Leinan, 2012:299, ISBN 978-82-471-3915-8 (printed ver.) ISBN 978-82-471-3916-5 (electronic ver.) ISSN 1503-8181.

“Large-Deformation behaviour of thermoplastics at various stress states”
Anne Serine Ognedal, 2012:298, ISBN 978-82-471-3913-4 (printed ver.) ISBN 978-82-471-3914-1 (electronic ver.) ISSN 1503-8181.

“Hardening accelerator for fly ash blended cement”
Kien Dinh Hoang, 2012:366, ISBN 978-82-471-4063-5 (printed ver.) ISBN 978-82-471-4064-2 (electronic ver.) ISSN 1503-8181.

“From molecular structure to mechanical properties”
Jianyang Wu, 2013:186, ISBN 978-82-471-4485-5 (printed ver.) ISBN 978-82-471-4486-2 (electronic ver.) ISSN 1503-8181.

“Experimental and numerical study of hybrid concrete structures”
Linn Grepstad Nes, 2013:259, ISBN 978-82-471-4644-6 (printed ver.) ISBN 978-82-471-4645-3 (electronic ver.) ISSN 1503-8181.

“Mechanics of ultra-thin multi crystalline silicon wafers”
Saber Saffar, 2013:199, ISBN 978-82-471-4511-1 (printed ver.) ISBN 978-82-471-4513-5 (electronic ver). ISSN 1503-8181.

“Through process modelling of welded aluminium structures”
Anizahyati Alisibramulisi, 2013:325, ISBN 978-82-471-4788-7 (printed ver.) ISBN 978-82-471-4789-4 (electronic ver.) ISSN 1503-8181.

“Combined blast and fragment loading on steel plates”
Knut Gaarder Rakvåg, 2013:361, ISBN978-82-471-4872-3 (printed ver.) ISBN 978-82-4873-0 (electronic ver.). ISSN 1503-8181.

“Characterization and modelling of the anisotropic behaviour of high-strength aluminium alloy”
Marion Fourmeau, 2014:37, ISBN 978-82-326-0008-3 (printed ver.) ISBN 978-82-326-0009-0 (electronic ver.) ISSN 1503-8181.

“Behaviour of threated steel fasteners at elevated deformation rates”
Henning Fransplass, 2014:65, ISBN 978-82-326-0054-0 (printed ver.) ISBN 978-82-326-0055-7 (electronic ver.) ISSN 1503-8181.

“Sedimentation and Bleeding”
Ya Peng, 2014:89, ISBN 978-82-326-0102-8 (printed ver.) ISBN 978-82-326-0103-5 (electric ver.) ISSN 1503-8181.

“Impact against X65 offshore pipelines”
Martin Kristoffersen, 2014:362, ISBN 978-82-326-0636-8 (printed ver.) ISBN 978-82-326-0637-5 (electronic ver.) ISSN 1503-8181.

“Formability of aluminium alloy subjected to prestrain by rolling”
Dmitry Vysochinskiy, 2014:363,, ISBN 978-82-326-0638-2 (printed ver.) ISBN 978-82-326-0639-9 (electronic ver.) ISSN 1503-8181.

“Experimental and numerical study of Yielding, Work-Hardening and anisotropy in textured AA6xxx alloys using crystal plasticity models”
Mikhail Khadyko, 2015:28, ISBN 978-82-326-0724-2 (printed ver.) ISBN 978-82-326-0725-9 (electronic ver.) ISSN 1503-8181.

“Behaviour and Modelling of AA6xxx Aluminium Alloys Under a Wide Range of Temperatures and Strain Rates”
Vincent Vilamosa, 2015:63, ISBN 978-82-326-0786-0 (printed ver.) ISBN 978-82-326-0787-7 (electronic ver.) ISSN 1503-8181.

“A Probabilistic Approach in Failure Modelling of Aluminium High Pressure Die-Castings”
Octavian Knoll, 2015:137, ISBN 978-82-326-0930-7 (printed ver.) ISBN 978-82-326-0931-4 (electronic ver.) ISSN 1503-8181.

“Ice Abrasion on Marine Concrete Structures”
Egil Møen, 2015:189, ISBN 978-82-326-1034-1 (printed ver.) ISBN 978-82-326-1035-8 (electronic ver.) ISSN 1503-8181.

“Fibre Orientation in Steel-Fibre-Reinforced Concrete”
Giedrius Zirgulis, 2015:229, ISBN 978-82-326-1114-0 (printed ver.) ISBN 978-82-326-1115-7 (electronic ver.) ISSN 1503-8181.

“Effect of spatial variation and possible interference of localised corrosion on the residual capacity of a reinforced concrete beam”
Mohammad Mahdi Kioumarsi, 2015:282, ISBN 978-82-326-1220-8 (printed ver.) ISBN 978-82-1221-5 (electronic ver.) ISSN 1503-8181.

“The role of concrete resistivity in chloride-induced macro-cell corrosion”
Karla Horbostel, 2015:324, ISBN 978-82-326-1304-5 (printed ver.) ISBN 978-82-326-1305-2 (electonic ver.) ISSN 1503-8181.

“Flowable fibre-reinforced concrete for structural applications”
Elena Vidal Sarmiento, 2015-335, ISBN 978-82-326-1324-3 (printed ver.) ISBN 978-82-326-1325-0 (electronic ver.) ISSN 1503-8181.

“Development of chushed sand for concrete production with microproportioning”
Rolands Cepuritis, 2016:19, ISBN 978-82-326-1382-3 (printed ver.) ISBN 978-82-326-1383-0 (electronic ver.) ISSN 1503-8181.

“Withdrawal properties of threaded rods embedded in glued-laminated timer elements”
Haris Stamatopoulos, 2016:48, ISBN 978-82-326-1436-3 (printed ver.) ISBN 978-82-326-1437-0 (electronic ver.) ISSN 1503-8181.

“An Experimental and numerical study of thermoplastics at large deformation”
Marius Andersen, 2016:191, ISBN 978-82-326-1720-3 (printed ver.) ISBN 978-82-326-1721-0 (electronic ver.) ISSN 1503-8181.

“Modeling and Simulation of Ballistic Impact”
Jens Kristian Holmen, 2016:240, ISBN 978-82-326-1818-7 (printed ver). ISBN 978-82-326-1819-4 (electronic ver.) ISSN 1503-8181.

“Early age crack assessment of concrete structures”
Anja B. Estensen Klausen, 2016:256, ISBN 978-82-326-1850-7 (printed ver). ISBN 978-82-326-1851-4 (electronic ver.) ISSN 1503-8181.

“Uncertainty quantification and sensitivity analysis for cardiovascular models”
Vinzenz Gregor Eck, 2016:234, ISBN 978-82-326-1806-4 (printed ver.) ISBN 978-82-326-1807-1 (electronic ver.) ISSN 1503-8181.

“Dynamic behaviour of existing and new railway catenary systems under Norwegain conditions”
Petter Røe Nåvik, 2016:298, ISBN 978-82-326-1935-1 (printed ver.) ISBN 978-82-326-1934-4 (electronic ver.) ISSN 1503-8181.

“Mechanical behaviour of particle-filled elastomers at various temperatures”
Arne Ilseng, 2016-295, ISBN978-82-326-1928-3 (printed ver.) ISBN 978-82-326-1929-0 (electronic ver.) ISSN 1503-8181.

“Nanotechnology for Anti-Icing Application”
Zhiwei He, 2016:348, ISBN 978-82-326-2038-8 (printed ver.) ISBN 978-82-326-2019-5 (electronic ver.) ISSN 1503-8181.

“Conduction Mechanisms in Conductive Adhesives with Metal-Coated Polyer Spheres”
Sigurd Rolland Pettersen, 2016:349, ISBN 978-326-2040-1 (printed ver,) ISBN 978-82-326-2041-8 (electronic ver.) ISSN 1503-8181.

“The interaction between calcium lignosulfonate and cement”
Alessia Colombo, 2017:20, ISBN 978-82-326-2122-4 (printed ver.) ISBN 978-82-326-2123-1 (electronic ver.) ISSN 1503-8181.

“Behaviour and Modelling of Flexible Structures Subjected to Blast Loading”
Vegard Aune, 2017:101, ISBN 978-82-326-2274-0 (printed ver.) ISBN 978-82-326-2275-7 (electronic ver.) ISSN 1503-8181.

“Behaviour of steel connections under quasi-static and impact loading”
Erik Løhre Grimsmo, 2017:159, ISBN 978-82-326-2390-7 (printed ver.) ISBN 978-82-326-2391-4 (electronic ver.) ISSN 1503-8181.

“An experimental and numerical study of cortical bone at he macro and Nano-scale”
Masoud Ramenzanzadehkoldeh,, 2017:208, ISBN 978-82-326-2488-1 (printed ver.) ISBN 978-82-326-2489-8 (electronic ver.) ISSN 1503-8181.

“Optoelectrical Properties of a Novel Organic Semiconductor: 6,13-Dichloropentacene”
Mao Wang, 2017:130, ISBN 978-82-326-2332-7 (printed ver.) ISBN 978-82-326-2333-4) (electronic ver.) ISSN 1503-8181.

“Core-shell structured microgels and their behavior at oil and water interface”
Yi Gong, 2017:182, ISBN 978-82-326-2436-2 (printed. ver.) ISBN 978-82-326-2437-9 (electronic ver.) ISSN 1503-8181.

“Aspects of design of reinforced concrete structures using nonliear finite element analyses”
Morten Engen, 2017:149, ISBN 978-82-326-2370-9 (printed ver.) ISBN 978-82-326-2371-6 (electronic ver.) ISSN 1503-8181.

“Numerical studies on ductile failure of aluminiumfailure of aluminium alloys”
Lars Edvard Dæhli, 2017:284, ISBN 978-82-326-2636-6 (printed ver.) ISBN 978-82-326-2637-3 (electronic ver.) ISSN 1503-8181.

“Modelling and Assessment of Hydrogen Embrittlement in Steels and Nickel Alloys”
Haiyang Yu, 2017:278, ISBN 978-82-326-2624-3 (printed. ver.) ISBN 978-82-326-2625-0 (electronic ver.) ISSN 1503-8181.